# Quantifying and Modelling Post-Wildfire Sediment Production in Waterton Lakes National Park

by

Markus Fleming

A thesis
presented to the University of Waterloo
in fulfillment of the
thesis requirement for the degree of
Master of Science
in
Geography

Waterloo, Ontario, Canada, 2021

## Author's Declaration

I hereby declare that I am the sole author of this thesis. This is a true copy of the thesis, including any required final revisions, as accepted by my examiners.
I understand that my thesis may be made electronically available to the public.

## Abstract

High-severity wildfires can increase sediment mobility and erosion rates in burned landscapes which increase the delivery of fine sediment to receiving streams. The downstream propagation of these pyrogenic materials can have significant implications for ecosystem and human health implications. The identification of areas prone to differing levels of sediment erosion is necessary for watershed managers to prioritize critical areas that may require best management practices to reduce sediment transfer from hillslopes to receiving streams. Knowledge of sediment erodibility and runoff rates at the site scale and incorporation of these data in watershed scale sediment erosion models such as the Revised Universal Soil Loss Equation (RUSLE) is critical for landscape managers to mitigate the effects of soil erosion. The objectives of this study are to 1) quantify runoff and sediment erosion rates for dominant soil textures using a rainfall simulator at the plot scale to provide estimates of sediment erodibility and yield, 2) model post-wildfire erosion at the watershed-scale to identify critical areas of sediment erosion and 3) identify priority management zones in Waterton Lakes National Park and recommend management options for the implementation of best management practices. Runoff and sediment erosion rates of various soil textures were measured using a rainfall simulator using an $I_{10}$ rainfall intensity. The rainfall simulation data were used in RUSLE to determine watershed-scale sediment yields and to identify priority management areas. In the present study, a low rainfall intensity (33 mm $hr^{-1}$) produced runoff and sediment erosion over a range of soil textures following a wildfire. Finer soil textures produced higher runoff rates and sediment yields compared to coarse soil textures on burned soils. RUSLE provided first-order sediment erosion estimates following wildfire and has the potential to identify areas of varying erosion rates at the watershed-scale, in a GIS environment, for use by land managers that may want to reduce sediment from potentially entering nearby streams.

## Acknowledgements

I want to thank my supervisor, Dr. Michael Stone, for his encouragement, support, guidance, and advice throughout my Master's experience. I would also like to thank Dr. Miles Dyck for co-supervising and providing advice and support during my Master's program. Thank you to Dr. Uldis Silins and the Southern Rockies Watershed Project team for the use of their facilities and rainfall simulator. I want to thank the *for*Water Network for providing funding to Dr. Stone to conduct this research.

Thank you to Quinn Decent for being an accommodating and knowledgeable field team leader and supporting me through my Master's program. Thank you to Rafaela Maltauro and Brittany Francescangeli for helping with the fieldwork and creating an exciting field season.

I want to thank my parents, Ashley Fleming, and Christine Fleming, for supporting and encouraging me through this entire process. Thank you to my best friend, Rebecca Garlick, for giving me a space to talk about the challenges and successes of my Masters, encouraging my work, and being a fantastic friend.

# Table of Contents

# List of Figures

# List of Tables

# Chapter 1 : Introduction

## 1.1 Problem Statement

Climate change-associated increases in extreme rainfall events lead to vegetation growth followed by longer, hotter periods and droughts which soil and vegetation moisture content is reduced, leading to more fuel for wildfires, which are expected to grow in frequency in severity over the next decade (Flannigan et al., 2013; Westerling et al., 2006). Wildfire threats to water supplies have been recognized within Canada and globally (Robinne et al., 2016; 2019; Nunes et al., 2018). Wildfires can lead to increases in the amount of precipitation that reaches the land surface, resulting in increased runoff of solids and associated contaminants (Williams et al., 2019; Moody and Martin, 2001). These impacts have even been observed at large basin scales in systems with already deteriorated source water quality (Emmerton et al., 2020). Wildfires can increase water temperature (Wagner et al., 2014) and alter water chemistry changes. For example, higher concentrations of suspended sediment (Silins et al., 2009; Kunze and Stednick, 2006), metals (Abraham et al., 2017), nutrients (Silins et al., 2014; Kunze and Stednick, 2006), and other contaminants (Crouch et al., 2006; Kalabokidis, 2000) have been observed in receiving waters flowing across wildfire impacted landscapes. Post-wildfire releases of bioavailable phosphorus from sediments to the water column can be long-lasting, contributing to the proliferation of bacteria and algae for decades or longer (Emelko et al., 2016; Stone et al., 2014; Watt et al., 2021). These effects can often be observed over considerable downstream distance; for example, it was recently shown that anthropogenic and climate-exacerbated landscape disturbances converge to alter phosphorus bioavailability in an oligotrophic river (Watt et al., 2021). These nutrient releases also fuel increases in abundance and diversity of macroinvertebrates (Martens et al., 2019) and the development of riverbed biofilms that result in more variable water quality (Stone et al., 2011). Collectively, these shifts in source water quality can result in costly challenges for drinking water treatment (Price et al., 2017; Emelko and Sham, 2014; Emelko et al., 2011) and emphasize the need for techno-ecological approaches to mitigate some of these threats at the source (Blackburn et al., 2021; Kirisits et al., 2019).

Increased knowledge of sediment erosion processes on burned landscapes is especially critical for mitigating wildfire threats to water quality and treatability (Robichaud et al., 2016b; Krishnappan et al., 2009). After a wildfire, sediment mobility and erosion rates increase due to the loss of vegetation (Karamesouti et al., 2016) which can increase the transport of fine sediment from hillslopes to streams and the probability of hazards occurring, such as mass wasting and floods (Hosseini et al., 2018; Shakesby and Doerr, 2006). Mass wasting can further alter streams flow and reduce water availability downstream. Accordingly, the identification of major areas of sediment source delivery from the landscape to receiving waters is critical to selecting and

deploying best management practices (BMPs) for risk mitigation (Robichaud, 2005; Collins et al., 2020; Krishnappan et al., 2009).

Sediment erosion and runoff models are used to simulate sediment yield, identify potential areas of risk for sediment transfer to streams, and determine the probability that sediment erosion will occur under a range of hydro-meteorological conditions. Hosseini et al. (2018) highlighted the need to quantify sediment loss and risk to aquatic environments. Due to the lack of field data on post-wildfire soil characteristics, it is difficult to accurately estimate sediment erosion from models as most sediment erosion models were not specifically designed for this purpose (Fernández and Vega, 2016). Rainfall simulators deployed at the plot scale can be used to generate soil erodibility data required for sediment erosion models. This type of analysis can be used to measure the time-to-start of runoff and the runoff rate from a set storm intensity and this approach has been previously applied to post-wildfire environments (Covert and Jordan, 2009; Pierson et al., 2001; Benavides-Solorio and MacDonald, 2001). Data generated from rainfall simulation experiments are then used as model parameters to estimate sediment erosion.

The Revised Universal Soil Loss Equation (RUSLE) model, initially developed for agricultural applications, has been used as a tool to estimate post-wildfire sediment erosion, and identify areas that with varying levels of risk to sediment erosion in burnt watersheds (Renard et al., 1991; Moody et al., 2013). Sediment erosion models coupled with Geographic Information Systems (GIS) have been used to create maps of sediment erosion potential at spatial scales ranging from the plot- to the watershed scales (Wu et al., 2013). Combining GIS with soil erosion models is an effective way to analyze data within the GIS platform to visualize model outputs (Grunwald and Qi, 2006). RUSLE is commonly used within a GIS framework because it is easy to implement and has fewer data requirements than other more complex and data-rich soil erosion models (Wu et al., 2013).

Several studies have attempted to estimate post-wildfire sediment erosion, but a critical challenge is to accurately predict the amount of soil loss (Fernández and Vega, 2016; Vieira et al., 2018; Robichaud et al., 2016; Esteves et al., 2012; Karamesouti et al., 2016; Meusburger et al., 2010; Vieira et al., 2014). Although several previous post wildfire erosion modelling studies have been conducted in the United States and Europe, few studies have investigated post-wildfire soil erosion in glaciated, forested source water regions located on the eastern slopes of the Canadian Rocky Mountains. This area is a critical forested source water region that supplies ~80% of drinking water supplies for Alberta's settled central and southern regions (Silins et al., 2009). Despite the critical importance of this region for water supply and the potential risk of post-wildfire sediment to degrade surface water quality, no studies to date have been conducted to quantify and model post-wildfire sediment production on the eastern slopes of the Rocky Mountains in southern Alberta.

## 1.2 Literature Review

### *1.2.1 Climate Change and Wildfire*

Climate change has both positive and negative impacts on global forests (Allen et al., 2010). The positive effects include increased water use efficiency and longer growing season. However, the negative effects include increased stress and mortality from climate-driven changes of forest insects and pathogens, droughts and higher temperatures causing forest mortality and wildfires (Allen et al., 2010). Consequently, more frequently droughts caused by warmer temperatures have increased wildfire activity (Westerling et al., 2006; Flannigan et al., 2009; Allen et al., 2010). Notably, in western North America, fire prone areas are strongly associated with drought and warmer temperatures which often increase frequency and intensity of wildfire (Westerling et al., 2006). Changes in fire frequency and intensity is largely due to previous fire suppression activity, which contributes to increased fuel loads (Allen et al., 2010). Larger fuel loads combined with drought can create favorable conditions that promote large scale high-intensity fires (Flannigan et al., 2009).

Over the last few decades fires typically burned larger areas which have been disturbed more frequently at greater burn severities and this has created a concern for post-wildfire human safety, regional economies, global climate, and ecosystem services (Flannigan et al., 2009; Larson-Nash et al., 2018). Furthermore, post-wildfire responses, which include typically hydro-geomorphic processes, carbon storage, ecosystem disturbances, and water quality concerns, can affect a much larger area than just the burned basins (Moody et al., 2013); particularly areas that are downstream of the burned area (Robichaud et al., 2016; Larson-Nash et al., 2018). The impact on hydrological ecosystem services is concerning in mountainous regions. This is especially true on the eastern slopes of the Rocky Mountains which are critical water source water regions (Hauer et al., 2016; Silins et al., 2009).

Hydrological processes on burned landscapes change significantly following a wildfire. Post-wildfire soils are typically water repellant and have decreased infiltrations rates that can significantly increase runoff rates compared to pre-burn conditions (Silins et al., 2009). Changes in the post-wildfire rainfall-runoff response can create floods and debris flows from short and frequent rainfall events, rather than longer and infrequent storm events (Moody et al., 2013). These authors report that peak stream discharge and sediment fluxes correlate with maximum rainfall intensities that are 30-minutes or less in duration (Spigel and Robichaud, 2007). The increased sediment flux is due to lower sediment thresholds and larger erosion rates that increase sediment production in the burned area (Silins et al., 2009).

### *1.2.2 Sediment Erosion*

Quantifying post-wildfire sediment erosion prediction is complicated because factors such as sediment availability, soil erodibility and sediment supply vary considerably in landscapes where topography, vegetation moisture conditions and fire intensity are highly variable (Moody et al., 2013). Soil porosity, composition, structure infiltration capacity and particle aggregation are key parameters that control soil erodibility (Varela at el., 2010). Soil erodibility is a function of soil texture, organic matter, soil structure, and permeability and can be calculated either from erodibility nomographs or physically based equations based on empirical data sets (Renard et al., 1991; Varela et al., 2010). The particle size distribution does not change in low severity fires. However, if temperatures are greater than 400°C particles can fuse together creating larger fractions of silt and sand. Additionally, the particle size distribution can have increased sand and silt fractions when clay particles are eroded during rainfall generated runoff (Varela et al., 2010).

Sediment availability is increased following a wildfire because the fire consumes the canopy, duff and litter layers thus exposing large areas to erosive forces. Furthermore, when soil aggregates are altered from the soil heating during the fire, aggregate stability can be reduced thus making sediment more susceptible to transport (Shakesby and Doerr, 2006; Hosseini et al., 2018). This change in aggregate stability further alters the soil structure which can reduce infiltration capacity and increase soil hydrophobicity (Moody et al., 2013). Following wildfire, the reduction in the infiltration capacity and increase in soil hydrophobicity are related to the consumption of organic matter, which plays a critical role in controlling aggregate stability and soil properties (Varela et al., 2010; Mataix-Solera et al., 2011).

Post-wildfire rainfall-runoff typically increases erosion rates in watersheds (Pierson et al., 2001). The runoff rates can be several orders of magnitude higher than the pre-wildfire conditions (Wilson et al., 2018), and lead to higher concentrations of suspended sediment and nutrients concentrations propagated downstream which are subsequently stored in the lower reaches of the stream network (Hosseini et al., 2018; Feikema et al., 2011). Additionally, the combustion of vegetation and organic matter, the interactions of fire with the soil surface, and the deposition of ash and charcoal associated metals are released and redeposited on the soil surface (Abraham et al., 2017).

### *1.2.3 Methods to Evaluate Post-Wildfire Sediment Erosion*

Soil erosion related to landscape disturbances, such as forest harvesting, agriculture, and urbanization has been widely studied and processes controlling erosion are generally well understood (Pulley and Collins, 2019; Santikari and Murdoch, 2019; Anne Naeth and Chanasyk, 1996; Hancock et al., 2020). However, there is a need to quantify key processes for post-wildfire prediction of rainfall-runoff erosion because of the highly variable changes in soil characteristics (Shakesby and Doerr, 2006). It is often difficult to obtain accurate sediment yields or identify areas at-risk to erosion using traditional methods, thus modifying current or developing new methods

would be beneficial for post-wildfire erosion predictions and assessments (Moody et al., 2013). Furthermore, most methods used to measure sediment erosion and rainfall-runoff estimation are developed for unburned basins, thus creating a need to evaluate erosion processes in burned basins (Moody et al., 2013). Additionally, in burned basins spatial variability in the extent of burn severity can result in heterogeneous behavior in soil water repellency and ash depth in a patch like manner (Shakesby and Doerr, 2006).

Previous studies of post-wildfire sediment erosion have used a variety of measurement techniques including infiltrometers (Moody and Ebel, 2014), sediment fences (Fernández and Vega, 2016), and rainfall simulators (Covert and Jordan, 2009; Pierson et al., 2001; Benavides-Solorio and MacDonald, 2001). Moody and Ebel (2014) used infiltrometers to determine the active depth, magnitude and time-to-start of runoff at the plot scale from naturally occurring rainfall events. Sediment fences have been used to measure sediment erosion on hillslopes following rainfall events (Fernández and Vega, 2016). Rainfall simulators are also used to determine runoff and sediment erosion rates for a given rainfall intensity. The advantage of rainfall simulators is that they can be strategically placed to evaluate the effects of factors such as slope, soil type, burn severity, and the forest floor type on sediment erosion rates (Covert and Jordan, 2009). Rainfall simulators have been deployed at the plot scale to validate the rainfall erosivity and soil erodibility in conjunction with soil properties in agricultural land cover (Meyer and Harmon, 1979; Matula, 2009; Hänsel et al., 2016; Boulange et al., 2019) and a recent increase in burned landscapes (Benavides-Solorio and MacDonald, 2001; Pierson et al., 2001; Covert and Jordan, 2009; Robichaud et al., 2016a; Larsen-Nash et al., 2018). However, they have not been used to directly measure post-wildfire effects on runoff and sediment erosion on the eastern slopes of the Rocky Mountains, particularly in snowmelt dominated critical source water regions that typically produce abundant supplies of high-quality water (Spencer et al., 2019).

Rainfall simulators are generally categorized into two basic designs based on nozzle type. The first type of nozzle is a drip tube and the second is a pressure valve nozzle (Boulange et al., 2019; Covert and Jordan, 2009). Rainfall intensity can be adjusted with rainfall simulators using pressurized nozzles, valves, varying nozzle sizes and different pumps (Boulange et al., 2019). Rainfall simulators must accurately reflect natural rainfall characteristics such as intensity, drop size, and velocity of the raindrops (Boulange et al., 2019). The drop size and velocity are determined using photography and videos with a gridded backdrop (Covert and Jordan, 2009). To obtain a rainfall intensity the simulator needs to be calibrated prior to the rainfall erosion experiment by covering the plot to keep it dry and collecting the rainfall running from the cover for a given interval (Covert and Jordan, 2009). This calibration process is repeated until the desired rainfall intensity is achieved.

The primary cause of post-wildfire erosion is from high-intensity, short-duration storm events because of the capacity of these storms to detach and transport surface particles (Spigel and

Robichaud, 2007). An intensity-duration-frequency (IDF) curve can be used to determine return period of storm events using empirical or theoretical approaches (Koutsoyiannis et al., 1998). Rainfall data is used with IDF approaches to estimate rainfall intensity, rainfall duration, and frequency of storm events (Requena et al., 2019), which can then be used in rainfall simulation to analyze runoff rates and sediment erosion on experimental plots. Accordingly, rainfall simulators deployed in post-wildfire environments must be calibrated according to storm events that occur to create runoff conditions that promote erosion (Covert and Jordan, 2009).

### *1.2.4 Sediment Export and Runoff Models*

Various sediment erosion models have been used to predict soil erosion rates or soil loss following a wildfire. These models include the Water Erosion Prediction Project (WEPP), the Morgan-Morgan-Finney (MMF) model, Pan-European Soil Erosion Risk Assessment (PESERA), and the (Revised) Universal Soil Loss Equation (R)USLE. WEPP is a physical-based model that predicts soil loss and runoff at large-scales (Fernández and Vega, 2018). PESERA is a physical-based model used to estimate long-term erosion rates at large spatial scales based on physical processes controlling sheet and rill erosion (Kirkby et al., 2009; Fernández and Vega, 2016). The MMF model is a simplified erosion model that was designed to simulate annual runoff and erosion rates (Hosseini et al., 2018). Similar, to the MMF model, USLE and its revised version, RUSLE, are empirical-based models that estimate annual sediment yields at various scales (Renard et al., 1991).

The RUSLE model includes five factors that influence the annual loss of sediment. The R-factor represents the rainfall energy and precipitation volume. The K-factor accounts for soil parameters that govern erosion potential. Soil parameters reflected in the K-factor include particle-size, percent organic matter, soil structure, and permeability (Alewell et al., 2019). The LS-factor is a measure of impact of runoff energy for a given slope length. The C-factor describes the vegetation cover and management practices. The P-factor is described as the human intervention practice based on our understanding of soil erosion (Alewell et al., 2019). The utility of the widely used RUSLE model is that it is easy to implement into a Geographic Information System (GIS) framework and compared to more mechanistic models it has relatively modest. Notably, it is widely used as a management tool to identify critical areas of concern of sediment erosion that require the implementation for best management practices (BMPs; Moody et al., 2013; Wu et al., 2013).

Geographic Information Systems are useful tools for performing geographic database management, geovisualization analysis and scientific and mathematical analysis between multiple datasets. Thus, making GIS capable of providing a reliable decision support system to evaluate areas of concern of sediment erosion from spatial analysis techniques at various scales (Dragićević et al., 2015). Furthermore, GIS can output the data visually through maps or in the form of tables and graphs (Grunwald and Qi, 2006). For post-wildfire modelling GIS can be used for burn

severity mapping (Lanorte et al., 2019; Fox et al., 2016) and effectively evaluate sediment erosion at various spatial scales (Terranova et al., 2009; Meusburger et al., 2010; Mitasova et al., 2013). Mapping sediment erosion with RUSLE provides an opportunity to integrate spatial layers for the five factors listed above and identify critical annual soil loss areas. It also provides first estimation in post-wildfire sediment erosion (Moody et al., 2013; Lim et al., 2005). Moreover, the visualization of areas experiencing sediment erosion can help planners and managers identify critical areas (i.e., hydrologically connected hillslopes and receiving streams) for the deployment of best management practices to mitigate the erosion potential.

### 1.3 Research Objectives

The primary goal of this research is to determine the effect of the Kenow wildfire on erodibility and sediment yields in Waterton Lakes National Park located in SW Alberta, Canada. The specific objectives of the study are to:

1) Quantify post-wildfire runoff and sediment erosion for dominant soil textures using rainfall simulations at the plot scale to provide estimates of sediment erodibility and yield.

2) Model post-wildfire erosion at the watershed scale to identify critical areas of sediment erosion.

3) Identify priority management zones in Waterton Lakes National Park and propose management options for the implementation of best management practices.

# Chapter 2 : Methods

## 2.1 Experimental Design

Rainfall simulators were deployed at the plot scale for a range of soil textures to quantify post-wildfire sediment production in two watersheds located in Waterton Lakes National Park (WLNP). Results of the plot erosion study were used as input data to the Revised Universal Soil Loss Equation model to simulate erosion at the watershed scale. Maps of erosion potential (high, medium, and low) were produced to identify critical zones that may present a risk to surface water quality.

## 2.2 Study Area

### *2.2.1 Study Area Description*

Waterton Lakes National Park is located on the eastern slopes of the Rocky Mountains in SW Alberta (Figure 2.1). The geology of the Park consists primarily of Proterozoic sedimentary materials that were forced over the younger Mesozoic rocks which make up the foothills of the Park (Coen & Holland, 1976). Currently, there are no glaciers in the WLNP, but previous glacial activity has altered the landscape. Surficial parent materials in the study area consist of thick deposits of glacial-fluvial derived sands and gravels (Coen & Holland, 1976). Alpine glaciers shaped much of the mountain-scape within WLNP which created U-shaped valleys and cirques while continental glaciers shaped the foothills in the lower areas leaving significant depositional features such as eskers and kames (WPIS,2019; Coen & Holland, 1976). Glacial deposits comprise most of the surficial materials in WLNP which include variable mixtures of sands, silts, clays, and gravels (Figure 2.2; WPIS, 2019).

Cameron Creek and Blakiston Creek drain two of the larger watersheds in WLNP that were severely burned during the Kenow wildfire (Figure 2.1). Cameron Creek flows within a heavily incised V-shaped valley, while Blakiston Creek flows across a U-shaped valley created from retreating glaciers. The lower section of Blakiston Creek has a broad floodplain separating the steeper hillslopes from the stream. Therefore, the connectivity between hillslopes and Blakiston Creek is relatively low, whereas the valley walls of Cameron Creek are more tightly connected hydrologically and thus represent a more direct pathway from the hillslopes to the stream.

Pacific Maritime weather systems that strongly influence the climate of Waterton Lakes National Park are less frequent and mixed with influential Arctic Continental air masses. The average annual precipitation is 1072 mm, the majority of which falls as snow (Parks Canada, 2018b). Using meteorological data from three weather stations for the period 2008 to 2017, Silins (unpublished) conducted an intensity-duration-frequency (IDF) analysis and determined storm events in WLNP. The intensity for 2- and 100-year storm events are 15.5 mm $hr^{-1}$ and 93.8 mm $hr^{-1}$, respectively.

Each of the watersheds under investigation has a weather station, located at Waterton Lakes Red Rock (Blakiston Creek) and Akamina Pass (Cameron Creek), while the third is situated at the Park's entrance.

The Pacific Maritime and Arctic Continental systems create a unique environment in WLNP where diverse vegetation types can flourish (Parks Canada, 2018c). Forty-five vegetation types have been identified in the Park and 16 are significant because they are rare or threatened. Additionally, the Park is also home to a unique plant known as the Waterton moonwort (*Botrychium x wateronese*), only found in Waterton Park (WLNPRG, 2020). The tree species typically found in the Park are Engelmann spruce (*picea engelmannii*), Douglas fir (*pseudotsuga menziesii*), Whitebark pine (*pinus albicaulis*), and Lodgepole pine (*pinus contorta*; USGS, 2007).

In 2017, the Kenow Mountain wildfire severely burned a nearly contiguous area of 19,303 Ha in WLNP (Figure 2.3; Parks Canada, 2018a). Cameron Creek and Blakiston Creek experienced an extreme severity burn throughout their drainage network, exposing extensive patches of soils and post-wildfire pyrogenic materials in near-stream riparian areas. The present study was conducted 22 months after the Kenow wildfire, during which some vegetation regrowth occurred.

### 2.3 Study Site Selection and Plot Characteristics

Six sites were selected in both Blakiston Creek and Cameron Creek watersheds and three additional reference (unburned) sites were selected in the Yarrow Creek watershed. In total 36 rainfall erosion experiments (each site sampled in triplicate) were conducted for the burned basins and a total of 6 rainfall erosion experiments were conducted for the reference basin. A previous study of soils in Waterton Lakes National Park identified seven main soil texture classes (Parks Canada, unpublished). In the present study, four soil texture classes were evaluated because they predominate the soil textural composition in areas adjacent to streams in Blakiston and Cameron watersheds (Figure 2.4). These four soil textures were clay loam, loam, sandy loam, and sand. Soil samples were collected at each study site and the soil texture of these materials were determined in the laboratory using sieves (ASTM, 2017). The mean slope of all the plots was 20.34% and ranged from 7.87 to 36.59% (Table 2.1). The mean slope for the dominant soil textures was 22.31% for clay loam, 17.88 for loam, 21.00% for sandy loam, 19.66 for sand, and 26.75 for reference, respectively.

Study sites located in Cameron and Blakiston Creeks were severely burned during the Kenow wildfire, but vegetation growth was observed 10 months after the wildfire (Figure 2.5). Vegetation at study sites in Cameron Creek watershed consisted of fireweed (*Chamerion angustifolium*) and mixed grasses (Figure 2.5b). However, fireweed regrowth was predominant in the forested area adjacent to Blakiston Creek while grasses and some flowers were more common in the meadow area. Differential vegetation regrowth was observed throughout the study area (Figure 2.5d).

Notably, at least one plot at each site had some live vegetation cover, including fireweeds, grasses, and moss. For the reference basin experiments, vegetation ground cover was removed from one plot at each site while the other plot was not disturbed.

## 2.4 Rainfall Simulator Description

### *2.4.1 Rainfall Simulator Design and Assembly*

The portable rainfall simulator described by Covert and Jordan (2009) was used in this research. The rainfall simulator consists of three support legs connected to a rectangular wooden platform. A (¼ inch HH-14WSQ) spray nozzle was attached to the centre of the platform and a plumb bob was used to centre the rainfall simulator over each experimental plot. The simulator was positioned at a height of 3 m over the plot to achieve a consistent terminal velocity for the simulated rainfall (Figure 2.6). A ball valve was attached to the hose to adjust the pressure of the water flowing to the nozzle and therefore regulate the rainfall intensity. A 4-stroke Honda Wx10 water pump was used to pump water to the rainfall simulator from an 80 L container.

### *2.4.2 Rainfall Simulations*

Simulated rainfall intensities used in the study are presented in Table 2.1. Initially, the target intensity was 24.1 mm $hr^{-1}$ (2-3-year storm event based on the IDF analysis) because of the equipment and practical limitations in the study. However, after conducting the rainfall experiments at two sites, this target intensity was adjusted to 32.8 mm $hr^{-1}$ ($I_{30}$) because a stronger rainfall intensity was required to consistently achieve runoff production. The adjusted rainfall intensity is comparable to a 10-year storm event ($I_{10}$) for Cameron Creek and a 3-year storm event ($I_3$) for Blakiston Creek. Despite efforts to maintain constant rainfall intensities for each plot, there were technical issues at sites 6a and 7. They include increases in pump speed and changes in pressure from the ball valve attached to the rainfall simulation hose. These technical issues were addressed with recalibration of the rainfall simulator system to the target $I_{30}$ of the study.

The rainfall simulator tripod was placed upright after a suitable area for the plot was identified. A windscreen was then fixed between two legs against the dominant wind direction and stretched to minimize any excess water from creating abnormal raindrop splash erosion. The legs were extended, and the simulator was levelled above the plot at a constant height. The plot frame was installed, and the plumb bob was centred above the frame. Three representative surface samples and one soil profile sample were gathered within 1 m of the plot. These samples were doubled bagged and stored at room temperature for subsequent particle size analysis.

The plot frame was recessed approximately 5 cm into the ground to prevent any inflow or outflow of water from the plot during the simulation (Figure 2.7). Surrounding surface material was placed on the sides of the frame to create a natural soil seal. To prevent excess water from entering the

sampling bottles a tarpaulin was placed over the spout. To ensure the plot remained dry a tarpaulin covered the plot while the pump was started, and an even distribution of rainfall was falling on the plot. Once the target intensity was achieved the tarpaulin was removed. Each rainfall simulation lasted for 20 minutes and if no runoff was produced the simulation continued for an additional 20 minutes. Most simulations were completed after 40 minutes. After each simulation the equipment was removed, and the site was returned to a pre-disturbance state as much as possible.

## 2.5 Laboratory Analysis

### *2.5.1 Runoff and Sediment Analysis*

Runoff was collected in 250 mL plastic bottles during each rainfall simulation. The time of runoff initiation was recorded when the first drop of water entered the bottle. Samples were collected at two- or five-minute intervals from the start-of-runoff, depending on the runoff rate during the experiment. Two intervals (2,5 min) were chosen to ensure that there would be enough runoff in the sampling bottle for laboratory analysis. Runoff rates were determined by calculating the volume (mm $hr^{-1}$) of water in each sample and dividing it by the time for each sample collection.

The total suspended solids concentrations from the runoff samples were calculated using the ASTM D3977 Standard Test Method for Determining Sediment Concentrations in Water Samples (ASTM, 2006). Runoff samples were passed through glass microfiber filters (Whatman® glass microfiber filters, Grade GF/A, diameter 55 mm) using a vacuum pump. The samples were then oven dried at 100 C for one hour then weighed to determine the mass of sediment in the runoff samples. Sediment concentrations were a product of sediment mass (g) per unit volume (L) of runoff. The sediment yields (g $m^{-1}$ $hr^{-1}$) at the plot scale were calculated as the product of sediment concentration (g $L^{-1}$) and runoff rate (L $hr^{-1}$) divided by the plot area (0.7784 $m^2$).

The soil samples from each study plot were collected in plastic bags and shipped to the University of Waterloo. Particle size distribution was determined by mass using a mechanical sieve shaker set to half phi intervals from 63 microns to 4 mm for the sand fraction (ASTM, 2017). Soil moisture content were determined gravimetrically using standards methods (ASTM, 2019).

## 2.6 GIS Modelling Analysis

RUSLE can be implemented into a GIS framework over various spatial scale because it is an empirical model that does not require a large data set (Wu et al., 2013). RUSLE was used in this study to estimate soil loss in the Blakiston and Cameron watersheds. GIS in this study was used to prescreen the watershed for possible study site locations. The goal was to identify locations where high hillslope connectivity to the river represented high priority management areas for the implementation of erosion best management practices to mitigate sediment production and transport to rivers. By assessing sediment erodibility and yields in high priority management zones

visual representations of potential risk zones are provided for identifying locations for the implementation of best management practices to reduce contaminants from entering the river system and propagating downstream.

### *2.6.1 GIS Environment*

A combination of ArcGIS 10.7.1 (ESRI, 2020) and Python 2.7 were used in this study. These tools permit RUSLE to be processed in a GIS framework through ArcGIS's ArcToolbox system and python scripts. Additionally, these two approaches enhance the reproducibility of RUSLE for future studies as they provide other users with accessibility to the methodology of the GIS analysis portion. The data used in the GIS analysis is based on data from field and laboratory experiments, as well as data from secondary sources (Appendix A, Table A.1). A 1 m resolution DEM was provided by Parks Canada, 3 m resolution vegetation cover was provided by Planet Team (2020), and a burn scar derived from 30 m resolution Landsat-8 imagery (USGS, 2019) was used as supplementary data for data input.

### *2.6.2 Revised Universal Soil Loss Equation*

RUSLE uses raster layers for its factors to create a soil loss surface based on the drainage basins within the Blakiston and Cameron watersheds. The parameters for RUSLE were based on field data collected from the rainfall simulations as well as satellite imagery (Appendix A, Table A.1). RUSLE was implemented into the GIS environment by creating a surface layer for each parameter of the RUSLE equation in ArcGIS 10.7.1 and sediment erosion was estimated using Python 2.7.

However, RUSLE does not explicitly model infiltration, overland flow, particle detachment, or sediment transport, but rather, it represents these processes through its factors (Larsen and MacDonald, 2007). These factors are soil loss (A; t $ha^{-1}$ $yr^{-1}$), rainfall-runoff erosivity (R; MJ mm $ha^{-1}$ $hr^{-1}$), soil erodibility (K; t hr $MJ^{-1}$ $mm^{-1}$), slope length and steepness (LS; dimensionless), cover-management (C; dimensionless), and conservation practice (P; dimensionless; Renard et al., 1991). The units presented for the rainfall simulation portion of this study have been modified for a single 1 hr storm event at the plot scale rather than annual soil loss estimation. However, for the modelling portion of the study the units follow those outlined by Renard et al. (1991) and uses the equation:

$$A = R * K * LS * C * P \quad (2.1)$$

The R-factor for single storm events was calculated using the Silins' (unpublished) IDF analysis in conjunction with the rainfall volume produced for the given $I_{30}$. The rainfall erosivity was calculated as described by Alewell et al. (2019) using the equation:

$$R = \left(0.29\left(1 - 0.72e^{(-0.05I_{30})}\right) * v_r\right) * I_{30} \quad (2.2)$$

Where, $I_{30}$ is the rainfall intensity (mm hr$^{-1}$) of a 30-min storm event, and $v_r$ is the rainfall volume (mm) during the storm event.

The R-factor for the mean annual erosivity was calculated using daily rainfall data from 2005 to 2018 for the months of April to October. Following the equation suggested by Hui et al. (2010):

$$R = 0.264F^{1.5} \quad (2.3)$$

Where, $F$ is the Fournier Index, which has been modified to estimate $R$ for areas that do not have detailed climate data (Hui et al., 2010). The Fournier Index follows the equation (Hui et al., 2010):

$$F = \sum_{i=1}^{7} \frac{r_i^2}{P} \quad (2.4)$$

Where, $r_i$ is the monthly precipitation and $P$ is the annual precipitation.

Using equations 2.3 and 2.4 an erosivity factor of 337.53 MJ mm hr$^{-1}$ ha$^{-1}$ was calculated and used to estimate annual soil loss at the watershed scale.

The K-factor was determined by rearranging RUSLE to solve for K based on the values determined from the other factors at the plot scale, and follows the equation:

$$K = \frac{A}{(R*LS*C)} \quad (2.5)$$

The K-factor at the watershed scale was determined using a soil texture map provided by Parks Canada and assigning the mean erodibility values from the field data to the provided soil textures. The accuracy of the map was assessed by comparing soil particle size data from the previous study.

The LS-factor at the plot scale used the field measurements of the slope length and degrees. Slope length was obtained by measuring the angle and length of the slope at the plot frame. The angle was converted into a slope percentage so that it can be used in the equation below. The LS-factor was calculated using the equation described by Stone and Hillborn (2012):

$$LS = (0.065 + 0.0456(s) + 0.006541(s)^2) * \left(\frac{l}{22.1}\right)^{NN} \quad (2.6)$$

Where, *s* is the slope percent, *l* is the slope length (m), *NN* is a variable that varies based on the slope gradient (Alewell et al., 2019). In this study *NN* set to 0.5 as suggested by Stone and Hillborn (2012) with slope percent greater than 5%.

The LS-factor at the watershed scale was derived from a 3 m resolution DEM by performing surface analysis. These techniques include obtaining a flow direction, flow accumulation, and a slope surface from the equation proposed by Mitasova et al. (2001):

$$LS = \left(Power\left(\left(\frac{FlowAcc * res}{22.1}\right), 0.4\right)\right) * \left(Power\left(\left(\frac{Sin((SlopeDeg * 0.01745))}{0.09}\right), 1.4\right) * 1.4\right) \quad (2.7)$$

Where, *Power* is the power function found in ArcToolbox, *FlowAcc* is the flow accumulation layer, *res* is the resolution of the raster, *Sin* is the sin function found in ArcToolbox, and *SlopeDeg* is the slope layer in degrees.

The post-wildfire C-factor values were obtained using the Soil-Adjusted Vegetation Index for both the plot- and watershed scale. The reference sites used a C-factor of 0.002 suggested by Breiby (2006) for forested land covers. SAVI has less variation than the NDVI under low vegetation conditions (Kuo et al., 2016), thus it was more appropriate to use for this study. It was obtained using the equation:

$$SAVI = \frac{(NIR - Red)(1 + L)}{(NIR + Red + L)} \quad (2.8)$$

Where, *L* is an adjustment length and was assumed to be 0.1, NIR is the near-infrared band, and Red is the red band.

$$C = -a * SAVI + 1 \quad (2.9)$$

Where, *a* is equal to 1.18 (Kuo et al., 2016).

The P-factor was set to a constant of one because there are no fire erosion mitigation practices currently in place within the Park.

### *2.6.3 RUSLE implementation into GIS*

The implementation of RUSLE into the GIS-framework followed the methods outlined by Mitasova et al. (2001; 2013) but RUSLE was incorporated using python scripts for spatial analysis. Python scripts provided a more flexible and streamlined data analysis process. RUSLE required

three scripts to integrate into the GIS-framework fully. The first calculated the LS-factor, while the second computed soil loss, and the final script calculated erosion and deposition derived from slope aspect and RUSLE. The number of extreme outliers, because of the mountainous terrain topography variability, was reduced by constraining the slope data.

The LS-factor was constrained to slopes less than 30 degrees (60 percent slopes) to keep within range of the values suggested by Renard et al. (1994) and reduce extreme values that would contribute to excessive soil loss. The LS-factor was determined using equation 2.7 from section 2.6.2. Additionally, any values of the LS-factor that were still extreme were constrained to values less than 300 to eliminate unusually high outliers of soil loss further. The five factors' spatial layers of RUSLE computed soil loss were quantified using equation 2.1 from 2.5.1.

After determining soil loss for the two basins, sediment flow direction, based on equations proposed by Mitasova et al. (2013), was calculated by determining the x and y directions of soil loss for a given slope and aspect then multiplying the cosine of the sediment flow aspect by the tangent of the sediment flow slope for both the x and y directions, thus identifying the severity of erosion and deposition at the watershed scale.

### 2.7 Statistical Analysis

A one-way analysis of variance (ANOVA) was performed to test differences in means of runoff rate, sediment yield, and erodibility. Assumptions of normality and variance of each dataset were evaluated. Post-hoc comparisons between means of soil textures were conducted using Tukey HSD tests. Statistical significance of the data was assessed at a p-value of 0.05. All statistical analyses were performed in R version 3.6.3 (R Core Team, 2019).

## 2.8 Tables and Figures

*Table 2.1a: Rainfall intensities and rainfall erosivity of plots at sites 1 to 7.*

| Site | 1a | 1b | 1c | 2a | 2b | 2c | 3a | 3b | 3c | 4a | 4b | 4c | 5a | 5b | 5c | 6a | 6b | 6c | 7a | 7b | 7c |
|---|---|---|---|---|---|---|---|---|---|---|---|---|---|---|---|---|---|---|---|---|---|
| Soil Texture | Clay Loam | Clay Loam | Clay Loam | Clay Loam | Clay Loam | Clay Loam | Clay Loam | Clay Loam | Clay Loam | Loam | Loam | Loam | Loam | Loam | Loam | Loam | Loam | Loam | Sandy Loam | Sandy Loam | Sandy Loam |
| Rainfall Erosivity (MJ mm $hr^{-1}$ $yr^{-1}$) | 89.47 | 89.47 | 89.47 | 111.1 | 111.1 | 111.1 | 88.86 | 88.86 | 88.86 | 89.47 | 89.47 | 89.47 | 89.47 | 89.47 | 89.47 | 268.24 | 88.86 | 88.86 | 88.86 | 88.86 | 88.86 |
| Rainfall Intensity (mm $hr^{-1}$) | 32.8 | 32.8 | 32.8 | 36.1 | 36.1 | 36.1 | 32.7 | 32.7 | 32.7 | 32.8 | 32.8 | 32.8 | 32.8 | 32.8 | 32.8 | 54 | 32.7 | 32.7 | 32.7 | 32.7 | 32.7 |
| Rainfall Volume (mm) | 10.93 | 10.93 | 10.93 | 12.03 | 12.03 | 12.03 | 10.90 | 10.90 | 10.90 | 10.93 | 10.93 | 10.93 | 10.93 | 10.93 | 10.93 | 18.00 | 10.90 | 10.90 | 10.90 | 10.90 | 10.90 |
| Slope Percent | 23.27 | 21.44 | 27.73 | 17.09 | 26.61 | 17.27 | 22.35 | 23.45 | 21.62 | 14.41 | 18.53 | 26.61 | 24.01 | 12.10 | 14.77 | 23.09 | 18.90 | 13.70 | 25.86 | 26.23 | 19.08 |

*Table 2.2b: Rainfall intensities and rainfall erosivity of plots at sites 8 to 15.*

| Site | 8a | 8b | 8c | 9a | 9b | 9c | 10a | 10b | 10c | 11a | 11b | 11c | 12a | 12b | 12c | 13a | 13b | 14a | 14b | 15a | 15b |
|---|---|---|---|---|---|---|---|---|---|---|---|---|---|---|---|---|---|---|---|---|---|
| Soil Texture | Sandy Loam | Sandy Loam | Sandy Loam | Sandy Loam | Sandy Loam | Sandy Loam | Sand | Sand | Sand | Sand | Sand | Sand | Sand | Sand | Sand | Reference | Reference | Reference | Reference | Reference | Reference |
| Rainfall Erosivity (MJ mm $hr^{-1}$ $yr^{-1}$) | 88.86 | 88.86 | 88.86 | 88.86 | 88.86 | 88.86 | 43.61 | 43.61 | 43.61 | 89.47 | 89.47 | 89.47 | 43.61 | 43.61 | 43.61 | 89.47 | 89.47 | 89.47 | 89.47 | 89.47 | 89.47 |
| Rainfall Intensity (mm $hr^{-1}$) | 32.7 | 32.7 | 32.7 | 32.7 | 32.7 | 32.7 | 24.1 | 24.1 | 24.1 | 32.8 | 32.8 | 32.8 | 24.1 | 24.1 | 24.1 | 32.8 | 32.8 | 32.8 | 32.8 | 32.8 | 32.8 |
| Rainfall Volume (mm) | 10.90 | 10.90 | 10.90 | 10.90 | 10.90 | 10.90 | 8.00 | 8.00 | 8.00 | 10.93 | 10.93 | 10.93 | 8.00 | 8.00 | 8.00 | 10.93 | 10.93 | 10.93 | 10.93 | 10.93 | 10.93 |
| Slope Percent | 20.35 | 15.30 | 21.62 | 17.09 | 23.82 | 19.62 | 7.87 | 8.75 | 8.92 | 21.99 | 32.88 | 36.59 | 19.62 | 19.44 | 21.07 | 27.73 | 34.63 | 30.00 | 22.72 | 11.39 | 34.04 |

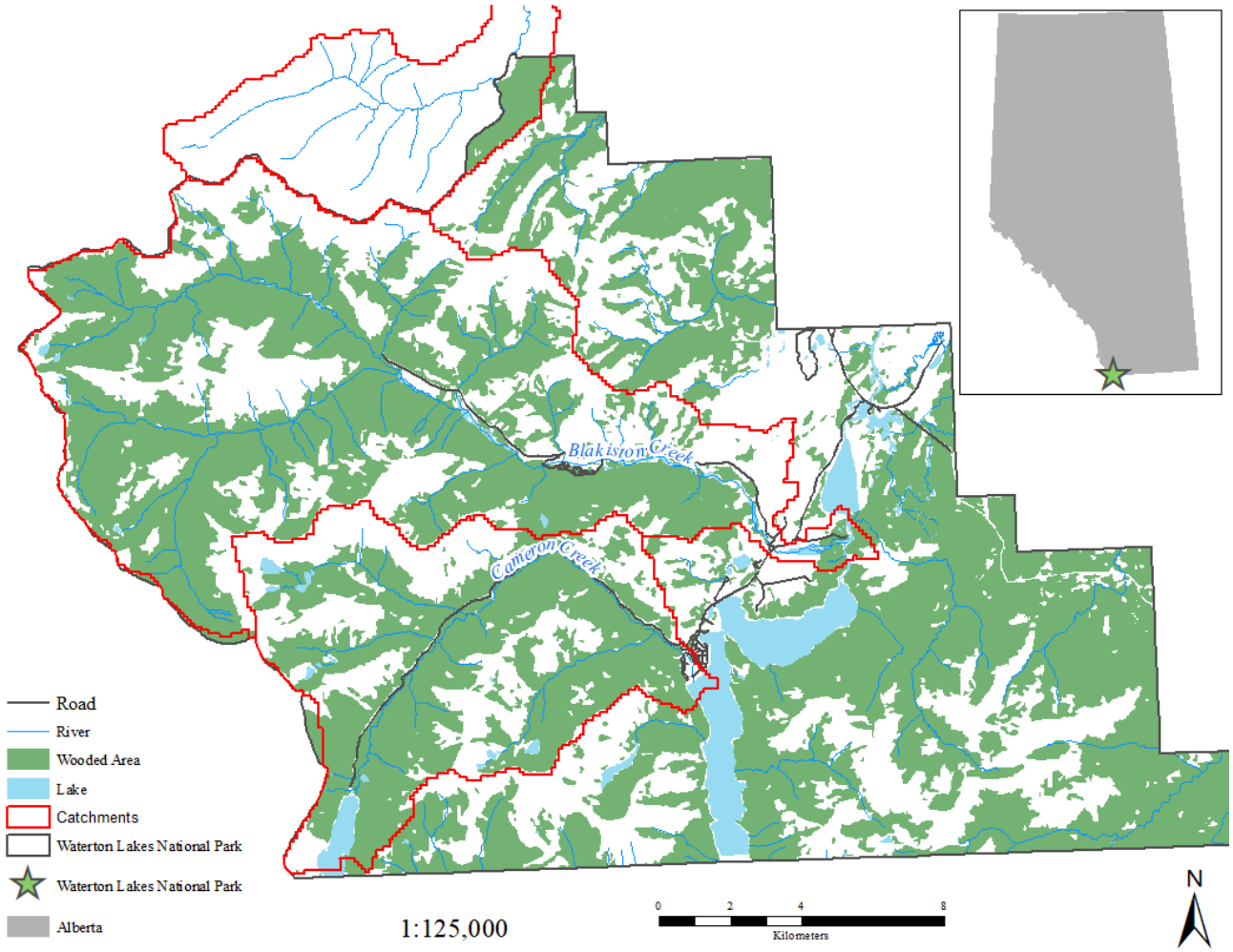


*Figure 2.1 Location of Waterton Lakes National Park in Alberta with study area catchments.*

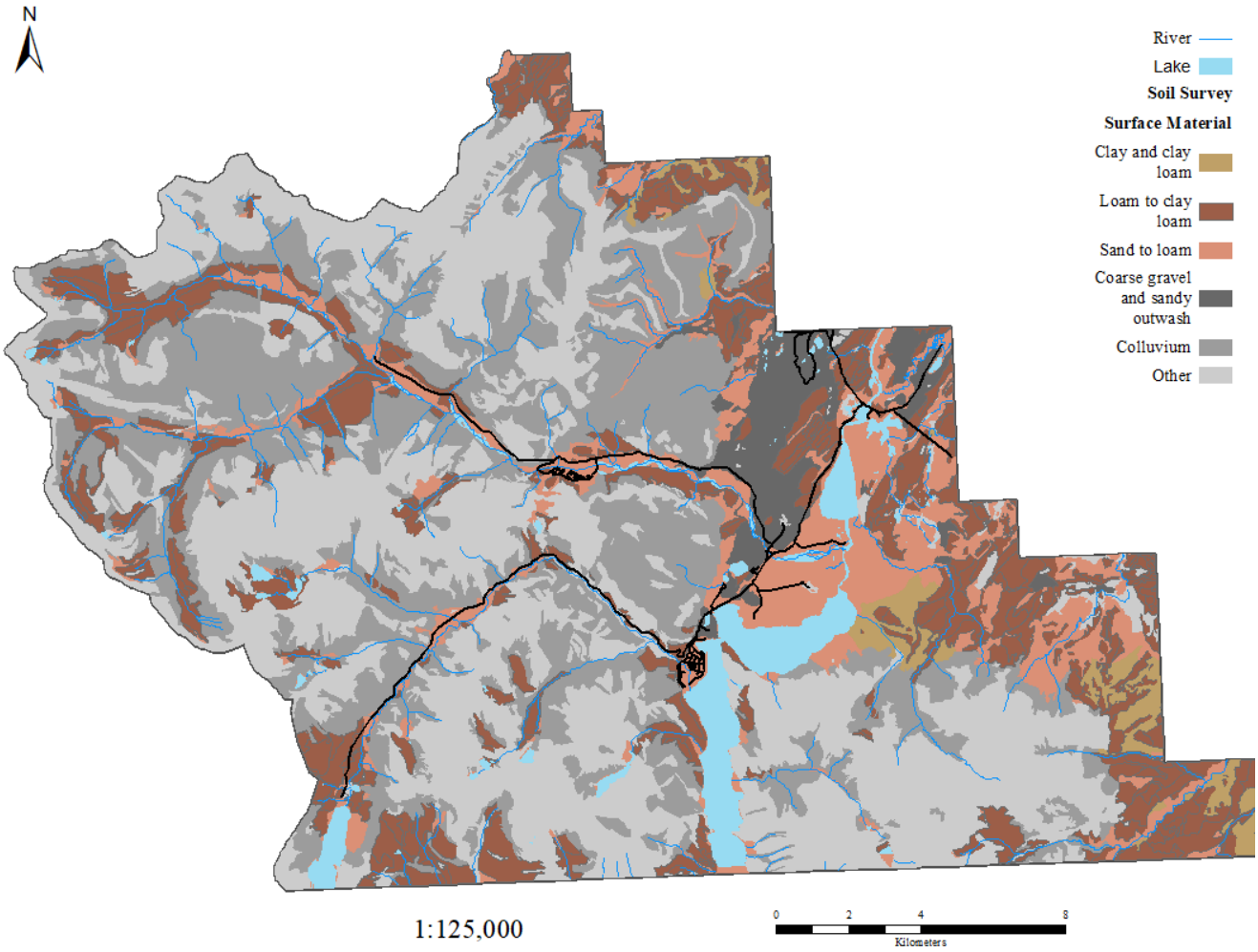


*Figure 2.2: Surficial geology in WLNP.*

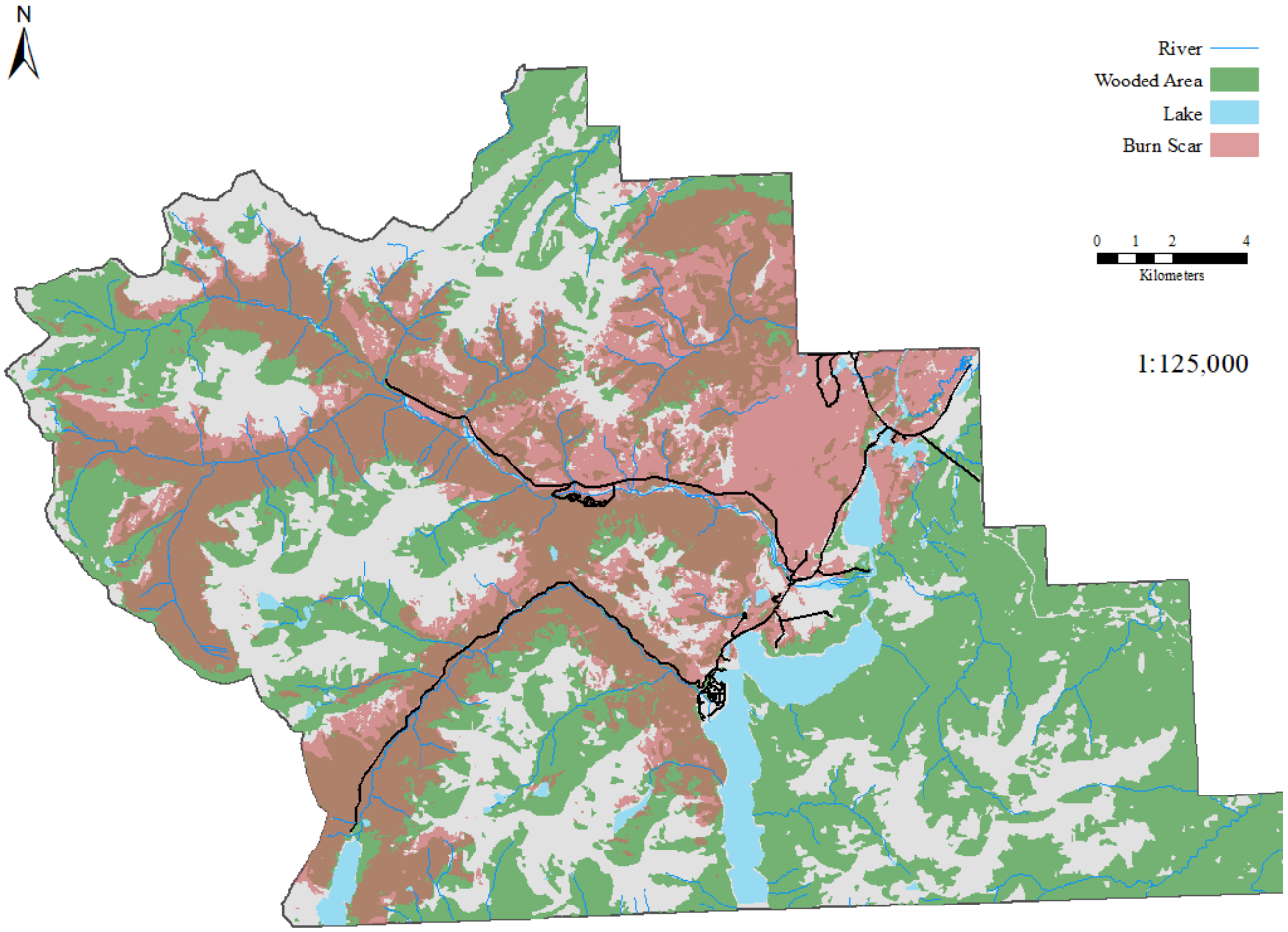


*Figure 2.3: WLNP vegetation cover and burn scar extent.*

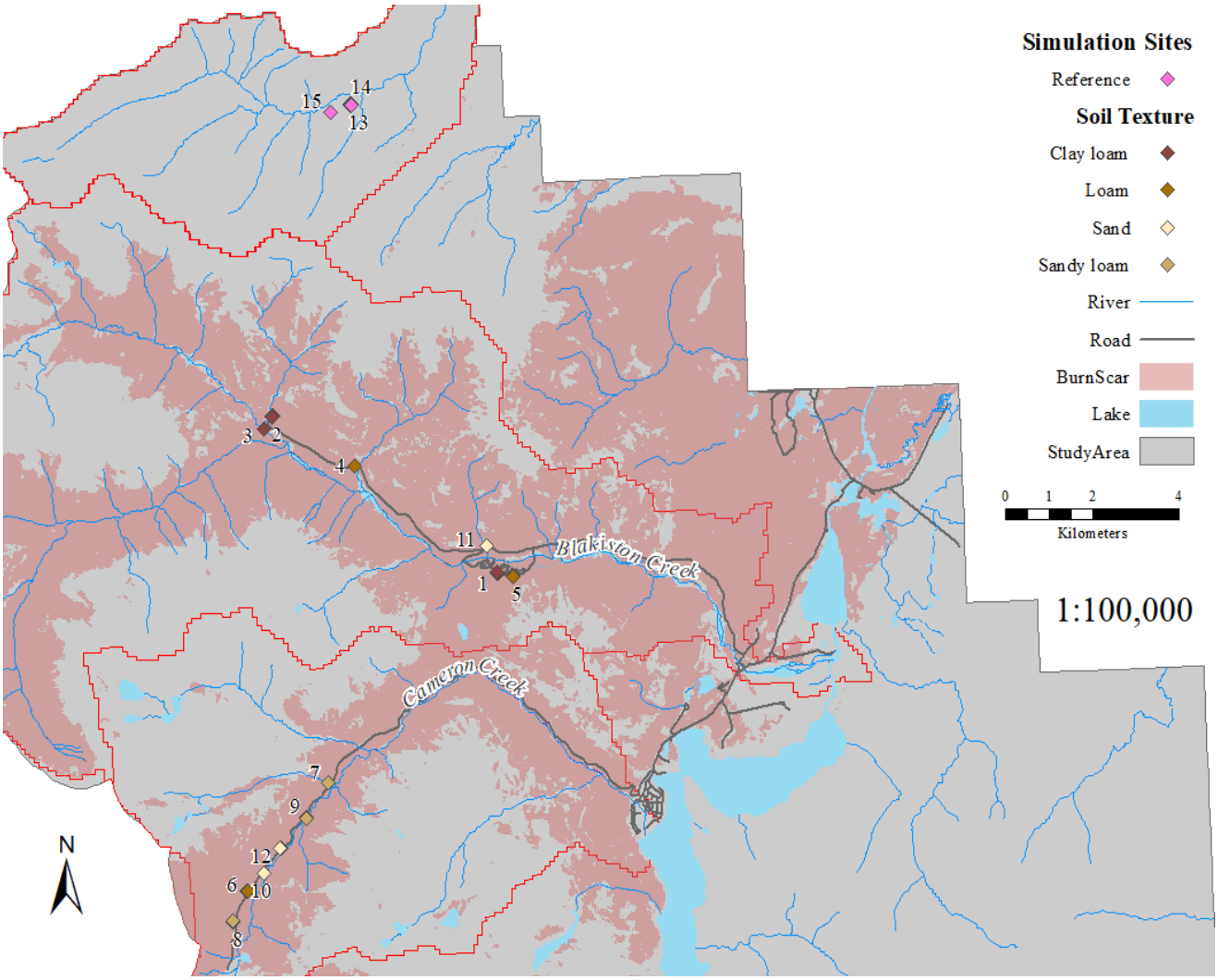


*Figure 2.4: Rainfall simulation locations in the study catchments.*


*Figure 2.5: Impacted forest from the wildfire (A). Emerging vegetation (B). Sparce vegetation (C). Mix of sparce and emerging vegetation (D).*

*Figure 2.6: Rainfall simulator setup and design with windscreen at Site 10a.*

*Figure 2.7: Rainfall simulation plot frame and sample collection setup with emerging vegetation at Site 5b.*

# Chapter 3 : Results

The results of the rainfall simulation and erosion modelling are presented in this Chapter. The first section introduces the data summarized from the rainfall simulations in conjunction with the laboratory analysis while the second section presents the data from the GIS analysis.

## 3.1 Field and Laboratory Experiments

### *3.1.1 Runoff Rates*

Runoff rates measured during rainfall erosion experiments are presented for each soil texture in Table 3.1. Variation in runoff rates within and between the soil textures are illustrated in Figure 3.1. Runoff rates were significantly different for each soil texture (ANOVA, $p = 0.001$) and these were based on significant differences between clay loam and reference (adjusted $p = 0.007$), clay loam and loam (adjusted $p = 0.041$), as well as clay loam and sand (adjusted $p = 0.001$) after performing the Tukey HSD tests (Figure 3.1).

Runoff rates for clay loam soils were relatively similar for each site (Figure 3.2). Clay loam sites had a mean runoff rate of 4.16 mm $hr^{-1}$. The mean runoff rate for site 1, 2, and 3 was 2.99 mm $hr^{-1}$, 4.99 mm $hr^{-1}$, and 4.49 mm $hr^{-1}$, respectively. The runoff characteristics from all sites on the clay loam plots varied over time. In one case the rising limb and peak of the hydrograph increased rapidly then slowly receded compared to the other two replicates as shown in Figure 3.2. For example, runoff rates from site 1a were comparatively lower than site 3a.

The runoff pattern from loam soils varied among sites and had a mean runoff rate of 1.25 mm $hr^{-1}$ (Figure 3.3). Site 4 had the lowest runoff rate for loam with a mean runoff rate of 0.02 mm $hr^{-1}$. Site 5 had the highest mean runoff rate of 2.55 mm $hr^{-1}$. The mean runoff rate for site 6 was 1.14 mm $hr^{-1}$. Due to a mechanical error in the rainfall simulator controls, the rainfall intensity for the experiment at site 6a was higher by a factor of 1.6. Accordingly, data from this experiment were excluded from the statistical analysis to evaluate the effect of soil texture on runoff rates where rainfall intensity was controlled.

Sandy loam soils had a mean runoff rate of 2.00 mm $hr^{-1}$ and the data for this soil texture are presented in Figure 3.4. The mean runoff rate at site 7 was 2.45 mm $hr^{-1}$. Site 8 had the lowest runoff rates among the sandy loam sites, with a mean of 0.45 mm $hr^{-1}$ while site 9 had a mean runoff rate of 3.10 mm $hr^{-1}$. Compared to the two other plots site 7a had a much greater runoff rate. Site 8 was the only sandy loam sites where experiments were run longer than 20 minutes. All three plots at site 9 were different with 9a having a steady increase in runoff rate while, 9b had a lower and steadier runoff rate. At site 9c runoff peaked early in the simulation then steadily declined before plateauing towards the end of the experiment.

The runoff rates from sand soils were the lowest among soil texture categories in the burned basins, with a mean runoff rate of 0.13 mm $hr^{-1}$ (Figure 3.5). The mean runoff rate for site 10 was 0.19 mm $hr^{-1}$. Site 11 had low runoff rates with a mean runoff rate of 0.003 mm $hr^{-1}$. The pattern of runoff rates for site 12 plots varied quite a bit from each other, and the mean was 0.19 mm $hr^{-1}$. For all sites with sand texture runoff experiments were extended to 40-minute simulations with only a few plots remaining in the desired 20-minute length.

Runoff rates at the reference sites were low, averaging 0.27 mm $hr^{-1}$ (Figure 3.6). For the exposed plots (vegetation removed), the runoff rate was 0.47 mm $hr^{-1}$ and the undisturbed was 0.11 mm $hr^{-1}$. The mean runoff rate for site 13 was 0.27 mm $hr^{-1}$. Site 14 had a mean runoff rate was 0.47 mm $hr^{-1}$. The mean runoff rate for site 15 was 0.06 mm $hr^{-1}$ while, site 15 was different from both sites 13 and 14. At these sites 15 the experiments were conducted for 40-minutes, and the disturbed plot (15a) did not produce any runoff.

*3.1.2 Sediment Yield*

Sediment yield determined from laboratory analysis is presented in Table 3.1. Variation in sediment yields within and between soil textures are illustrated in Figure 3.7. While there was no significant difference in sediment yield ($p$ = 0.065), the data show that there was a significant difference in sediment yield between clay loam and sand (adjusted $p$ = 0.045) using the Tukey HSD test (Figure 3.7).

Clay loam had a mean sediment yield of 28.77 g $m^{-2}$ $hr^{-1}$ and was the highest among the soil texture categories (Figure 3.8). The mean sediment yield at sites 1, 2, and 3 was 14.16 g $m^{-2}$ $hr^{-1}$, 55.70 g $m^{-2}$ $hr^{-1}$ and 16.44 g $m^{-2}$ $hr^{-1}$, respectively. The sediment yield patterns were different from the runoff rate patterns as there was much more variability between the plots within the sites. For example, sediment yields from site 1a were comparatively lower than site 1c. However, site 3 had little variability amongst the plots and had much lower sediment yields to the runoff rates, comparatively to the clay loam sites.

The sediment yields for loam varied considerably across sites and the mean was 7.35 g $m^{-2}$ $hr^{-1}$ (Figure 3.9). Site 4 had low sediment yields with a mean of 0.13 g $m^{-2}$ $hr^{-1}$. Site 4b did not produce any sediment yield from the two 20-minute experiments. Site 5 had a mean sediment yield of 16.55 g $m^{-2}$ $hr^{-1}$. The mean sediment yield for site 6 was 4.40 g $m^{-2}$ $hr^{-1}$. The sediment yield patterns of the loam sites follow a similar pattern of their respective runoff rates. Again, due to a mechanical error in the rainfall simulator controls, the rainfall intensity for the experiment at site 6a was higher by a factor of 1.6. Accordingly, data from this experiment were excluded from the statistical analysis to evaluate the effect of soil texture on sediment yield where rainfall intensity was controlled.

Sediment yields for sandy loam had a mean sediment yield of 6.89 g $m^{-2}$ $hr^{-1}$ and the data for this soil texture are presented in Figure 3.10. The mean sediment yield for site 7 was 9.22 g $m^{-2}$ $hr^{-1}$. Site 8 had a mean sediment yield of 1.78 g $m^{-2}$ $hr^{-1}$. The mean sediment yield for site 9 was 9.68 g $m^{-2}$ $hr^{-1}$. The patterns of the sediment yield followed the runoff rates, comparable to what occurred for the loam sites. Most plots with the sandy loam soil texture had low sediment yields, except for sites 7a and 9c. These two plots are comparable to the lower sediment yields of clay loam plots.

The sediment yields for sand were the lowest with a mean of 0.38 g $m^{-2}$ $hr^{-1}$ (Figure 3.11). The mean sediment yield for site 10 was 0.58 g $m^{-2}$ $hr^{-1}$. The mean sediment yield at site 11 was also low at 0.34 g $m^{-2}$ $hr^{-1}$. Site 12 had the lowest mean sediment yield of 0.22 g $m^{-2}$ $hr^{-1}$. Like the patterns of the sediment yield for loam, the sandy loam sites followed runoff rates.

Surprisingly, the sediment yields for the disturbed reference sites were quite high compared to most of the burnt soil textures (Figure 3.12), with a mean sediment yield of 14.42 g $m^{-2}$ $hr^{-1}$. The undisturbed mean sediment yield was 1.86 g $m^{-2}$ $hr^{-1}$. The two plots at site 13 had vastly different sediment yields, with 13a having its ground cover removed. Site 13a had quite a high total sediment yield 41.36 g $m^{-2}$ $hr^{-1}$, and 13b had a much lower total sediment yield 5.42 g $m^{-2}$ $hr^{-1}$. Site 14a had its ground cover untouched, which resulted in a negligible total sediment yield. Whereas 14b had the ground cover removed, it was able to produce a total sediment yield of 1.90 g $m^{-2}$ $hr^{-1}$. The mean sediment yield for site 14 was 0.95 g $m^{-2}$ $hr^{-1}$. Sediment yield did not occur at 15a, even with the removal of the ground cover. However, 15b produced a total sediment yield of 0.16 g $m^{-2}$ $hr^{-1}$, while still having an untouched ground cover. The mean sediment yield at site 15 was 0.08 g $m^{-2}$ $hr^{-1}$.

### *3.1.3 Erodibility*

The erodibility estimates were obtained from a rearrangement of RUSLE at the plot scale for each of the dominant soil textures and reference sites. These results are presented in Table 3.1 and the variations of erodibility are illustrated in Figure 3.13. There is a significant difference in erodibility ($p$ = 0.018). The data show that there were significant differences in erodibility between the reference and dominant soil classes of WLNP using the Tukey HSD test (Figure 3.13). The p-adjusted for reference and clay loam was 0.04, for reference and loam was 0.038, for reference and sandy loam was 0.025, and for reference and sand was 0.022.

Erodibility of clay loam sites for Waterton Lakes National Park had a mean erodibility of 0.24 g hr $MJ^{-1}$ $mm^{-1}$. The mean erodibility at site 1 was 0.13 g hr $MJ^{-1}$ $mm^{-1}$. The mean erodibility for site 2 was 0.47 g hr $MJ^{-1}$ $mm^{-1}$. Site 3 had a mean erodibility of 0.12 g hr $MJ^{-1}$ $mm^{-1}$.

The erodibility of loam was the second highest with a mean of 0.14 g hr $MJ^{-1}$ $mm^{-1}$. Site 4 had low erodibility with mean of 0.0012 g hr $MJ^{-1}$ $mm^{-1}$. Site 4b did not have any sediment production

because there was no erodibility for the plot. Site 5 had an erodibility of 0.36 g hr $MJ^{-1}$ $mm^{-1}$. The mean erodibility rate for site 6 was 0.03 g hr $MJ^{-1}$ $mm^{-1}$.

The mean erodibility for sandy loam was 0.06 g hr $MJ^{-1}$ $mm^{-1}$. The mean erodibility for site 7 was 0.05 g hr $MJ^{-1}$ $mm^{-1}$. The mean erodibility for site 8 being 0.009 g hr $MJ^{-1}$ $mm^{-1}$. The mean erodibility for site 9 was 0.05 g hr $MJ^{-1}$ $mm^{-1}$.

Sand soils had a mean erodibility of 0.01 g hr $MJ^{-1}$ $mm^{-1}$ making it the lowest erodibility of the soil textures analysed in this study. The mean erodibility for site 10 was 0.03 g hr $MJ^{-1}$ $mm^{-1}$. The mean erodibility at site 11 was also low at 0.0008 g hr $MJ^{-1}$ $mm^{-1}$. Site 12 had a mean erodibility of 0.002 g hr $MJ^{-1}$ $mm^{-1}$.

The mean erodibility for the uncovered reference plots was 5.30 g hr $MJ^{-1}$ $mm^{-1}$, which was the highest for all rainfall simulation sites, and the mean erodibility for the undisturbed reference plots was 0.73 g hr $MJ^{-1}$ $mm^{-1}$. With the removal of the ground cover at 13a the erodibility was quite high at 12.17 g hr $MJ^{-1}$ mm-1. Site 13b had a much lower erodibility with 2.14 g hr $MJ^{-1}$ $mm^{-1}$. Site 14a had an erodibility of 0.002 of g hr $MJ^{-1}$ $mm^{-1}$ with an untouched ground cover. The mean erodibility for site 14 was 1.86 g hr $MJ^{-1}$ $mm^{-1}$. Whereas 14b produced an erodibility of 3.72 g hr $MJ^{-1}$ $mm^{-1}$ with the removal of the ground cover. As mentioned, there was no erodibility at 15a, even with the removal of the ground cover. At 15b the erodibility was 0.05 g hr $MJ^{-1}$ $mm^{-1}$, with an untouched ground cover. The mean erodibility at site 15 was 0.03 g hr $MJ^{-1}$ $mm^{-1}$.

## 3.2 Modelling

### *3.2.1 Modelling Sediment Erosion using RUSLE*

Estimates of annual sediment yield at the plot scale for each of the dominant soil textures and reference sites are presented in Table 3.2 and the variations of RUSLE are illustrated in Figure 3.14. There is a significant difference in erodibility ($p$ = 0.046). The data show that there was a significant difference in erodibility between clay loam and sand (adjusted $p$ = 0.03) using the Tukey HSD test (Figure 3.14). Table 3.3 shows the mean values of the RUSLE factors for each site, excluding the R- and P- factors because they were constant values.

Annual sediment yield ranged from 0.00 to 3.89 t $ha^{-1}$ $yr^{-1}$. The mean sediment yield for clay loam is 0.95 t $ha^{-1}$ $yr^{-1}$. Loam had a mean annual sediment yield of 0.29 t $ha^{-1}$ $yr^{-1}$. The mean annual sediment yield for sandy loam was 0.26 t $ha^{-1}$ $yr^{-1}$ and for sand was 0.03 t $ha^{-1}$ $yr^{-1}$. For the reference sites the mean annual sediment yield was 0.25 t $ha^{-1}$ $yr^{-1}$. The most notable mean values for the burnt sites were site 6 with a mean annual sediment yield of 1.999 t $ha^{-1}$ $yr^{-1}$. For the RUSLE modelling site 6a was included in the analysis because the rainfall erosivity factor was made constant across all plots. Although, the erodibility was still derived from its original rainfall intensity producing a higher sediment yield. Conversely to this site, site 4 had a mean annual

sediment yield of 0.005 t $ha^{-1}$ $yr^{-1}$. Interestingly, sites 6 and 4 both were classified as having a loam soil texture. The notable mean values for the reference sites were site 13 with a sediment yield of 0.652 t $ha^{-1}$ $yr^{-1}$ and site 15 with a sediment yield of 0.004 t $ha^{-1}$ $yr^{-1}$.

The results for erodibility ranged from 0.00 to 0.01 t hr $MJ^{-1}$ $mm^{-1}$ for the burnt sites with a mean of 0.001 t hr $MJ^{-1}$ $mm^{-1}$. The erodibility for the reference sites ranged from 0.00 to 0.12 t hr $MJ^{-1}$ $mm^{-1}$ with a mean of 0.0302 t hr $MJ^{-1}$ $mm^{-1}$. The mean erodibility of clay loam from RUSLE is 0.0024 t hr $MJ^{-1}$ $mm^{-1}$. For loam the mean erodibility was 0.0014 t hr $MJ^{-1}$ $mm^{-1}$. Sandy loam had a mean erodibility of 0.0005 t hr $MJ^{-1}$ $mm^{-1}$. The mean erodibility of sand was 0.0001 t hr $MJ^{-1}$ $mm^{-1}$.

The results for the LS-factor ranged from 1.68 to 20.86 across all sites at the plot scale. Site 1 had a mean of 9.95. The mean for site 2 was 7.56. The LS-factor mean at site 3 was 8.77. Site 4 had a mean LS-factor of 7.22. The mean for site 5 was 5.62. For site 6 the mean was 4.72. The mean for site 7 was 9.63. Site 8 had a LS-factor mean of 6.36. The mean for site 9 was 7.88. The LS-factor mean for site 10 was 1.74. For site 11 the mean was 14.58. The mean LS-factor at site 12 was 7.37. The mean for site 13 was 15.76. The mean for site 14 was 11.36. Finally, the mean for site 15 was 10.61.

While the C-factor was derived from Remote Sensing and GIS analysis it was used for the plot scale estimations as well. The results for the C-factor ranged from 0.10 to 0.49 across all sites. Site 1 had a mean of 0.17. The mean for site 2 was 0.18. The mean for site 3 was 0.17. The mean C-factor for site 4 was 0.18. Site 5 had a mean of 0.15. For site 6 the mean C-factor was 0.44 The mean for site 7 was 0.21. The C-factor mean for site 8 was 0.29. Site 9 had a mean of 0.16. The mean for site 10 was 0.32. For site 11 the mean was 0.23. Finally, site 12 had a mean C-factor value of 0.37.

### *3.2.2 GIS Analysis*

The RUSLE factors that were upscaled for use with GIS were the K- and LS-factors. The R- and P-factor had constant values of 337.53 and 1, respectively. The C-factor values were already established for the watershed scale since they were derived from satellite imagery that covered the study area and downscaled for the plot scale analysis of RUSLE.

The K-factor had only three values present at the watershed scale as result of little data availability for soil texture of the Park at this scale. Figure 3.15 shows that the distribution of the three values, which were 0, 0.0007, and 0.0019 t hr $MJ^{-1}$ $mm^{-1}$, throughout Blakiston Creek and Cameron Creek watersheds. The higher erodible material is for the most part on the steeper slopes, with some of it being on gentler slopes. Most of the erodible material is along the two main tributaries. The less erodible material is generally on the shallower slopes where material has a higher erodibility threshold. Additionally, some of the channels feeding into Blakiston and Cameron Creek are on

steep, bare rock slopes that generally does not have immediate erodible material around them until they approach the channels they are feeding.

The LS-factor ranged from 0 to 6018.56 with a mean of 3.82 and a standard deviation of 22.00 (Figure 3.16). Steep slopes caused visually unnatural flow paths with high LS values, even with the removal of extremely steep slopes. However, there are visually natural looking flow paths with high LS values that lead to channels. Blakiston Creek has lower LS-factor values close to and on the floodplain portion of the valley. The small channel incisions of the channels flowing into Blakiston have higher LS values on their valley walls compared to the floodplain values. Cameron Creek has mid to low LS-factor values within proximity of the river. The lower values tend to be on the western side of Cameron Creek on the west side of the road, and surrounding Cameron Lake. Additionally, there were some LS-values from the surface water of the lakes, as the DEM captured the parts of the lakes, but those values were low

The C-factor ranged from 0 to 1 with a mean of 0.36 and a standard deviation of 0.23 (Figure 3.17). Lower values of C represent areas with more vegetation, conversely higher values represent areas with less vegetation. The lower values of C were mostly at the lower reaches of the two valleys, particularly in the meadow areas of Blakiston Creek and near the stream banks of Cameron Creek. The lowest values were areas that had minimal or no impact from the Kenow Fire. The highest values were generally areas that consisted of bare rock near the mountain peaks. The higher values were on steep slopes and areas that had little vegetation regrowth following the fire.

The sediment erosion and deposition map (Figure 3.18) shows the severity of areas where soil is more erodible or areas of deposition. Negative values represent erosion where positive values represent deposition. Based on the data available and the methods used values fell in the range of -160.60 to 153.39 t $ha^{-1}$ $yr^{-1}$. The mean value is -0.99 t $ha^{-1}$ $yr^{-1}$ indicating more erosion than deposition and the standard deviation is 1.49. The south-facing slopes of the two valleys experienced greater erosion rates compared to any other direction. Conversely, the north-facing slopes had more deposition than any other direction.

### 3.3 Tables and Figures

*Table 3.1: Summary of rainfall simulation experiments. Site 6a was removed from loam for this analysis because it was out of the controlled rainfall intensity.*

| | Soil Texture | | | | | | | | | | | | | | | | | |
|---|---|---|---|---|---|---|---|---|---|---|---|---|---|---|---|---|---|---|
| | Reference (natural) | | | Reference (disturbed) | | | Clay Loam | | | Loam* | | | Sandy Loam | | | Sand | | |
| | Mean | Std.dev. | N | Mean | Std.dev. | N | Mean | Std.dev. | N | Mean | Std.dev. | N | Mean | Std.dev. | N | Mean | Std.dev. | N |
| Runoff Rate ($mm\ hr^{-1}$) | 0.11 | 0.00 | 3 | 0.42 | 0.41 | 3 | 4.16 | 2.77 | 9 | 1.25 | 1.88 | 8 | 2.00 | 2.75 | 9 | 0.13 | 0.16 | 9 |
| Sediment Yield ($g\ m^{-2}\ hr^{-1}$) | 1.86 | 3.08 | 3 | 14.42 | 23.35 | 3 | 28.76 | 39.17 | 9 | 7.35 | 11.87 | 8 | 6.90 | 9.54 | 9 | 0.39 | 0.51 | 9 |
| Erodibility ($g\ hr\ MJ^{-1}\ mm^{-1}$) | 0.73 | 1.22 | 3 | 5.30 | 6.23 | 3 | 0.24 | 0.33 | 9 | 0.14 | 0.30 | 8 | 0.06 | 0.09 | 9 | 0.01 | 0.03 | 9 |
| Slope (%) | 32.87 | 2.50 | 3 | 20.60 | 8.35 | 3 | 22.32 | 3.60 | 9 | 17.88 | 5.17 | 8 | 20.99 | 3.76 | 9 | 19.49 | 10.26 | 9 |

*Table 3.2: Estimations of RUSLE parameters at the plot scale. Site 6a was removed from loam for this analysis because it was out of the controlled rainfall intensity.*

| | Reference | | | | | | Soil Texture | | | | | | | | | | | |
|---|---|---|---|---|---|---|---|---|---|---|---|---|---|---|---|---|---|---|
| | Vegetation | | | Without Vegetation | | | Clay Loam | | | Loam* | | | Sandy Loam | | | Sand | | |
| | Mean | Std.dev. | N | Mean | Std.dev. | N | Mean | Std.dev. | N | Mean | Std.dev. | N | Mean | Std.dev. | N | Mean | Std.dev. | N |
| A-Factor (t $ha^{-1}$ $yr^{-1}$) | 0.094 | 0.156 | 3 | 0.415 | 0.543 | 3 | 0.950 | 1.188 | 9 | 0.278 | 0.447 | 8 | 0.261 | 0.364 | 9 | 0.025 | 0.037 | 9 |
| R-Factor (MJ mm $hr^{-1}$ $yr^{-1}$) | 337.53 | 0.00 | 3 | 337.53 | 0.00 | 3 | 337.53 | 0.00 | 9 | 337.53 | 0.00 | 8 | 337.53 | 0.00 | 9 | 337.53 | 0.00 | 9 |
| K-Factor (t hr $MJ^{-1}$ $mm^{-1}$) | 0.0073 | 0.0121 | 3 | 0.0530 | 0.0624 | 3 | 0.0024 | 0.0033 | 9 | 0.0014 | 0.0029 | 8 | 0.0005 | 0.0009 | 9 | 0.0001 | 0.0003 | 9 |
| LS-Factor | 13.69 | 4.92 | 3 | 13.41 | 9.15 | 3 | 8.76 | 2.36 | 9 | 5.99 | 2.97 | 8 | 7.96 | 2.24 | 9 | 7.90 | 6.91 | 9 |
| C-factor | 0.002 | 0.000 | 3 | 0.002 | 0.000 | 3 | 0.17 | 0.04 | 9 | 0.23 | 0.13 | 8 | 0.22 | 0.06 | 9 | 0.31 | 0.09 | 9 |

*Table 3.3: Mean RUSLE factor values for each experiment site at the plot scale. The R- and P-factors were excluded because they were set as constants for each site.*

| Site | Soil Texture | n | Annual Soil Loss ($t\ ha^{-1}\ yr^{-1}$) | Soil Erodibility ($t\ hr\ MJ^{-1}\ mm^{-1}$) | LS-Factor | C-Factor |
|---|---|---|---|---|---|---|
| 1 | Clay Loam | 3 | 0.533 | 0.00127 | 9.95 | 0.17 |
| 2 | Clay Loam | 3 | 1.693 | 0.00466 | 7.56 | 0.18 |
| 3 | Clay Loam | 3 | 0.625 | 0.00118 | 8.77 | 0.17 |
| 4 | Loam | 3 | 0.005 | 0.00001 | 7.22 | 0.18 |
| 5 | Loam | 3 | 0.625 | 0.00362 | 5.62 | 0.15 |
| 6 | Loam | 3 | 1.999 | 0.00156 | 6.03 | 0.45 |
| 7 | Sandy Loam | 3 | 0.351 | 0.00055 | 9.63 | 0.21 |
| 8 | Sandy Loam | 3 | 0.067 | 0.00009 | 6.36 | 0.29 |
| 9 | Sandy Loam | 3 | 0.365 | 0.00100 | 7.88 | 0.16 |
| 10 | Sand | 3 | 0.046 | 0.00032 | 1.74 | 0.32 |
| 11 | Sand | 3 | 0.013 | 0.00001 | 14.58 | 0.23 |
| 12 | Sand | 3 | 0.015 | 0.00002 | 7.37 | 0.37 |
| 13 | Reference | 2 | 0.652 | 0.07155 | 15.76 | 0.002 |
| 14 | Reference | 2 | 0.108 | 0.01862 | 11.36 | 0.002 |
| 15 | Reference | 2 | 0.004 | 0.00030 | 10.61 | 0.002 |

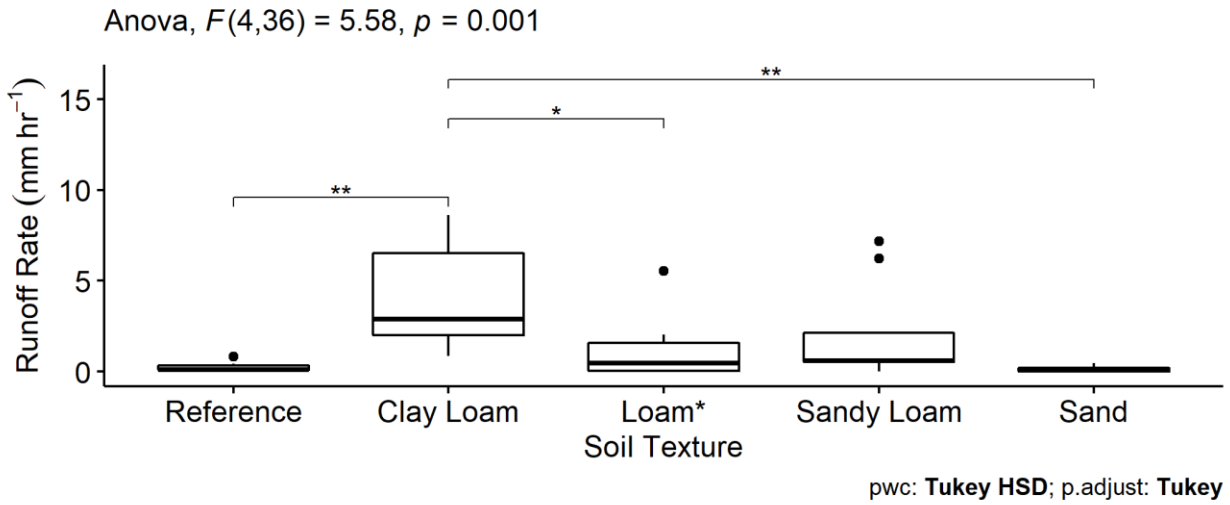


*Figure 3.1: Runoff rate (mm hr$^{-1}$) as a function of soil texture with ANOVA and pairwise comparison results. *Site 6a was removed from loam for this analysis because it was out of the controlled rainfall intensity.*

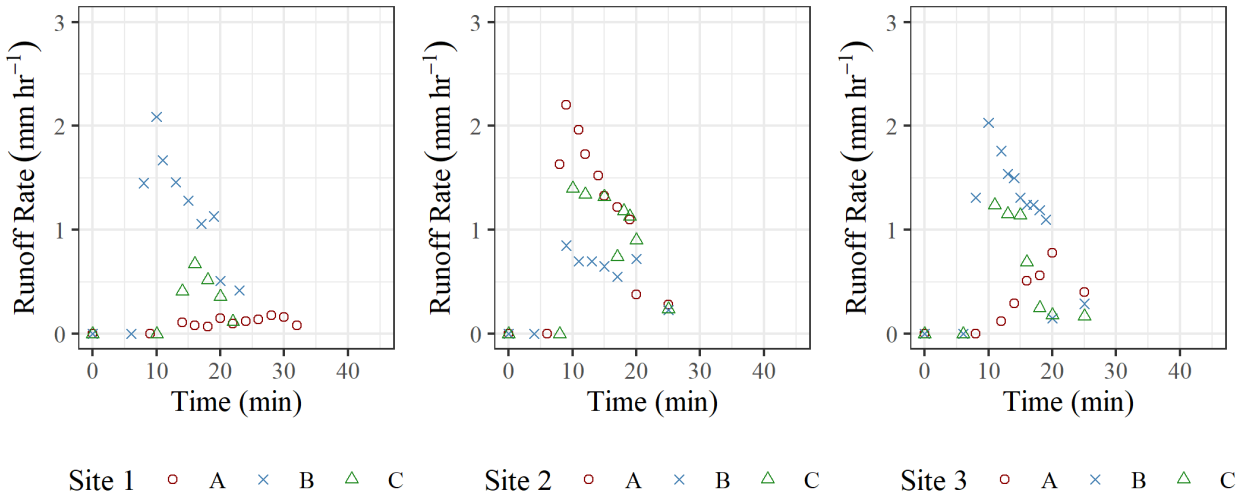


*Figure 3.2: Runoff rates for clay loam sites (mm hr$^{-1}$).*

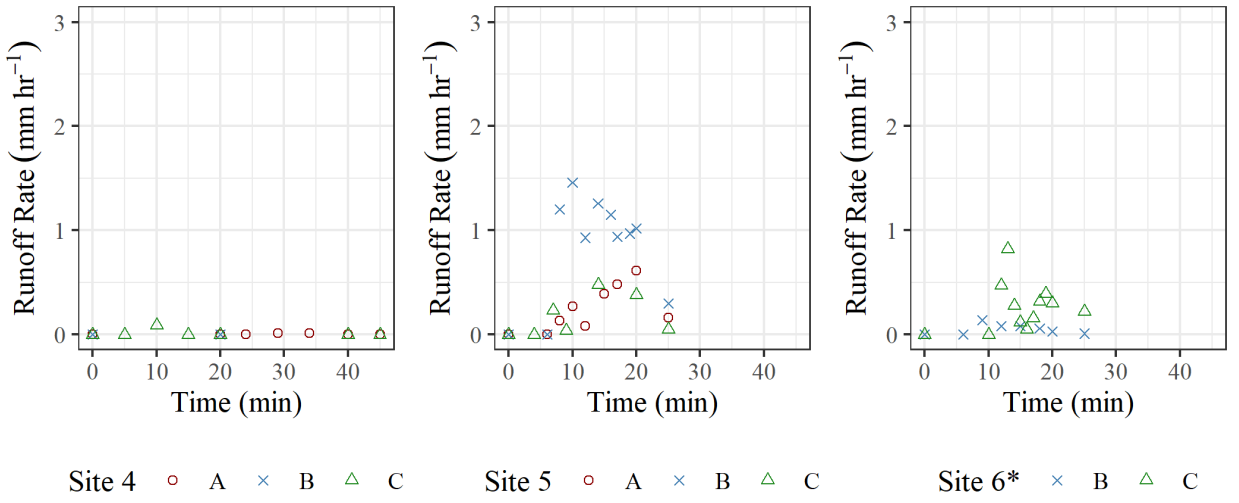


*Figure 3.3: Runoff rates for loam sites (mm hr$^{-1}$). Site 6a was removed for this analysis because it was out of the controlled rainfall intensity.*

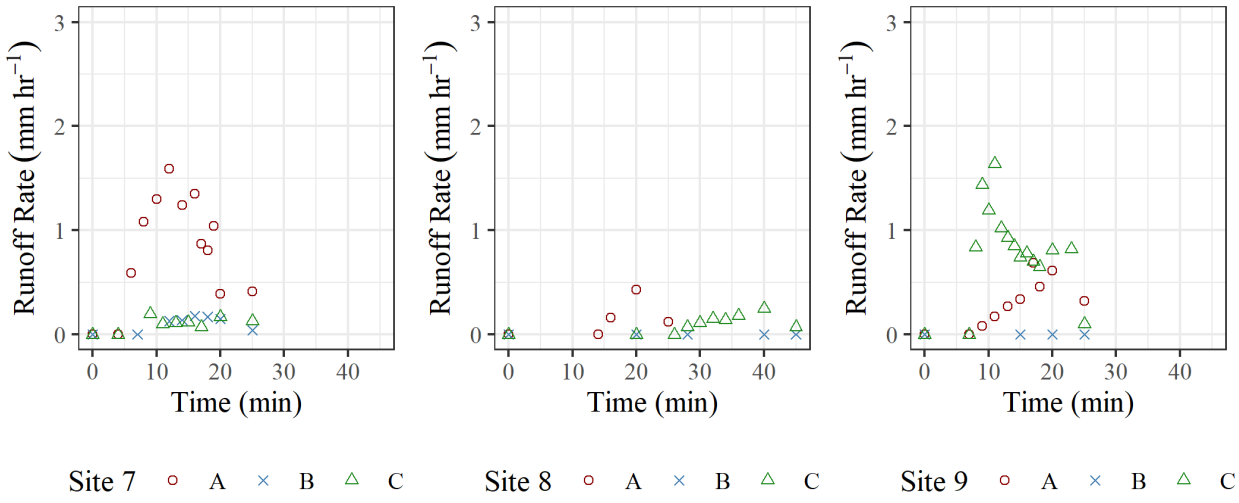


*Figure 3.4: Runoff rates for sandy loam sites (mm hr$^{-1}$).*

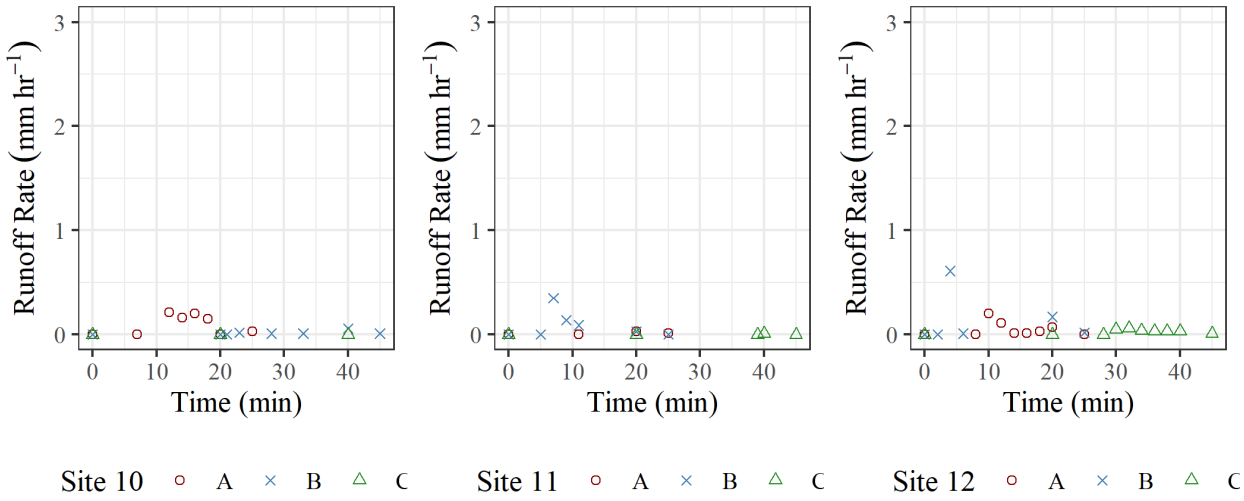


*Figure 3.5: Runoff rates for sand sites (mm hr$^{-1}$).*

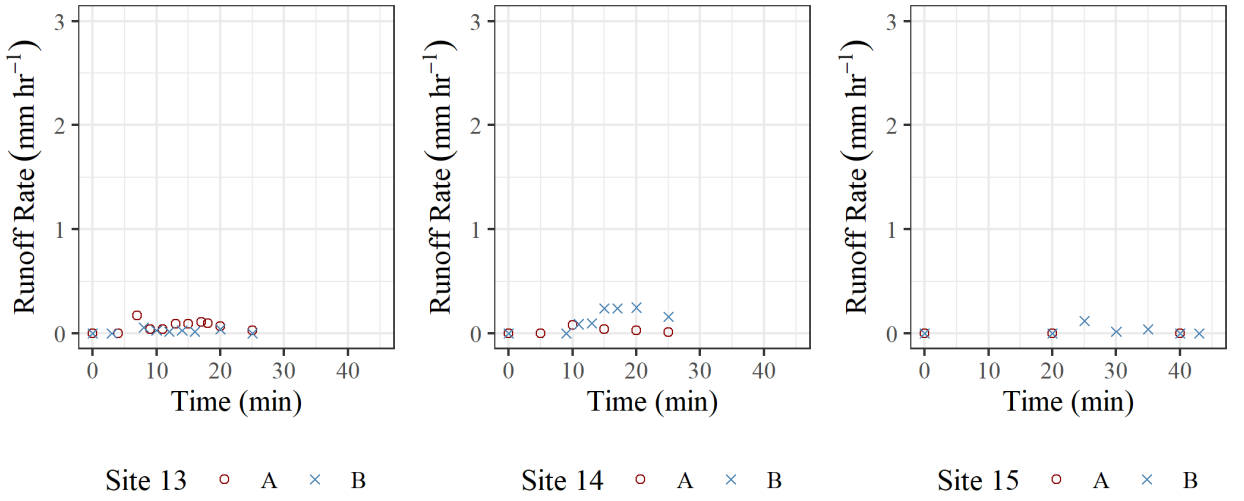


*Figure 3.6: Runoff rates for reference sites (mm hr$^{-1}$).*

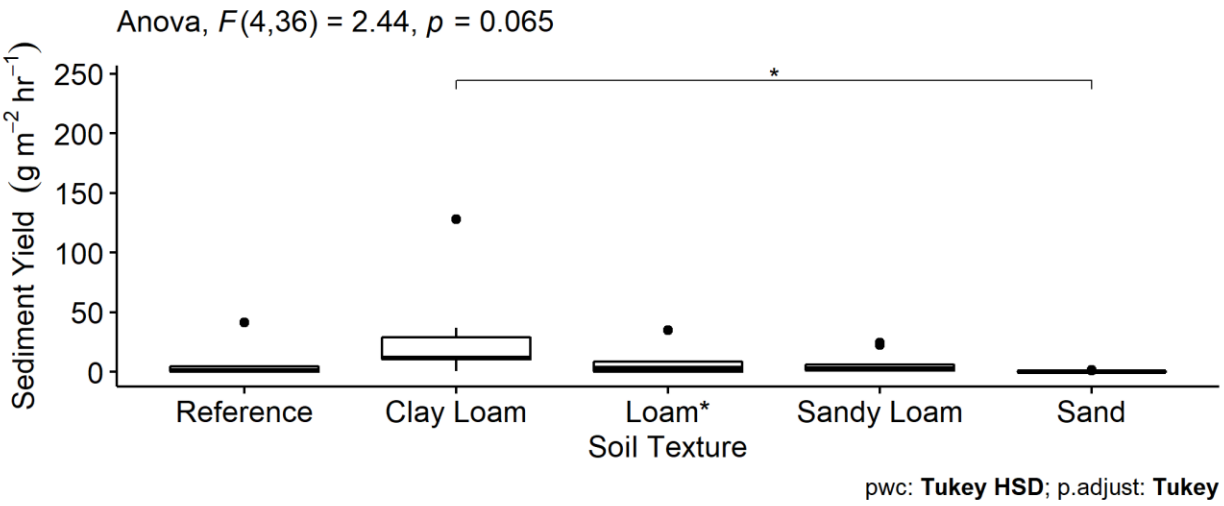


*Figure 3.7: Sediment yield (g m $^{-2}$ hr$^{-1}$) as a function of soil texture with ANOVA and pairwise comparison results. *Site 6a was removed from loam for this analysis because it was out of the controlled rainfall intensity.*

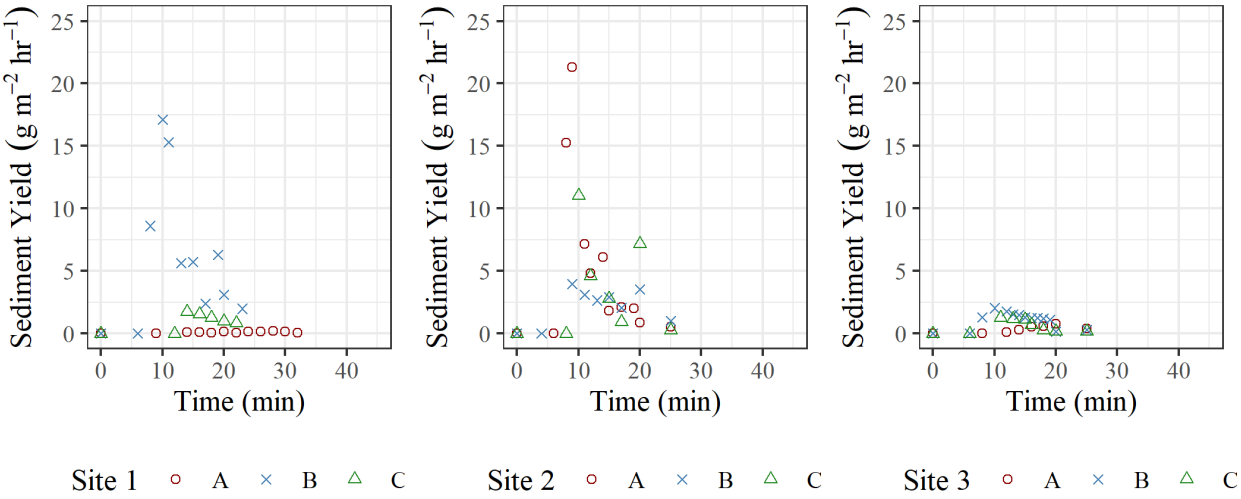


*Figure 3.8: Sediment yield for clay loam sites (g m $^{-2}$ hr$^{-1}$).*

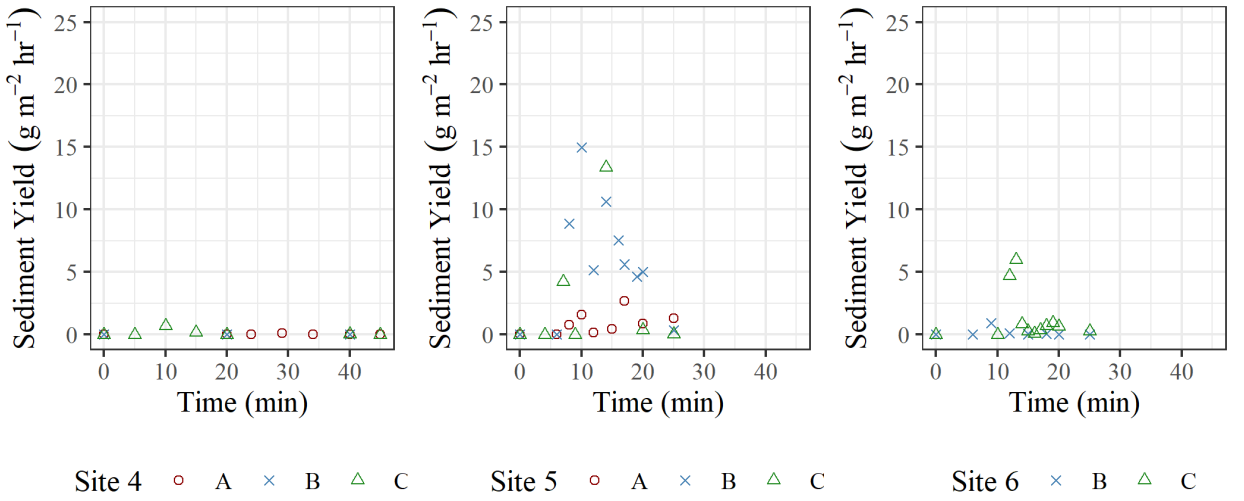


*Figure 3.9: Sediment yield for loam sites (g m $^{-2}$ hr$^{-1}$). Site 6a was removed for this analysis because it was out of the controlled rainfall intensity.*

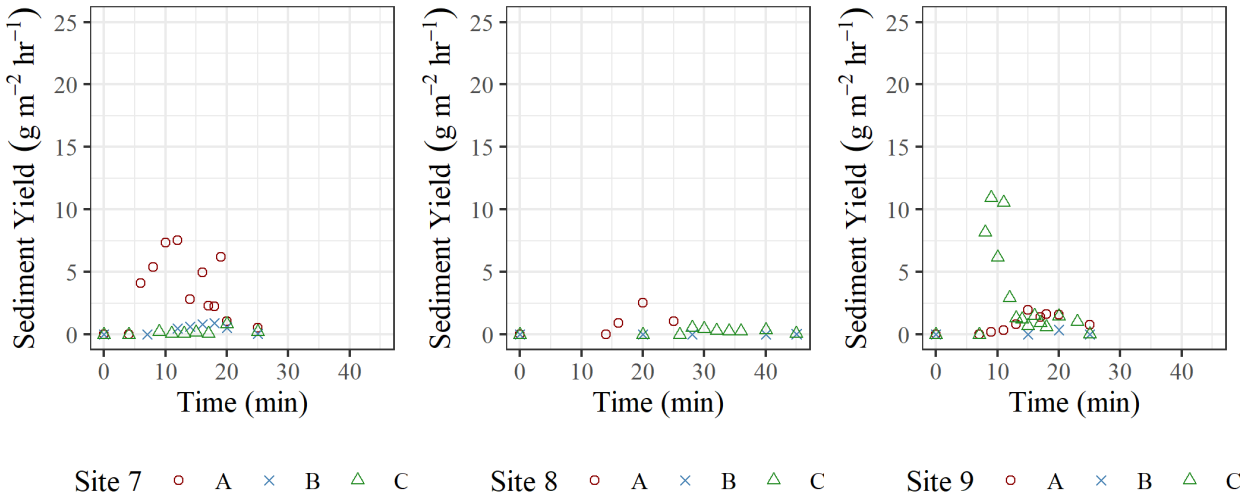


*Figure 3.10: Sediment yield for sandy loam sites (g m $^{-2}$ hr$^{-1}$).*

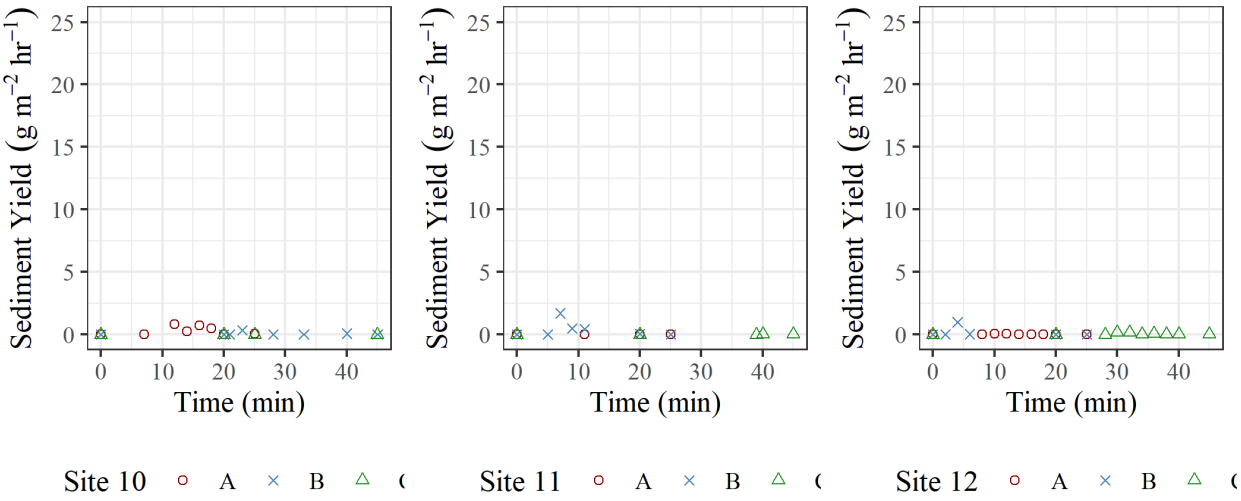


*Figure 3.11: Sediment yield for sand sites (g m $^{-2}$ hr$^{-1}$).*

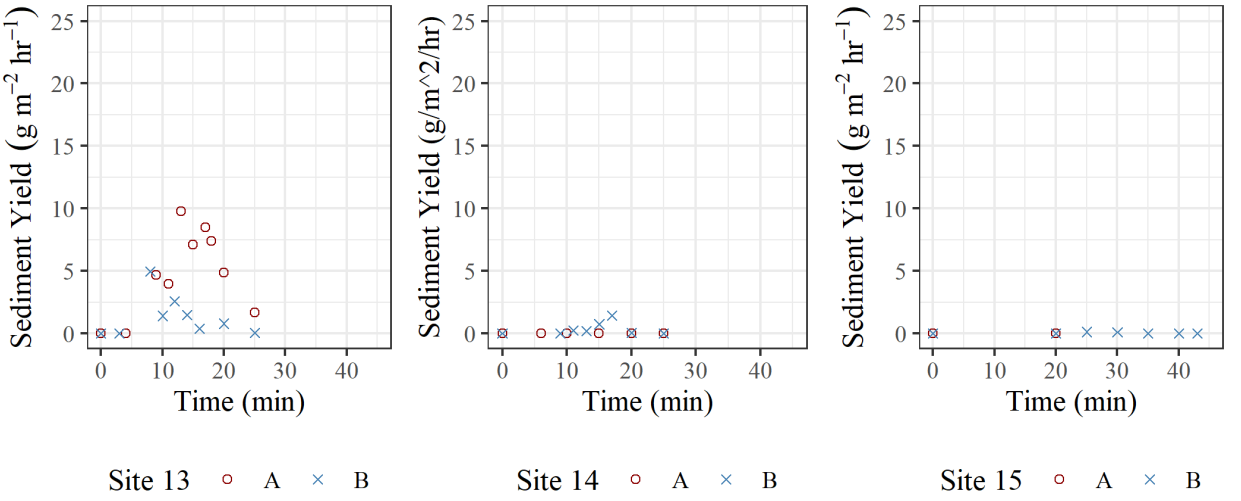


*Figure 3.12: Sediment yield for reference sites (g m $^{-2}$ hr$^{-1}$).*

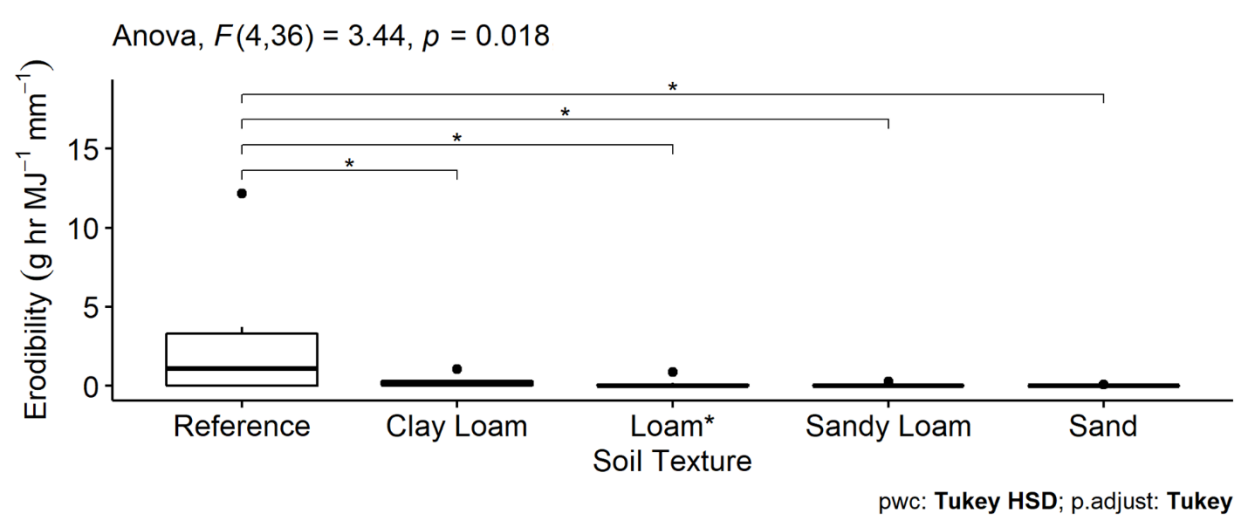


*Figure 3.13: Erodibility (g hr $MJ^{-1}$ $mm^{-1}$) as a function of soil texture with ANOVA and pairwise comparison results. *Site 6a was removed from loam for this analysis because it was out of the controlled rainfall intensity.*

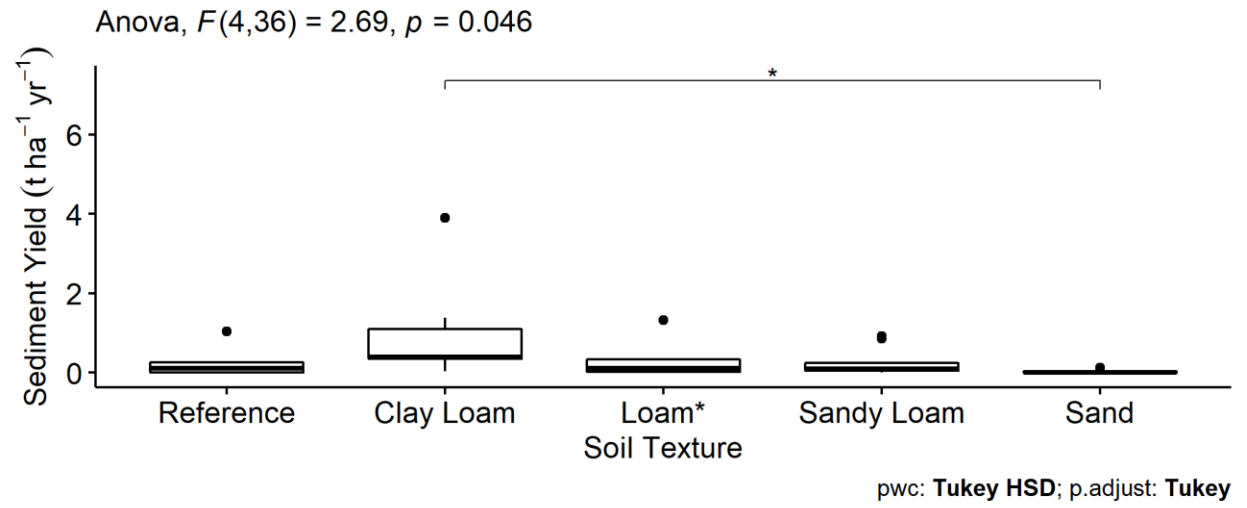


*Figure 3.14: Sediment yield (t $ha^{-1}$ $yr^{-1}$) as a function of soil texture with ANOVA and pairwise comparison results. *Site 6a was removed from loam for this analysis because it was out of the controlled rainfall intensity.*

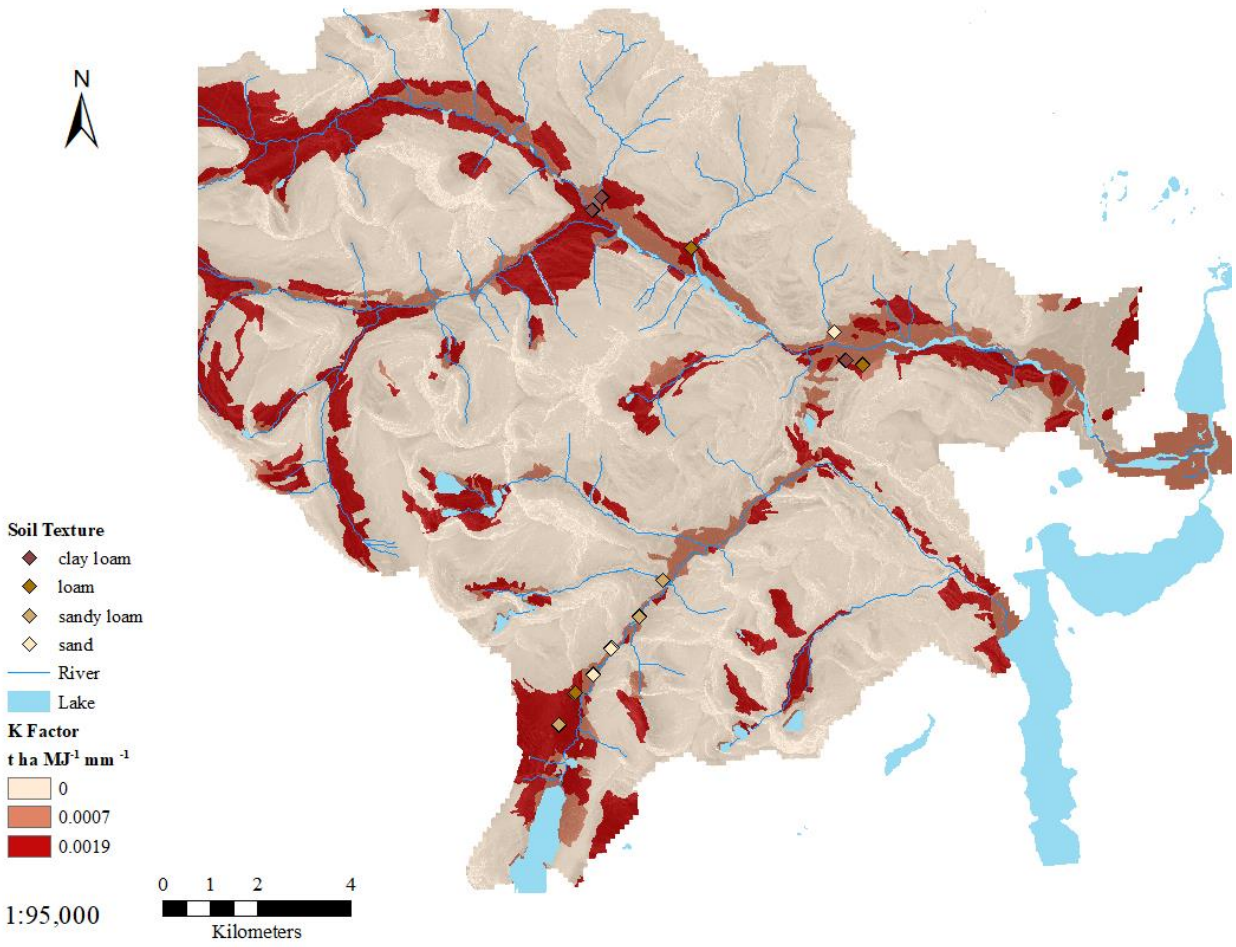


*Figure 3.15: K-factor distribution for Blakiston Creek and Cameron Creek watersheds.*

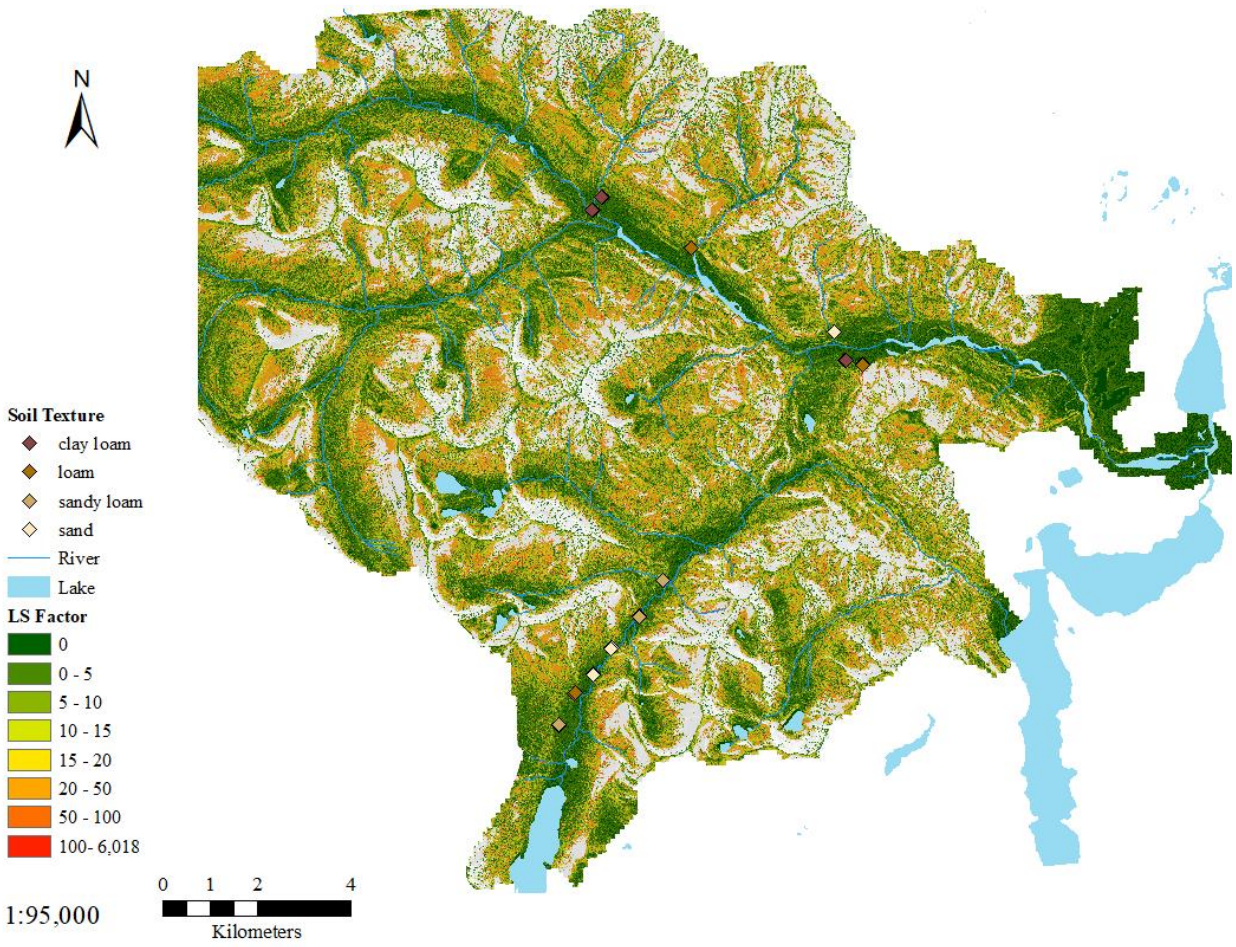


*Figure 3.16: LS-factor values for Blakiston Creek and Cameron Creek watersheds.*

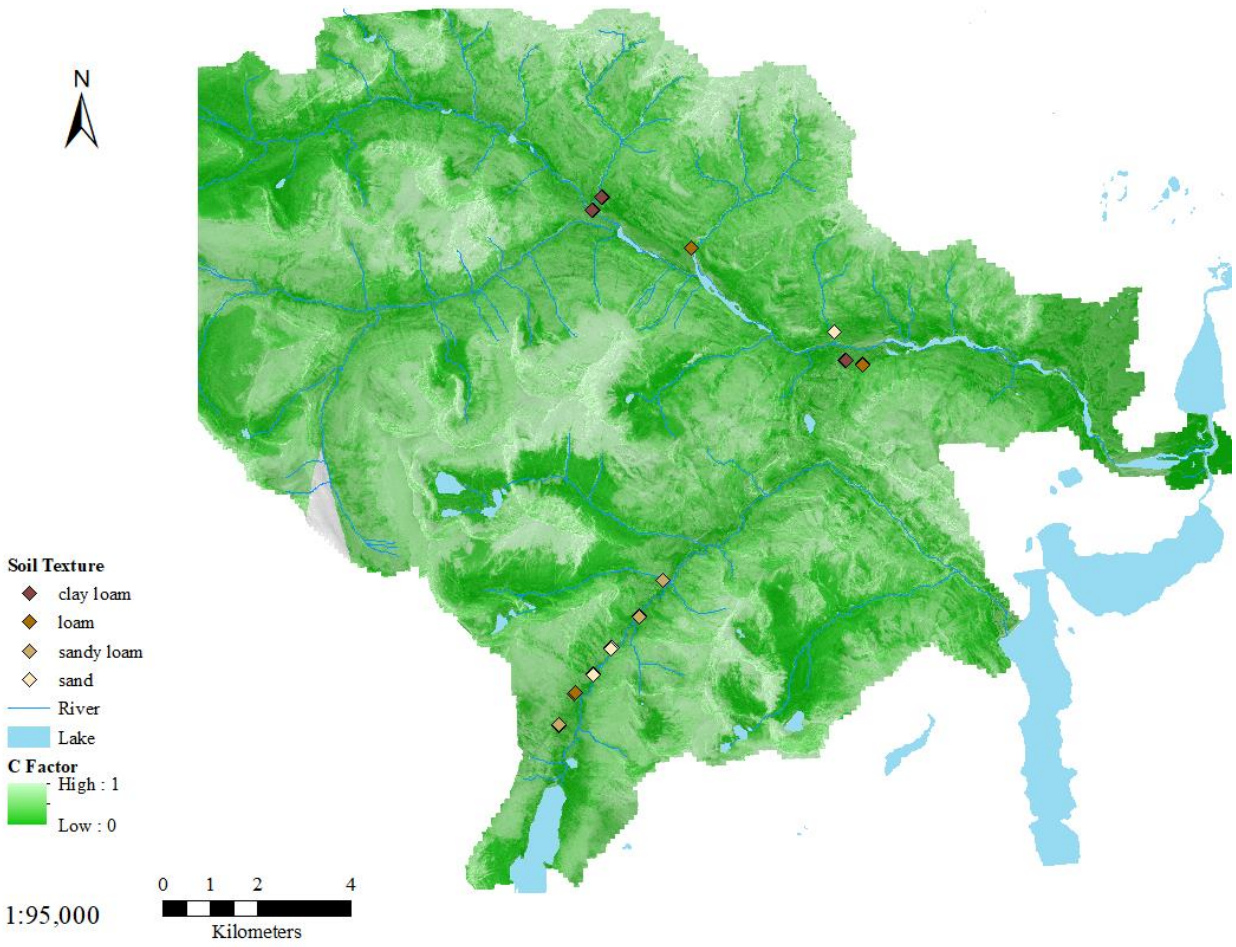


*Figure 3.17: Distribution of C-factor values for Blakiston Creek and Cameron Creek watersheds.*

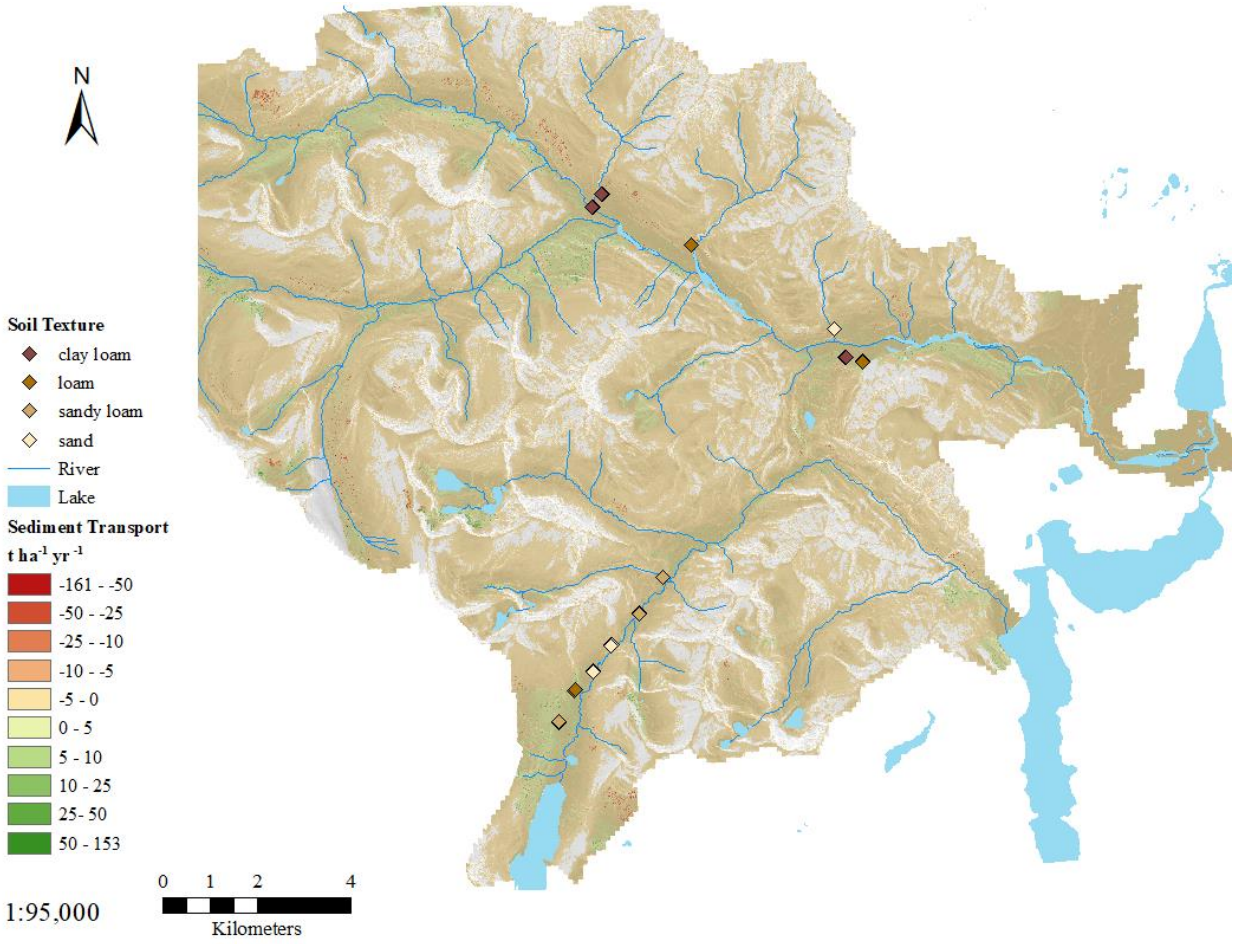


*Figure 3.18: Distribution of erosion and deposition severity throughout Blakiston Creek and Cameron Creek watersheds. Negative values represent sediment erosion and positive values represent sediment deposition.*

# Chapter 4 : Discussion

## 4.1 Introduction

Post-wildfire sediment erosion has been studied in a wide range of hydro-climatic and physiographic regions globally, including Colorado (Benavides-Solorio and MacDonald, 2001; Larsen and MacDonald, 2007), Nevada (Pierson et al., 2001), Utah (Robichaud et al., 2019), Montana (Woods and Balfour, 2010; Robichaud et al., 2016a; Spigel and Robichaud, 2007), the Mediterranean (Lanorte et al., 2019; Fernández et al., 2010; Fernández and Vega, 2016; Fernández and Vega, 2018; Karamesouti et al., 2016; Hosseini et al., 2003), and Australia (Blake et al., 2020; Sheridan et al., 2007; Feikema et al., 2011). In contrast, very few post-wildfire erosion studies have been conducted in critical forested source water regions of Canada (Robichaud et al., 2013).

The present study is the first to quantify and model post-wildfire hillslope erosion in Waterton Lakes National Park in southwestern Alberta. A rainfall simulator was deployed at the plot scale for a range of soil textures was used in two watersheds (Cameron, Blakiston) to measure soil erosivity, runoff rates, and sediment yield. Data from the field erosion experiments were used as input parameters to a sediment transport model (RUSLE) to produce soil erosion maps for watershed planning and water quality management. Results of the previous chapter are discussed in the following sections (4.2) factors impacting runoff rates, (4.3) factors impacting sediment erosion and (4.4) modelling sediment erosion in Waterton Lakes National Park.

## 4.2 Factors impacting runoff rates in post-wildfire Waterton Lakes National Park (WLNP)

Surface runoff rates in WLNP varied across soil textures on post-wildfire soils during low-intensity rainfall events. These results support the concept that runoff rates increase following a wildfire (Benavides-Solorio and MacDonald, 2001; Spigel and Robichaud, 2007; Woods and Balfour, 2010; Larsen and MacDonald, 2007; Shakesby and Doerr, 2006). However, runoff rates in the present study are lower than previous research by a factor of 10.41. Possible reasons for the observed reduction in runoff rates include lower rainfall intensities, recovery of infiltration capacities, variations in microtopography, changes in ground cover, and spatial variation in soil texture. General trends from hillslope runoff studies show that factors controlling runoff include rainfall intensity (Benavides-Solorio and MacDonald, 2001; Spigel and Robichaud, 2007), infiltration (Larsen and MacDonald, 2007; Woods and Balfour, 2010), microtopography (Puntenney-Desmond et al., 2020; Lui et al., 2019; Jourgholami and Labelle, 2020), ground cover (Hartanto et al., 2002; Zhou et al., 2018; Puntenney-Desmond et al., 2020; Shakesby and Doerr, 2006), and particle size (Woods and Balfour, 2010; Jourgholami and Labelle, 2020), these factors on runoff will be discussed in the following subsections.

### *4.2.1 Implications of rainfall intensity and infiltration on runoff generation*

Soil erosion studies using high-intensity rainfall simulations have been conducted on post-wildfire soils (Benavides-Solorio and MacDonald, 2001; Woods and Balfour, 2010; Robichaud et al., 2016a), harvested soils (Puntenney-Desmond et al., 2020), heavily trafficked soils (Jourgholami and Labelle, 2020; Zemke, 2016) and undisturbed soils (Zhou et al., 2018; Benavides-Solorio and MacDonald, 2001; Puntenney-Desmond et al., 2020). In contrast to the use of high-intensity rainfall simulations, the current study found that simulated low-intensity high-frequency storm events were capable of producing runoff on most experimental plots in a severely burned post-wildfire environment 22 months following a wildfire and on undisturbed soils. Although rainfall intensities in the present study were lower than in previous research, comparable runoff rates were observed in previous studies. One explanation is that the lower rainfall intensities were insufficient to saturate soils and therefore reach infiltration capacity. However, at site 6a, which had the highest rainfall intensity, post-wildfire soils were mobilized and transported more easily. Thus, site 6a shows that higher rainfall intensities reach infiltration capacities quicker, and runoff rates are more notable than at simulations with lower rainfall intensities. Notably, because of a mechanical error in the rainfall simulator controls, the data from site 6a were excluded from the statistical analysis. Furthermore, this result should be taken with caution as this is only one example of high-intensity rainfall in the present study.

Post-wildfire infiltration rates are affected by the ash and subsurface hydrophobic layer after wildfire (Larsen and MacDonald, 2007; Woods and Balfour, 2010). The ash layer saturates from the bottom up and creates unique conditions producing infiltration excess overland flow in shallow depth ash. Furthermore, after ash layer saturation, runoff rates are dependent on rainfall intensity and the infiltration capacity of the underlying soil (Woods and Balfour, 2010). In the present study, some plots were not saturated, and infiltration capacities were not exceeded. This soil moisture condition observation is evident for sites 4 and 11 (Figure 4.1). Early ponding was observed in the rainfall simulation experiments but was followed by rapid infiltration and reduced runoff generation.

Another possible explanation for the runoff rates observed in the present study is a hydrophobic layer influencing the infiltration rates of the underlying soils by decreasing surface roughness and reducing the amount of water infiltrating the soils near or at the soil surface (Larsen and MacDonald, 2007). However, a natural water repellency layer can form from resins, waxes, and aromatic oils created by live vegetation, typically on hot, dry days on undisturbed soil surfaces (Puntenney-Desmond et al., 2020). Thus, runoff production on undisturbed soils with natural water repellency layer can be similar or more notable than disturbances in the same study area. In the present study, infiltration rates may have moderately recovered to pre-burn conditions on some plots. An explanation for this potential recovery is seen between plots at a site when comparing the runoff initiation. For instance, early runoff generation at site 3, plots 3b and 3c (Figure 3.2) occurred, whereas it took longer to generate runoff at site 3a. This finding supports previous

research investigating the decay of the hydrophobic layer and recovery of infiltration rates (Woods and Balfour, 2010; Larsen and MacDonald, 2007). However, infiltration capacity and ash layer presence must be interpreted cautiously because other factors could affect differences in runoff rates measured in these plots.

### *4.2.2 The influence of microtopography on runoff rates*

Microtopography can influence runoff rates via the presence of micro-depressions that store water and changes in flow-path length changes (Puntenney-Desmond et al., 2020; Lui et al., 2019; Jourgholami and Labelle, 2020). In the present study, the microtopography of experimental plots influenced the runoff rates. The most noticeable factor from the microtopography was the micro-depressions that created a ponding effect and reduced the runoff volume (Figure 4.2). These findings were similar to those described by Puntenney-Desmond et al. (2020), where ponding was observed on some plots caused by depression from harvest activity. The topographic depressions in the current study were likely naturally occurring from previous erosion events before developing a vegetation layer and tree roots near the soil surface. Additionally, micro-depressions were typically located at the back corners or in the middle of plots, with few at the spout of the plot frame. The location of the depressions is a possible explanation for the reduction in runoff rates because ponding limited water availability from entering sample bottles.

In addition to micro-depressions, potential changes to runoff rates include changes in flow-path length. Shorter flow-path lengths require more water to generate runoff (Lui et al., 2018). However, the runoff results from some plots suggest some flow-path lengths were short enough to reduce runoff rates, particularly plots with dynamic microtopography. For example, Figure 4.2a shows ponding from an experiment with no flow path for the water to move downslope. Furthermore, a flow path could not form because the water volume throughout the experiment was not enough to escape the micro-depression. Notably, the infiltration rates on that plot were exceptionally fast, with the ponded water infiltrating seconds after the experiment was over (Figure 4.2b). Similar cases, to a lesser degree, were observed on other plots as well.

### *4.2.3 The importance of ground cover on runoff rates*

Ground cover type plays a critical role in regulating runoff rates (Hartanto et al., 2002; Zhou et al., 2018; Puntenney-Desmond et al., 2020; Shakesby and Doerr, 2006). In this study, ground cover affected the runoff rates because of vegetation recovery, litter dams from debris and, soil hydrophobicity. Hydrophobic soils can reduce surface roughness and increase runoff rates (Larsen and MacDonald, 2007).

The relationship between vegetation recovery and runoff rates may partly be explained by leaf interception from the newly grown vegetation reducing the volume of water hitting the soil surface, resulting in decreased water availability (Hartanto et al., 2002). However, the present study could

not demonstrate that live vegetation played a critical role in runoff rates. It may be that there was not enough vegetation cover on plots to show any sign of runoff decreases compared to non-vegetated plots with similar soil textures. For example, site 5b had approximately 25% vegetation cover (Figure 2.7) but had the maximum runoff rate at site 5 (Figure 3.2). In contrast to this example, site 4a had approximately 35% leafy vegetation cover (Figure 4.3) but had the minimum runoff rate at site 4 (Figure 3.2). Although this was an observation, there is potential bias from the observers, and other factors could have increased the runoff rates on the vegetated plots.

Litter dams from debris can trap water in depressions and alter the lengths and directions of flow paths by making the path shorter or longer (Shakesby and Doerr et al., 2006; Zhou et al., 2018; Jourgholami and Labelle, 2020). In the present study, interaction between litter and runoff during rainfall simulations was observed. Remaining post-fire vegetation created litter dams that restricted runoff. For example, at site 2b, there was an exposed root that ran horizontally across the plot near the spout of the frame. This plot had the lowest runoff rates at the three site 2 plots. When comparing other factors between the plots, there are minimal differences in plot characteristics.

### *4.2.4 The effect of dominant particle size on runoff rates*

Few studies have specifically examined the role of soil texture on runoff rates in a post-wildfire environment (Woods and Balfour, 2010). In the present study, soil texture was a key factor influencing runoff rates and demonstrated that as particle size increases, runoff rates decreased due to increased infiltration capacity. These results are consistent with those obtained by Jourgholami and Labelle (2020), although their study focused on machine-trafficked soils.

One unanticipated outcome of the present study was that the loam soil texture had lower runoff rates than the sandy loam sites. This discrepancy could result from excluding an experiment that did not use the study's controlled rainfall intensity, resulting in fewer plots in the statistical analysis runoff rates as a function of soil texture. In addition to this result, two out of three sites (4 and 6) were influenced by a thick ash layer that did not saturate thoroughly throughout the experiments at site 4 and micro-depressions at site 6, considerably reducing runoff volume leaving the plots. Thus, runoff rates for loam might not reflect the actual runoff rates experienced in situ under normal conditions. Therefore, cautious interpretation of the results for runoff rates as a function of loam is required.

Reference runoff rates were much lower than the post-wildfire rates, particularly when compared against the fine-textured soils. Additionally, the reference sites are more in line with sand-textured soils in the burned basin. Furthermore, comparing the natural and disturbed runoff rates of the reference plots shows that ground cover plays an essential role in the volume of runoff generated. The disturbed plots were within a few meters of the natural plots at the same sites, and rainfall simulations were done on the same day for the two plots at each site in the reference basin. Another

possible reason why runoff rates seem low for the reference basin is that one plot (site 15a) did not have any runoff production. The lack of runoff for that plot can be attributed to it having a low slope combined with micro-depressions and litter dams from tree roots, even with the removal of ground cover. However, this observation must be interpreted with caution because the time constraints of the study did not allow for the analysis of dominant particle size analysis for the reference basin.

### 4.3 Factors impacting sediment erosion in post-wildfire Waterton Lakes National Park

Sediment erosion in WLNP varied between soil textures during low-intensity rainfall simulations. These results further support the idea that sediment erosion increases following a wildfire (Benavides-Solorio and MacDonald, 2001; Spigel and Robichaud, 2007; Larsen and MacDonald, 2007; Shakesby and Doerr, 2006). Although, the current study experienced lower sediment yields compared to previous studies. The lower sediment yields can be explained by low rainfall erosivity, ground cover differences, and dominant particle size variations. There is a considerable amount of literature on sediment erosion in hillslope environments that have shown that factors such as rainfall erosivity (Benavides-Solorio and MacDonald, 2005; Larsen and MacDonald, 2007) and ground cover (Hartanto et al., 2002; Zhou et al., 2018; Puntenney-Desmond et al., 2020; Shakesby and Doerr, 2006) affect sediment erosion. In this section, each of these factors that affect erosion will be discussed in the context of the present study and compared with previous research findings.

#### *4.3.1 The importance of rainfall erosivity on post-wildfire soils*

Rainfall erosivity influences sediment erosion in a post-wildfire environment (Larsen and MacDonald, 2007; Benavides-Solorio and MacDonald, 2005). Additionally, Larsen and MacDonald (2007) have noted that values of 5 - 20 MJ mm $ha^{-1}$ $h^{-1}$ were the minimum rainfall erosivity on recently burned soils to generate soil erosion. This study found that rainfall erosivity as low as 43.61 MJ mm $ha^{-1}$ $hr^{-1}$ can achieve sediment production on soils 22 months following a severe wildfire. A possibility is that the Kenow Wildfire's burn severity was destructive enough to slow the soil recovery rate in the study area, resulting in erodible soils in the two burned basins under low-intensity rainfall conditions.

In addition to the soil erosivity, there were some differences in sediment yields between sites with the same soil texture. These variations in sediment yields can be explained by the impact of rainfall erosivity when looking at the slight differences in rainfall intensity, thus causing differences in the particle detachment and transport from raindrop splash energy during the rainfall simulations. For example, the clay loam sites had differing rainfall erosivity values. Table 2.1a shows that sites 1 and 3 were similar, with site 2 being much higher. These differences resulted in site 2 having higher sediment yields than the other two sites, even with all three sites having a large percentage of bare soil exposed. However, the impact rainfall erosivity has on sediment erosion in this study

needs to be taken with caution because other factors also affect sediment erosion, such as ground cover (Benavides-Solorio and MacDonald, 2005) and soil texture.

### *4.3.2 The influence of ground cover on sediment erosion*

Ground cover plays a critical role in sediment production in forested environments because surface roughness, litter and vegetation cover, and soil exposure are the first-order controls governing sediment production (Puntenney-Desmond et al., 2020; Hartanto et al., 2002; Zhou et al., 2018; Shakesby and Doerr, 2006). The present study found that litter cover and soil exposure had the most influence on sediment production for the rainfall simulation experiments. This influence can be seen when comparing the disturbed and undisturbed plots, where the sediment production on disturbed plots was nearly an order of magnitude greater in most instances, except for the sand-textured soils.

Stem vegetation (15 to 45 cm tall) had little impact on reducing sediment erosion in the post-wildfire experiments. This outcome is contrary to previous studies that suggested that vegetation cover reduces sediment production by protecting against soil particle detachment (Hartanto et al., 2002; Zhou et al., 2018; Puntenney-Desmond et al., 2020; Shakesby and Doerr, 2006). It may be that the vegetation did not provide adequate raindrop interception for the plot surfaces resulting in the exposed soils still being susceptible to the erosive force of the simulated rain. However, sites 8b and 8c had a moss layer present which seemed to reduce the volume of sediment produced during those experiments (Figure 4.4). The impact of moss cover on sediment production may be explained by looking at the natural plots in the reference basin, which had a litter layer covering the soil surface and having a minute amount of soil loss for those experiments. This litter layer reduced the sediment yields of the natural plots by a factor of 7.75 compared to the sediment yields of the disturbed reference plots.

A note of caution is due here since most plots in the post-wildfire basins primarily consisted of exposed soils with little stem vegetation cover and even less leaf cover. Thus, it is difficult to determine the actual effect of vegetation cover following the Kenow wildfire. However, it is promising that the present study showed that litter cover and soil exposure played a role in determining sediment production.

### *4.3.3 The effect of dominant particle size on sediment erosion*

Very little was found in the literature regarding the effect dominant soil particle size has on sediment erosion for post-wildfire environments. Although, there have been studies on the effect of soil texture on sediment erosion on agricultural (Wischmeier and Smith, 1978) and machine trafficked soils (Jourgholami and Labelle, 2020). The current study determined that particle size is an essential factor for post-wildfire sediment erosion (Figure 3.7). The present findings on soil

texture and sediment erosion indicate that as the soil particle size increases, the volume of sediment eroded decreases, with clay loam having the highest and sand having the lowest soil erosion rates.

The influence of soil texture on sediment erosion is consistent with that of Jourgholami and Labelle (2020), who showed that clay textured soils have higher erosion rates than loam textured soils on disturbed soils. However, Wischmeier and Smith (1978) found that clay textured soils were less erodible than course-textured soils on agricultural plots because the clay soils had greater soil aggregate stability. The reason for the differences for clay textured soil erosion between the studies could be that the soil aggregate stability decreased following a disturbance that increased the soils' detachment rates (Shakesby and Doerr, 2006; Hosseini et al., 2018). Interestingly, loam textured soils produced more sediment than the sandy loams, even though loam sites had lower runoff rates than the sandy loam (Table 3.1). This finding can be attributed to the loam sites having a higher erodibility causing greater sediment concentrations in the runoff samples than the sandy loam sites.

Similar to the reference runoff rates, the natural reference sediment yields were lower than the disturbed yields, except for the sand textured soils (Table 3.1). A possible reason for the natural reference sites being higher than the sand sites is that site 13b had some soil exposed near the spout of the plot frame (Figure 4.5). This exposed soil increased sediment leaving the plot, resulting in a higher sediment yield than the other natural plots. In addition to the exposed soil at site 13b, site 13 had higher erodibility than any other site conducted in this study (Table 3.3), increasing the mean sediment yields for the reference sites. Furthermore, the reference sites were more erodible than the soil textures in the burned basin (Figure 3.13). Unfortunately, comparing the reference sites to the post-wildfire sites is somewhat limited because time constraints did not allow for soil texture analysis of the reference sites. Thus, making it challenging to compare soil textures of non-burned soils to burned soils for the present study. However, these findings may help us understand the impact of soil texture on sediment erosion in post-wildfire environments, particularly in critical source water regions at risk of the transport of post-wildfire contaminants.

### 4.4 Modelling sediment erosion in post-wildfire Waterton Lakes National Park

Sediment erosion in WLNP was modelled using the Revised Universal Soil Loss Equation (RUSLE) at the plot-scale for each site and watershed-scale for Blakiston Creek and Cameron Creek basins. Comparison of the present findings is in line with those of previous studies (Table 4.1). However, the current study's results are on the lower end of soil erosion than previous post-wildfire studies. These lower sediment yields found in the current study may be explained by the soil erodibility and cover management factors from RUSLE. While most sediment erosion modelling has been conducted on agricultural landscapes (Hancock et al., 2020; Renard et al., 1997; Wischmeier and Smith, 1978; Renard et al., 1991; Renard et al., 1994), there has been an increase in sediment erosion modelling in post-wildfire environments in recent years (Larsen and MacDonald, 2007; Blake et al., 2020; Fernández et al., 2010; Fernández and Vega, 2016;

Fernández and Vega, 2018), with a minor focus on the use of GIS to model sediment erosion (Lanorte et al., 2019).

The emerging literature on modelling sediment erosion in post-wildfire have attempted to adjust the K- and C-factor to account for the surface changes following a wildfire (Larsen and MacDonald, 2007; Lanorte et al., 2019; Fernández et al., 2010; Fernández and Vega, 2016; Fernández and Vega, 2018). However, the current study did not adjust the K-factor because it was determined using a different methodology from the other studies that adjusted the soil erodibility factor (Fernández et al., 2010; Fernández and Vega, 2016; Fernández and Vega, 2018). Furthermore, the C-factor was not altered because it was calculated using Remote Sensing techniques following the Kenow Wildfire, similar to Lanorte et al. (2019). The following subsections discuss the application of RUSLE and its factors, the application of RUSLE in a GIS framework, and the implications for best management practices in Waterton Lakes National Park.

### *4.4.1 Application of RUSLE to model erosion processes in Waterton Lakes National Park*

The present study standardized the annual rainfall erosivity across all sites to reduce variability from rainfall data on sediment yield prediction. The R-factor in the current study was much lower than most previous post-wildfire RUSLE studies (Table 4.2) except for the Larsen and MacDonald (2007) study. These differences in rainfall erosivity between the current study and Larsen and MacDonald (2007) compared to other studies can be explained by the other studies being in areas with high amounts of precipitation throughout a year. The Larsen and MacDonald (2007) study area was more similar to the present study area than the other studies and measured rainfall data between June and October for each year of the study with a mean rainfall erosivity of 286 MJ mm ha-1 hr-1. This study used historical rainfall data between April and October over 13 years to calculate a mean rainfall erosivity of 337.53 MJ mm ha-1 hr-1. A note of caution is due here with the current study's R-factor because some precipitation data may be snowfall precipitation for April and May. Thus, there may be some inaccuracy in the rainfall erosivity estimations for the present study.

Due to an inadequate amount of field data, the present study determined the K-factor by rearranging the RUSLE model to calculate soil erodibility using the field sediment yield data instead of the one suggested by Renard et al. (1991). However, the soil erodibility values were still within the range of previous studies that obtained their erodibility values through field measurements (Table 4.3), even though they were on the lower end. A possible reason the current study's soil erodibility is lower than previous studies could be that the K-factor was not adjusted to account for soil burn severity (Fernández et al., 2010; Fernández and Vega, 2016; Fernández and Vega, 2018). Instead, the rearranged version of RUSLE used in the present study calculated the post-wildfire erodibility, so there was no need to incorporate a soil burn severity into the modelling for predicting annual sediment yields.

There is a paucity of studies in the literature on the impact of slope length and steepness factor (LS-factor) on sediment erosion following wildfire (Blake et al., 2020). However, previous studies have documented their LS-values for their research, and the current study falls within a similar range (Table 4.4). The LS-factor was moderately similar across most sites in the current study, except for two sand sites (sites 10 and 11; Table 3.3). Moreover, site 10 had the lowest LS-values but the highest sediment yield for sand and, conversely, site 11 had the highest LS-factor and the lowest sediment yield for sand. A possible explanation for the differing sediment yields at sites 10 and 11 is that site 11 was in the meadow area of Blakiston Creek, which had more infiltration compared to other areas of the study, as discussed in section 4.2.1. Furthermore, in looking at the LS-values throughout the study, LS-factor has minimal impact on the amount of sediment yield estimated in the present study (Table 3.2).

The cover-management factor (C-factor) is a critical variable from RUSLE to estimate post-wildfire sediment yields (Fernández et al., 2010) because the C-factor describes the vegetation cover and management of an area (Benavides-Solorio and MacDonald, 2005; Renard et al., 1991). Larsen and MacDonald (2007) hypothesized that C-factor values should be at or close to a value of 1 following high-severity wildfire. However, field studies could only calculate values lower than this hypothesized value because of a lack of detailed forest soil data following a wildfire (Larsen and MacDonald, 2007; Fernández et al., 2010; Fernández and Vega, 2016; Fernández and Vega, 2018). The current study supports the C-factor values calculated in the previous field studies (Table 4.5) using Remote Sensing methods to estimate C-values. Furthermore, the C-factor values were highest for the sand textured sites and the lowest for the clay loam textured sites. Thus, there was more vegetation present on the finer-textured sites. It is difficult to explain why the fine-textured sites had higher vegetation than coarse-textured sites, but it may be related to the finer-textured sites tending to be in sediment deposition areas (Figure 4.6), resulting in minor soil disturbance for vegetation to grow. However, slope length and steepness did not seem to impact the amount of cover present at each site (Table 3.3).

Sediment yields in the present study were lower at the plot scale than previous studies that used RUSLE to model post-wildfire sediment erosion (Table 4.1). The data used for the R-factor, K-factor, LS-factor, and C-factor can explain the lower sediment yields observed. The rainfall erosivity values in the present study for RUSLE were substantial enough to generate sediment transport on most experimental plots. Although the K-factor was calculated using a rearrangement of the RUSLE equation, the initial erodibility data used was per stimulated storm event for each soil texture. It was then scaled to an annual erodibility for each soil texture to estimate the annual sediment yields for each plot. While the LS-factor was not an imperative factor in the amount of sediment produced in the present study, it was still necessary to estimate sediment yield (Table 3.2). The C-factor in the current study is estimated only for the rainfall simulation experiments and does not fully capture changes in C-values throughout the year and future values as vegetation increases in the study area. Overall, mean annual rainfall erosivity, current erodibility values and

cover-management values, and slope length and steepness provided the estimations of annual sediment yield in Waterton Lakes National Park 22 months following the wildfire.

### *4.4.2 Application of GIS to model erosion and deposition at the watershed scale*

Geographic Information Systems can be a valuable tool to analyze spatial data or simulate processes, such as areas at varying degrees of risk to sediment erosion (Terranova et al., 2009; Meusburger et al., 2010; Mitasova et al., 2013; Dragićević et al., 2015). GIS was used to model and identify sediment erosion and deposition areas throughout Blakiston Creek and Cameron Creek watersheds in the present study. The most compelling finding from the GIS analysis was that the Park mainly experienced low erosion rates with some low deposition rates (Figure 3.17). This result may be explained because large portions of the two watersheds had little vegetation cover following the wildfire. Another possible explanation of these results is that the watershed-scale RUSLE factors (K-, LS-, and C-factors) used to estimate sediment yields may be generalized when scaled up from the plot scale (Zhou et al., 2018). Except for the C-factor in the present study, it used Remote Sensing at the watershed scale and then scaled down for plot scale use in the RUSLE model.

The soil erodibility factor at the watershed scale was limited to three values (Figure 3.15) because the data available at that scale was a range of soil textures rather than a specific soil texture for a given location (Figure 2.2). This coarse soil texture data can lead to generalizations of sediment yields as the K-factor at the watershed scale in the current study represents the mean soil erodibility of multiple soil textures at a given location. A possible reason for the lack of data of soil textures throughout the Park is that there has been a lack of studies on obtaining detailed soil data and digitizing it for use in a GIS framework.

Similar to the LS-factor discussed in 4.4.1, little literature has discussed the impact of the slope length and steepness on sediment erosion post-wildfire (Blake et al., 2020; Mhaske et al., 2021). The high LS-values observed at the watershed scale can be attributed to calculating flow paths when creating the LS-factor dataset. Moreover, the mountain peaks and steep slopes can misrepresent slope steepness and length. However, the impact of these misrepresentations may be minimal because other RUSLE factors with zero values will produce no sediment erosion at those locations, such as the K-factor.

The C-factor in the present study is in line with Lanorte et al. (2019), who used the Soil Adjusted Vegetation Index (SAVI) to obtain C-values in the range of 0.32 – 0.98, compared to this study with a range of 0 to 1 at the watershed scale. Heavily forested areas unaffected by the Kenow Wildfire and bare rock mountain faces in the two watersheds of concern may explain the range of C-values for the current study. Low C-factor values calculated from SAVI are from the forested areas throughout the study area, and the high C-factor values are from the mountain faces. Furthermore, the C-factor in the present study represented small vegetation at the watershed scale

because of the satellite imagery having a resolution of 3 meters. However, a note of caution is due here since the C-factor could not compare and validate for in situ data and could only compare to previous studies (Table 4.5).

The current study was the first to model sediment erosion and deposition in a post-wildfire environment in Canada using the combination of GIS and RUSLE. While the sediment yields in the current study are comparable to previous studies (Table 4.6), it is challenging to compare the deposition measured from the GIS due to a lack of studies. Mhaske et al. (2021) showed that the probability of sediment deposition was mapped qualitatively but did not provide measured values of sediment deposition. Thus, the current study cannot compare the deposition measured to previous studies. Figures 3.16 and 4.6 need to be interpreted with caution because zero values are considered sediment erosion, thus giving the bias of more erosion predicted than present *in situ*, based on the data available and used in the current study.

### *4.4.3 Implications for planning and erosion management in Waterton Lakes National Park*

Most of Blakiston Creek and Cameron Creek watersheds experienced erosion but some deposition areas were also simulated after the Kenow Wildfire (Figure 4.6) and areas of concern for the transfer of pyrogenic materials to receiving streams were mapped (Figure 3.18 and Figure 4.6). These figures provide zones of erosion or deposition at a spatial resolution of 3 meters allowing for more precise identification of critical risk areas for implementing best management practices (BMPs) to reduce sediment entering the river system in Blakiston Creek and Cameron Creek. Figure 4.6 can help managers easily find the areas of deposition and erosion throughout the two watersheds. While Figure 3.18 can help managers know the erosion and deposition rates and use that information to prioritize areas that require BMPs. Interestingly, the erosion rates are low throughout WLNP, ranging from 0 to 5 t $ha^{-1}$ $yr^{-1}$ for riparian areas. Although, there may be some concern with sediment deposition in the floodplain of Blakiston Creek as it may store contaminants and be released later during flooding events (Figure 4.7).

Previous studies have investigated the effectiveness of various BMPs, such as installing erosion barriers, mulching, and seeding, following a wildfire (Robichaud, 2005; Robichaud et al., 2013; Covert, 2011). Seeding is the most cost-efficient approach with the most lasting effect because once established, the vegetation growth increases infiltration and reduces erosion for several years following a fire (Robichaud, 2005). Moreover, mulching provides the best short-term sediment erosion mitigation because it is an immediate ground cover over the disturbed soil (Robichaud et al., 2013). Furthermore, erosional barriers limit overland flow, promote sediment deposition, and reduce sediment transported downslope. These barriers tend to be straw wattles, straw bales, logs, and other natural and engineered structures (Robichaud, 2005).

In the context of the present study, these best management practices may be beneficial in reducing sediment from entering Blakiston Creek and Cameron Creek. However, there may be implications

of utilizing specific BMPs over others. For example, agricultural straw mulching may spread invasive vegetation species and limit the growth of native plants (Covert, 2011; Robichaud et al., 2013). Since Waterton Lakes National Park attempts to preserve native vegetation, this approach should be a low priority. Another example of an implication from BMPs is that erosional barriers using felled trees decrease in effectiveness over long periods because the storage capacity is exceeded and can no longer trap mobilized sediment (Robichaud, 2005). An example of the implications of seeding as a BMP is the length of time it takes to establish because the vegetation does not always grow within the first year following a fire (Robichaud, 2005). Given the timing of the current study, small vegetation has already grown in some areas, planners and managers may want to consider the use of seeding to help further reduce sediment erosion and apply log erosion barriers in areas prone to high erosion rates. Otherwise, planners and managers may not want to implement best management practices as most areas with high sediment erosion are far from riparian areas, and vegetation regrowth throughout the Park can reduce the low erosion rates experienced over most areas of concern.

## 4.5 Limitations

### *4.5.1 Limitations of field and laboratory experiments*

The limitations of the field experiments in the present study were mechanical constraints and determination and use of rainfall intensity and duration for simulation experiments in Waterton Lakes National Park. While there was an attempt to keep rainfall intensities constant at an intensity of 32.84 mm $hr^{-1}$, mechanical faults caused changes in rainfall intensities in some cases (sites 2 and 6a). In other instances, experiments (sites 10 and 12) were in their final stages of development to determine the appropriate intensity for other plot locations. Sites 10 and 12 intensities were lower at 24.1 mm $hr^{-1}$, which was still within an acceptable range of the median. Additionally, sites 2 and 6a had mechanical errors that resulted in greater rainfall intensities from the median of the study. Site 2 had a rainfall intensity of 36.1 mm $hr^{-1}$, which was close enough to the median that omission was not necessary. Site 6a had an intensity of 54 mm $hr^{-1}$, resulting in the exclusion of data for this plot to evaluate the effect of soil texture on runoff rates and sediment yield where rainfall intensities were controlled. However, site 6a was included for the annual watershed scale portion of this study because the rainfall erosivity was set to a constant value across all plots.

### *4.5.2 Limitations of Revised Universal Soil Loss Equation*

The limitations of the Revised Soil Loss Equation in the present study were associated with predicting post-wildfire sediment yields from errors in the input data and model errors. Previous studies discovered that RUSLE has difficulty predicting post-wildfire sediment yields due to model errors, errors in the input data, and errors in the data used for validation (Larsen and MacDonald, 2007; Lanorte et al., 2019; Fernández et al., 2010; Fernández and Vega, 2018; Blake et al., 2020). The input data errors include a lack of soil erodibility data at the watershed scale,

miscalculations in deriving LS-factor at the watershed scale, and lack of ground-truthing of C-factor values. The model errors include a lack of explicitly modelling certain erosion factors, such as sediment detachment, overland flow, infiltration, and sediment deposition (Larsen and MacDonald. 2007). Additionally, a lack of available data for the RUSLE factors creates deficiencies in predicting post-wildfire erosion at the watershed scale (Blake et al., 2020). In the current study, this was evident with the lack of soil texture and erodibility data for Waterton Lakes National Park, as most data was only available as point data. However, even with these limitations, RUSLE could still predict mean annual sediment erosion and deposition to identify priority management zones to reduce sediment transport into the Park's river system.

### *4.5.3 Limitations of Geographic Information Systems*

There were not many limitations with GIS in the current study because GIS is a tool that depends on the data provided by the user and the user's hardware processing power. Therefore, the data limitations for GIS were similar to those discussed in section 4.5.2, and the hardware processing power was not an issue in the present study. Although better processing power would have allowed for faster computation of the analysis at the watershed scale. Another limitation from the GIS was the visualization of sediment yield, where 0 values of sediment yield could not be separated from the erosion category.

## 4.6 Conclusions

### *4.6.1 Conclusions*

The primary goal of the current study was to evaluate the effect of the Kenow wildfire on erodibility and sediment yields in Waterton Lakes National Park at both the plot and watershed scale using rainfall simulators and an erosion model (RUSLE). The conclusions of this study were:

1) Low rainfall intensities (33 mm $hr^{-1}$) were of sufficient energy to produce runoff and sediment erosion on plots that did not have high infiltration rates from wildfire ash.
2) Runoff volume was low in some plot scale experiments due to ponding from micro-depressions found on plot scale topography.
3) The degree of ground cover (vegetation amount and type) are critical factors determining sediment erosion rates. However, stem vegetation (15 to 45 cm tall) cover did not reduce erosion rates.
4) Soil particle size was a key factor influencing runoff rates and sediment erosion in WLNP, because finer soil textures produced more runoff volume and sediment concentrations than the coarser soil textures.
5) RUSLE is an appropriate scenario development tool to model post-wildfire sediment erosion for post-wildfire planning and management.

6) The combination of GIS and RUSLE provides a suitable platform to simulate watershed-scale sediment erosion and deposition.

To my knowledge, this study is the first of its kind to evaluate runoff and sediment erosion data from a range of soil textures using rainfall simulations and scaling those results up to the watershed scale through a sediment erosion model (RUSLE) in a GIS framework to identify areas of concern to sediment erosion following a wildfire. However, this study is a first estimate of potential sediment yields in Waterton Lakes National Park because of the limitations present in the study. These limitations include soil data availability at the watershed-scale, availability, time constraints for the field season, and RUSLE which is an empirical model which lacks the capability of modelling runoff, sediment detachment, and infiltration processes.

### *4.6.2 Future Recommendations*

The present study demonstrated that low-intensity rainfall simulations on burned hillslopes conducted 22 months following a high-severity wildfire produced runoff and sediment erosion for a range of sites with various soil textures. Moreover, these data can be used in the Revised Soil Loss Equation to identify potential areas of concern for sediment erosion. Further research might explore:

1) More focused research using rainfall simulation experiments over a range of vegetation covers is required to evaluate the impact of vegetation regrowth on sediment erosion for differing soil textures following a wildfire.
2) Detailed rainfall simulations using a range of rainfall intensities is required to evaluate runoff rates, infiltration capacity and sediment erosion potential for a wider range of precipitation intensities that reflect the range of storm events that typically occur in Waterton Lakes National Park.
3) Post-wildfire hillslope studies are required to examine the connectivity between post-wildfire landscapes and receiving streams to compare plot-scale data with hillslope scale data.

## 4.7 Tables and Figures

*Table 4.1: Sediment yields of the current study for both field measurements and modelled yields compared to previous studies.*

| Citation | Study Area | Source | Value | Unit | Soil Texture | Type |
|---|---|---|---|---|---|---|
| Current Study | Waterton Lakes National Park, Alberta | Field Measurement | 0.001 - 1.28 | $t\ ha^{-1}\ hr^{-1}$ | Clay loam; loam; sandy loam; sand | Post-wildfire (severe) |
| Current Study | Waterton Lakes National Park, Alberta | RUSLE | 0.004 - 3.89 | $t\ ha^{-1}\ yr^{-1}$ | Clay loam; loam; sandy loam; sand | Post-wildfire (severe) |
| Fernández and Vega (2018) | NW Spain | RUSLE | 7.4 - 40.9 | $t\ ha^{-1}\ yr^{-1}$ | Sandy loam | Post-wildfire (severe) |
| Larsen and MacDonald (2007) | Colorado, United States | RUSLE | 10.3 | $t\ ha^{-1}\ yr^{-1}$ | Sandy loam; coarse sand | Post-wildfire (severe) |
| Blake et al. (2020) | south-western Australia | RUSLE | 0 - 94.5 | $t\ ha^{-1}\ yr^{-1}$ | N/A | Post-wildfire |
| Hancock et al. (2020). | Mulconda Creek, Australia | LiDAR/field | 0.8 - 4.8 | $t\ ha^{-1}\ yr^{-1}$ | Loamy sand; silty loam | Agriculture |
| Almagro et al. (2019) | Guariroba, Brazil | RUSLE | 2.2 | $t\ ha^{-1}\ yr^{-1}$ | Sand; sandy loam | Mixed Landcover |
| Terranova et al., (2009). | Calabria, Italy | RUSLE | 30 - 116 | $t\ ha^{-1}\ yr^{-1}$ | N/A | Mixed Landcover |

*Table 4.2: Mean rainfall erosivity of the current study for both field and modelled measurements compared to the mean rainfall erosivity of previous studies.*

| Citation | Study area | Source | Value | Unit | Soil Texture |
|---|---|---|---|---|---|
| Current Study | Waterton Lakes National Park, Alberta | Field Measurement | 88.86 | MJ mm $ha^{-1}$ $hr^{-1}$ $yr^{-1}$ | clay loam; loam; sandy loam; sand |
| Current Study | Waterton Lakes National Park, Alberta | RUSLE | 337.53 | MJ mm $ha^{-1}$ $hr^{-1}$ $yr^{-1}$ | clay loam; loam; sandy loam; sand |
| Fernadez and Vega (2018) | NW Spain | Field Measurement | 3440 | MJ mm $ha^{-1}$ $hr^{-1}$ $yr^{-1}$ | Sandy loam |
| Fernadez and Vega (2016) | NW, Spain | Field Measurement | 2780 | MJ mm $ha^{-1}$ $hr^{-1}$ $yr^{-1}$ | N/A |
| Fernadez et al. (2010) | Verin, Spain | Field Measurement | 1385.5 | MJ mm $ha^{-1}$ $hr^{-1}$ $yr^{-1}$ | N/A |
| Blake et al., (2020) | south-western Australia | RUSLE | 500 - 1188 | MJ mm $ha^{-1}$ $hr^{-1}$ $yr^{-1}$ | N/A |
| Almagro et al. (2019) | Guariroba, Brazil | RUSLE | 9042 | MJ mm $ha^{-1}$ $hr^{-1}$ $yr^{-1}$ | Sand; sandy loam |

*Table 4.3: Range of soil erodibility of the current study for both field and modelled measurements compared to the range of previous studies.*

| Citation | Study Area | Source | Value | Unit | Soil Texture | Type |
|---|---|---|---|---|---|---|
| Current Study | Waterton Lakes National Park, Alberta | Field Measurement | 0.00 - 0.01 | t hr $MJ^{-1}$ $mm^{-1}$ | clay loam; loam; sandy loam; sand | Post-wildfire (severe) |
| Fernadez and Vega (2018) | NW Spain | Field Measurement | 0.005 - 0.008 | t hr $MJ^{-1}$ $mm^{-1}$ | Sandy loam | Post-wildfire (severe) |
| Fernadez and Vega (2016) | NW, Spain | Field Measurement | 0.01 - 0.08 | t hr $MJ^{-1}$ $mm^{-1}$ | N/A | Post-wildfire (severe) |
| Fernadez et al. (2010) | NW, Spain | Field Measurement | 0.02 | t hr $MJ^{-1}$ $mm^{-1}$ | N/A | Post-wildfire (moderate) |
| Blake et al. (2020) | south-western Australia | RUSLE | 0.01 - 0.79 | t hr $MJ^{-1}$ $mm^{-1}$ | N/A | Pre-wildfire |
| Almagro et al. (2019) | Guariroba, Brazil | RUSLE | 0.03 - 0.04 | t hr $MJ^{-1}$ $mm^{-1}$ | Sand; sandy loam | Mixed Landcover |

*Table 4.4: Slope length and steepness of the current study for both field and modelled measurements compared to previous studies.*

| Citation | Study area | Source | Value | Soil Texture |
|---|---|---|---|---|
| Current Study | Waterton Lakes National Park, Alberta | Field Measurement | 1.68 - 20.68 | clay loam; loam; sandy loam; sand |
| Current Study | Waterton Lakes National Park, Alberta | GIS | 0 - 6019 | clay loam; loam; sandy loam; sand |
| Fernadez and Vega (2018) | NW Spain | Field Measurement | 6.06 - 8.94 | Sandy loam |
| Fernadez and Vega (2016) | NW, Spain | Field Measurement | 2.74 - 15.05 | N/A |
| Fernadez et al. (2010) | NW, Spain | Field Measurement | 6.37 - 8.70 | N/A |
| Blake et al., (2020) | south-western Australia | RUSLE | 0 - 23.5 | N/A |
| Almagro et al. (2019) | Guariroba, Brazil | RUSLE | 0.01 - 49.18 | Sand; sandy loam |

*Table 4.5: Range of C-factor values of the current study compared to previous studies.*

| Citation | Study Area | Source | Value | Type |
|---|---|---|---|---|
| Current Study | Waterton Lakes National Park, Alberta | Csavi | 0.1 - 0.49 | Post-wildfire (severe) |
| Blake et al. (2020) | south-western Australia | Literature | 0.01 - 0.3 | Post-wildfire (high) |
| Larsen and MacDonald (2007) | Colorado, USA | Field data | 0.2 | First year post-fire (severe) |
| Larsen and MacDonald (2007) | Colorado, USA | Field data | 0.05 | First year post-fire (moderate) |
| Larsen and MacDonald (2007) | Colorado, USA | Field data | 0.01 | First year post-fire (low) |
| Larsen and MacDonald (2007) | Colorado, USA | Field data | 0.03 | Third year post-fire (severe) |
| Larsen and MacDonald (2007) | Colorado, USA | Field data | 0.0006 | Fourth year post-fire (severe) |
| Fernadez et al. (2010) | NW, Spain | Field Measurement | 0.002 - 0.249 | Post-wildfire (severe) |
| Fernadez and Vega (2016) | NW, Spain | Field Measurement | 0.002 - 0.236 | Post-wildfire (moderate) |
| Fernadez and Vega (2018) | NW Spain | Field Measurement | 0.055 - 0.169 | Post-wildfire (severe) |
| Lanorte et al. (2019) | Basilicata, Italy | Csavi | 0.32 - 0.98 | Post-fire |
| Lanorte et al. (2019) | Basilicata, Italy | Land cover Classification | 0.001 - 0.265 | Pre-fire |
| Almagro et al. (2019) | Guariroba, Brazil | Literature | 0.02 | Pasture |
| Almagro et al. (2019) | Guariroba, Brazil | Literature | 0.03 | Eucalyptus |
| Almagro et al. (2019) | Guariroba, Brazil | Literature | 1 | Bare Soil |
| Almagro et al. (2019) | Guariroba, Brazil | CrA | 0.025 | Pasture |
| Almagro et al. (2019) | Guariroba, Brazil | CrA | 0.012 | Eucalyptus |
| Almagro et al. (2019) | Guariroba, Brazil | CrA | 0.033 | Bare Soil |
| Almagro et al. (2019) | Guariroba, Brazil | Cvk | 0.164 | Pasture |
| Almagro et al. (2019) | Guariroba, Brazil | Cvk | 0.027 | Eucalyptus |
| Almagro et al. (2019) | Guariroba, Brazil | Cvk | 0.37 | Bare Soil |

*Table 4.6: Sediment yields of the current study for modelled yields in a GIS-framework compared to previous studies.*

| Citation | Study Area | Source | Value | Unit | Soil Texture | Type |
|---|---|---|---|---|---|---|
| Current Study | Waterton Lakes National Park, Alberta | RUSLE | 0 - 161.6 | $t\ ha^{-1}\ yr^{-1}$ | Clay loam; loam; sandy loam; sand | Post-wildfire (severe) |
| Lanorte et al. (2019) | Basilicata, Italy | RUSLE | 8.64 - 31.48 | $t\ ha^{-1}\ yr^{-1}$ | N/A | Post-wildfire |
| Fernández and Vega (2018) | NW Spain | RUSLE | 7.4 - 40.9 | $t\ ha^{-1}\ yr^{-1}$ | Sandy loam | Post-wildfire (severe) |
| Larsen and MacDonald (2007) | Colorado, United States | RUSLE | 10.3 | $t\ ha^{-1}\ yr^{-1}$ | Sandy loam; coarse sand | Post-wildfire (severe) |
| Blake et al. (2020) | south-western Australia | RUSLE | 0 - 94.5 | $t\ ha^{-1}\ yr^{-1}$ | N/A | Post-wildfire |
| Hancock et al. (2020) | Mulconda Creek, Australia | LiDAR/field | 0.8 - 4.8 | $t\ ha^{-1}\ yr^{-1}$ | Loamy sand; silty loam | Agriculture |
| Almagro et al. (2019) | Guariroba, Brazil | RUSLE | 2.2 | $t\ ha^{-1}\ yr^{-1}$ | Sand; sandy loam | Mixed Landcover |
| Terranova et al. (2009) | Calabria, Italy | RUSLE | 30 - 116 | $t\ ha^{-1}\ yr^{-1}$ | N/A | Mixed Landcover |

*Figure 4.1: Rainfall simulation with unsaturated surface soil and ash layer at Site 4b.*

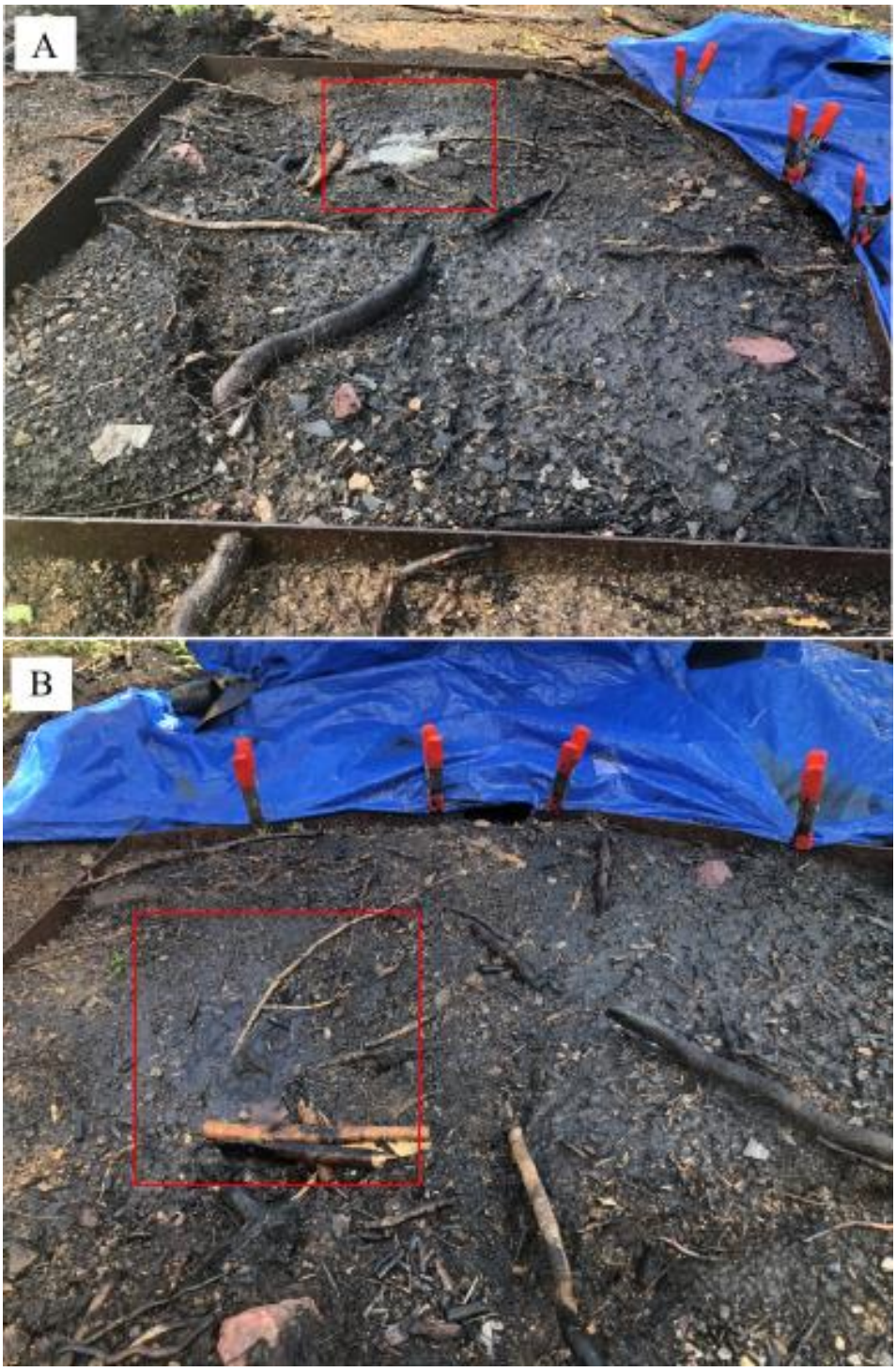


*Figure 4.2: Ponding present following the rainfall simulation at Site 12c (A). Seconds following the first photograph showing rapid infiltration of rainfall at sand-textured areas (B).*

*Figure 4.3: Fine ash before the rainfall simulation experiment at site 4a.*

*Figure 4.4: Moss cover before the rainfall simulation experiment at site 8b.*

*Figure 4.5: Exposed soil at site 13b before the rainfall simulation experiment.*

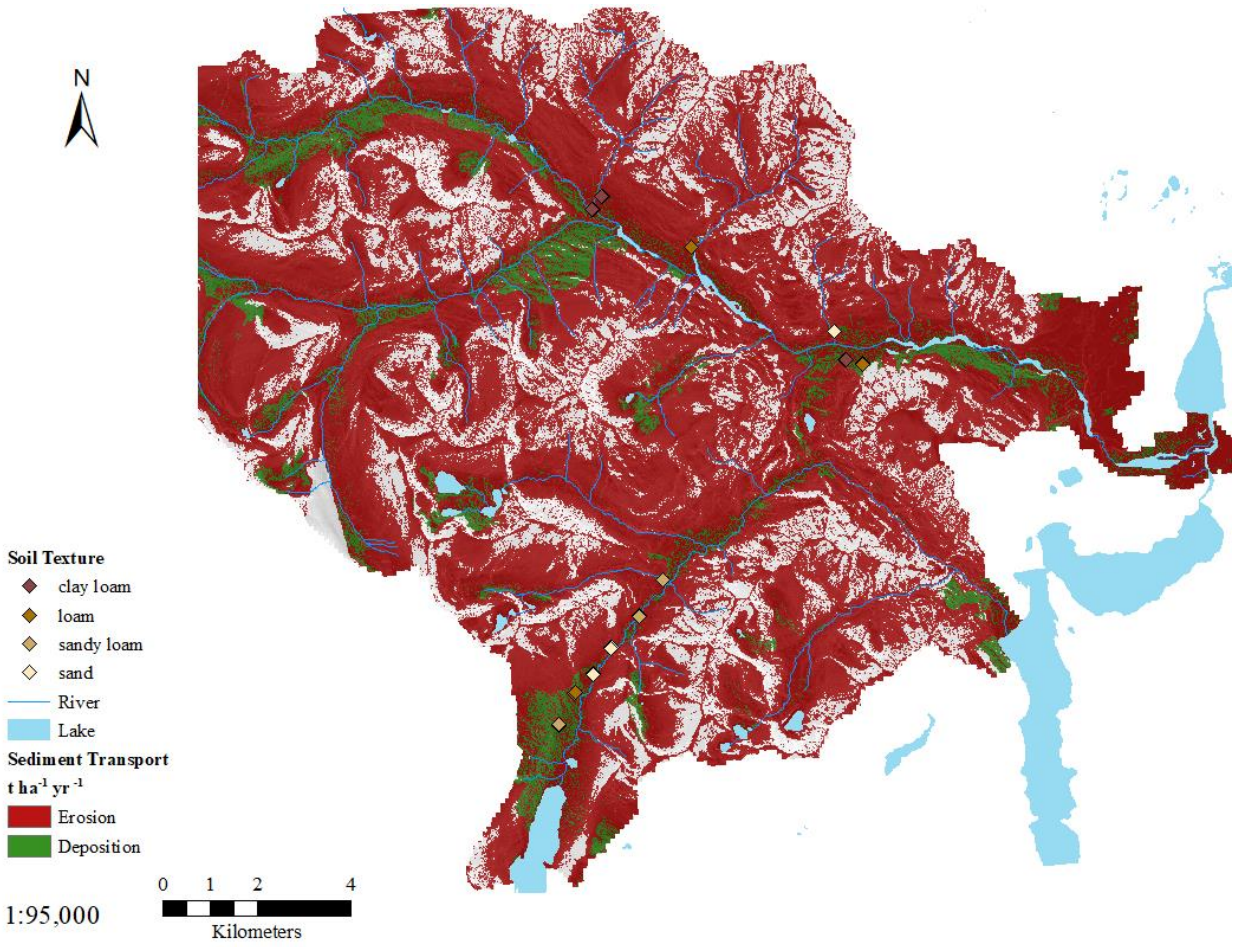


*Figure 4.6: Modelled erosion and deposition sites for Blakiston Creek and Cameron Creek watersheds.*

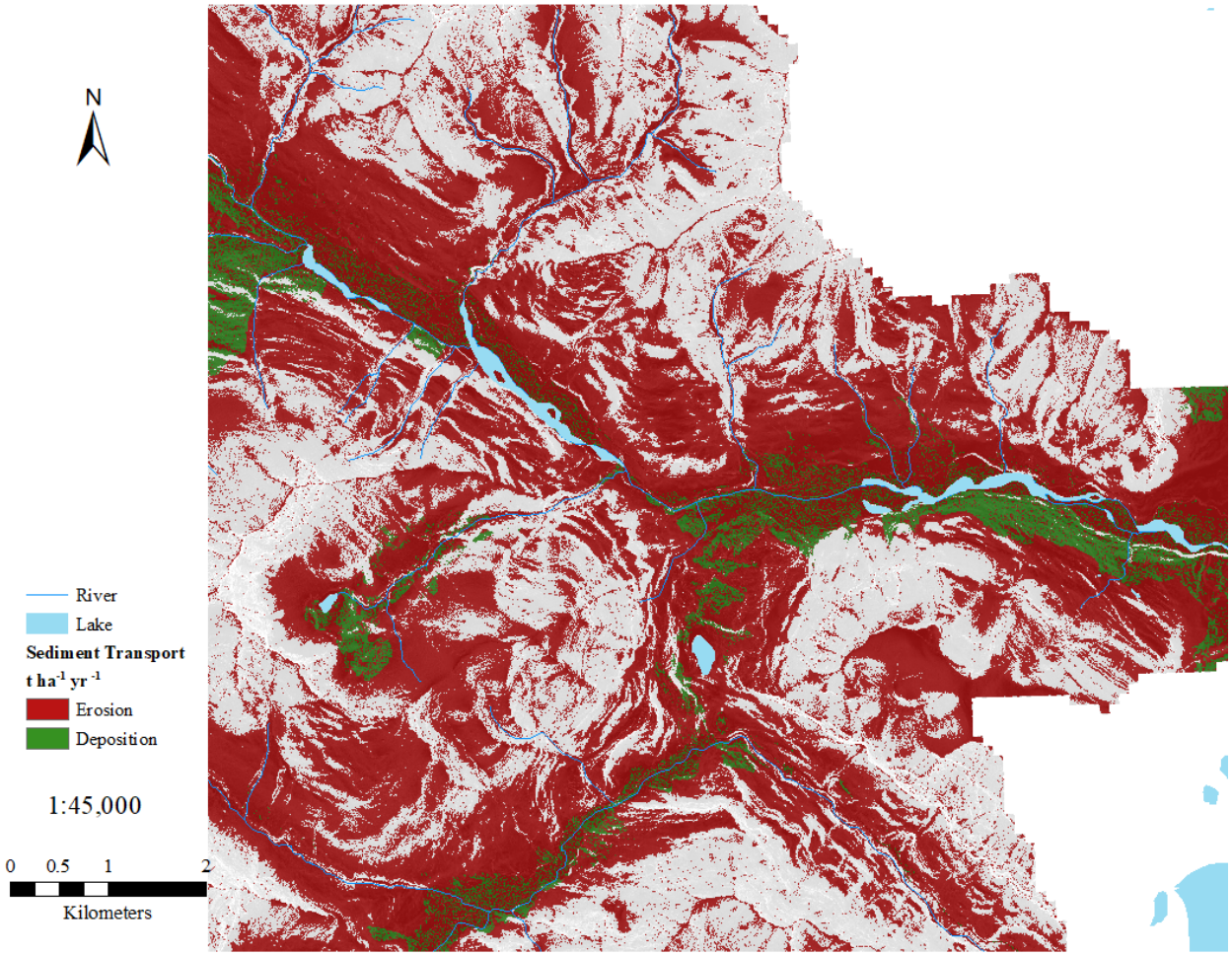


*Figure 4.7: Sediment deposition in the lower reaches of Blakiston Creek's floodplain.*

# References


Abraham, J., Dowling, K., & Florentine, S. (2017). Risk of post-fire metal mobilization into surface water resources: A review *Science of the Total Environment*, 599-600, 1740-1755. doi:https://doi.org/10.1016/j.scitotenv.2017.05.096

Alewell, C., Borrelli, P., Meusburger, K., & Panagos, P. (2019). Using the USLE: Chances, challenges and limitations of soil erosion modelling. *International Soil and Water Conservation Research*, *7*(3), 203-225. doi:https://doi.org/10.1016/j.iswcr.2019.05.004

Allen, C. D., Macalady, A. K., Chenchouni, H., Bachelet, D., McDowell, N., Vennetier, M., . . . Cobb, N. (2010). A global overview of drought and heat-induced tree mortality reveals emerging climate change risks for forests. *Forest Ecology and Management*, *259*(4), 660-684. doi:https://doi.org/10.1016/j.foreco.2009.09.001

Almagro, A., Thomé, T. C., Colman, C. B., Pereira, R. B., Marcato Junior, J., Rodrigues, D. B. B., & Oliveira, P. T. S. (2019). Improving cover and management factor (C-factor) estimation using remote sensing approaches for tropical regions. *International Soil and Water Conservation Research*, *7*(4), 325-334. doi:https://doi.org/10.1016/j.iswcr.2019.08.005

Anne Naeth, M., & Chanasyk, D. S. (1996). Runoff and sediment yield under grazing in foothills fescue grasslands of Alberta. JAWRA *Journal of the American Water Resources Association*, *32*(1), 89-95. doi:https://doi.org/10.1111/j.1752-1688.1996.tb03436.x

ASTM (2006) D 3977-97, Standard Test Method for Determining Sediment Concentration in Water Samples, Annual Book of Standards, Water and Environmental Technology, 2006, Volume 11.02.

ASTM (2017) D6913 / D6913M-17, Standard Test Methods for Particle-Size Distribution (Gradation) of Soils Using Sieve Analysis, ASTM International, West Conshohocken, PA, 2017, www.astm.org

Benavides-Solorio, J., & MacDonald, L. H. (2005). Measurement and prediction of post-fire erosion at the hillslope scale, Colorado front range. *International Journal of Wildland Fire*, *14*(4), 457-474. doi:https://doi.org/10.1071/WF05042

Benavides-Solorio, J., & MacDonald, L. H. (2001). Post-fire runoff and erosion from simulated rainfall on small plots, Colorado front range. *Hydrological Processes*, *15*(15), 2931-2952. doi:https://doi.org/10.1002/hyp.383

Blackburn, E.A.J, Dickson-Anderson, S., Stone, M., Emelko, M.B. (2021). Advancing on the promises of techno-ecological nature-based solutions: A framework for green technology in water supply and treatment. *Blue-Green Systems*, *3*(1), 81-94. doi:https://doi.org/10.2166/bgs.2021.008

Blake, D., Nyman, P., Nice, H., D'Souza, F. M. L., Kavazos, C. R. J., & Horwitz, P. (2020). Assessment of post-wildfire erosion risk and effects on water quality in south-western Australia. *International Journal of Wildland Fire*, *29*(3), 240-257. doi:https://doi.org/10.1071/WF18123

Breiby, T. (2006). Assessment of soil erosion risk within a sub watershed using GIS and RUSLE with a comparative analysis of the use of STATSGO and SSURGO soil databases. *Resource Analysis*, *8*, 1-22.

CanVec [geodatabase]. Government of Canada: Geospatial Data Extraction, 2017. Available: https://maps.canada.ca/czs/index-en.html (accessed Nov 18, 2018).

Coen, G. M., & Holland, W. D. (1976). Soils of Waterton Lakes National Park, Alberta. *Information Report. Alberta Institute of Pedology (Canada)*. no.NOR-X-65.

Colman, C. B., Oliveira, P. T. S., Almagro, A., Soares-Filho, B., & Rodrigues, D. B. B. (2019). Effects of climate and land-cover changes on soil erosion in Brazilian Pantanal. *Sustainability*, *11*(24), 7053. doi:https://doi.org/10.3390/su11247053

Collins, A. L., Blackwell, M., Boeckx, P., Chivers, C. A., Emelko, M., Evrard, O., ... & Zhang, Y. (2020) Sediment source fingerprinting: benchmarking recent outputs, remaining challenges and emerging themes. *Journal of Soils and Sediments*, *20*, 4160–4193. doi:https://doi.org/10.1007/s11368-020-02755-4.

Covert, A., & Jordan, P. (2009). A portable rainfall simulator: Techniques for understanding the effects of rainfall on soil erodibility

Covert, A. (2011). The effects of straw mulching on post-wildfire vegetation recovery in south eastern British Columbia. *Journal of Ecosystems and Management*, *11*(3). http://jem.forrex.org/index.php/jem/article/view/

Crouch, R. L., Timmenga, H. J., Barber, T. R., & Fuchsman, P. C. (2006). Post-fire surface water quality: Comparison of fire retardant versus wildfire-related effects. *Chemosphere*, *62*(6), 874-889. doi: https://doi.org/10.1016/j.chemosphere.2005.05.031

Dragićević, S., Lai, T., & Balram, S. (2015). GIS-based multicriteria evaluation with multiscale analysis to characterize urban landslide susceptibility in data-scarce environments. *Habitat international*, *45*, 114-125. doi:https://doi.org/10.1016/j.habitatint.2014.06.031

ESRI (2020). ArcGIS Desktop: Release 10.7.1. Redlands, CA: Environmental Systems Research Institute.

Emelko, M. B., Silins, U., Bladon, K. D., & Stone, M. (2011). Implications of land disturbance on drinking water treatability in a changing climate: Demonstrating the need for "source water supply and protection" strategies. *Water research*, *45*(2), 461-472. doi: https://doi.org/10.1016/j.watres.2010.08.051

Emelko, M., & Sham, C. H. (2014). *Wildfire impacts on water supplies and the potential for mitigation: Workshop Report*. Canadian Water Network.

Emelko, M.B., Stone, M., Silins, U., Allin, D., Collins, A.L., Williams, C.H.S., Martens, A.M., Bladon, K.D. (2016). Sediment-phosphorus dynamics can shift aquatic ecology and cause downstream

legacy effects after wildfire in large river systems. *Global Change Biology*, *22*, 1168-1184. doi:https://doi.org/10.1111/gcb.13073

Emmerton, C.A., Cooke, C., Hustins, S., Silins, U., Emelko, M.B., Lewis, T., Kruk, M.K., Taube, N., Zhu, D., Jackson, B., Stone, M., Kerr, J.G., Orwin, J.F. (2020). Severe western Canadian wildfire affects water quality even at large basin scales. *Water Research*, *183*, 116071. doi:https://doi.org/10.1016/j.watres.2020.116071

Esteves, T. C. J., Kirkby, M. J., Shakesby, R. A., Ferreira, A. J. D., Soares, J. A. A., Irvine, B. J., . . . Carreiras, M. A. (2012). Mitigating land degradation caused by wildfire: Application of the PESERA model to fire-affected sites in central Portugal. *Geoderma*, *191*, 40-50. doi:https://doi.org/10.1016/j.geoderma.2012.01.001

Feikema, P. M., Sheridan, G. J., Argent, R. M., Lane, P. N. J., & Grayson, R. B. (2011). Estimating catchment-scale impacts of wildfire on sediment and nutrient loads using the E2 catchment modelling framework. *Environmental Modelling & Software*, *26*(7), 913-928. doi:https://doi.org/10.1016/j.envsoft.2011.02.002

Fernández, C., Vega, J. A., & Vieira, D. C. S. (2010). Assessing soil erosion after fire and rehabilitation treatments in NW Spain: Performance of rusle and revised Morgan–Morgan–Finney models. *Land Degradation & Development*, *21*(1), 58-67. doi:https://doi.org/10.1002/ldr.965

Fernández, C., & Vega, J. A. (2016). Evaluation of RUSLE and PESERA models for predicting soil erosion losses in the first year after wildfire in NW Spain. *Geoderma*, *273*, 64-72. doi:https://doi.org/10.1016/j.geoderma.2016.03.016

Fernández, C., & Vega, J. A. (2018). Evaluation of the rusle and disturbed wepp erosion models for predicting soil loss in the first year after wildfire in NW Spain. *Environmental Research*, *165*, 279-285. doi:https://doi.org/10.1016/j.envres.2018.04.008

Flannigan, M., Krawchuk, M., Wotton, M., & Johnston, L. (2009). Implications of changing climate for global wildland fire. *International Journal of Wildland Fire*, *18*, 483-507. doi:https://doi.org/10.1071/WF08187

Flannigan, M., Cantin, A. S., De Groot, W. J., Wotton, M., Newbery, A., & Gowman, L. M. (2013). Global wildland fire season severity in the 21st century. *Forest Ecology and Management*, *294*, 54-61. doi: https://doi.org/10.1016/j.foreco.2012.10.022

Fox, D. M., Laaroussi, Y., Malkinson, L. D., Maselli, F., Andrieu, J., Bottai, L., & Wittenberg, L. (2016). POSTFIRE: A model to map forest fire burn scar and estimate runoff and soil erosion risks. *Remote Sensing Applications: Society and Environment*, *4*, 83-91. doi:https://doi.org/10.1016/j.rsase.2016.07.002

Grunwald, S., & Qi, C. (2006). GIS-based water quality modeling in the Sandusky watershed, Ohio, USA. JAWRA *Journal of the American Water Resources Association*, *42*(4), 957-973. doi:https://doi.org/10.1111/j.1752-1688.2006.tb04507.x

Hancock, G. R., Ovenden, M., Sharma, K., Rowlands, W., Gibson, A., & Wells, T. (2020). Soil erosion – the impact of grazing and regrowth trees. *Geoderma, 361*, 114102. doi:https://doi.org/10.1016/j.geoderma.2019.114102

Hänsel, P., Schindewolf, M., Eltner, A., Kaiser, A., & Schmidt, J. (2016). Feasibility of high-resolution soil erosion measurements by means of rainfall simulations and SfM photogrammetry. *Hydrology, 3*(4), 38. doi:https://doi.org/10.3390/hydrology3040038

Hartanto, H., Prabhu, R., Widayat, A. S., & Asdak, C. (2003). Factors affecting runoff and soil erosion: Plot-level soil loss monitoring for assessing sustainability of forest management. *Forest Ecology and Management, 180*(1-3), 361-374. doi:https://doi.org/10.1016/S0378-1127(02)00656-4

Hauer, F. R., Locke, H., Dreitz, V. J., Hebblewhite, M., Lowe, W. H., Muhlfeld, C. C., . . . Rood, S. B. (2016). Gravel-bed river floodplains are the ecological nexus of glaciated mountain landscapes. *Science Advances, 2*(6), e1600026. doi:https://doi.org/10.1126/sciadv.1600026

Hosseini, M., Nunes, J. P., Pelayo, O. G., Keizer, J. J., Ritsema, C., & Geissen, V. (2018). Developing generalized parameters for post-fire erosion risk assessment using the revised Morgan-Morgan-Finney model: A test for north-central Portuguese pine stands. *Catena, 165*, 358-368. doi:https://doi.org/10.1016/j.catena.2018.02.019

Hui, L., Xiaoling, C., Lim, K. J., Xiaobin, C., & Sagong, M. (2010). Assessment of soil erosion and sediment yield in Liao watershed, Jiangxi province, China, using USLE, GIS, and RS. *Journal of Earth Science, 21*(6), 941-953. doi:https://doi.org/10.1007/s12583-010-0147-4

Jourgholami, M., & Labelle, E. R. (2020). Effects of plot length and soil texture on runoff and sediment yield occurring on machine-trafficked soils in a mixed deciduous forest. *Annals of Forest Science, 77*(1), 1-11. doi:https://doi.org/10.1007/s13595-020-00938-0

Kalabokidis, K. D. (2000). Effects of wildfire suppression chemicals on people and the environment—a review. *Global Nest: The International Journal, 2*(2), 129-137.

Karamesouti, M., Petropoulos, G. P., Papanikolaou, I. D., Kairis, O., & Kosmas, K. (2016). Erosion rate predictions from PESERA and RUSLE at a Mediterranean site before and after a wildfire: Comparison & implications. *Geoderma, 261*, 44-58. doi:https://doi.org/10.1016/j.geoderma.2015.06.025

Kirisits, M.J., Emelko, M.B., Pinto, A. (2019). Applying biotechnology for drinking water biofiltration: Advancing science and practice. *Current Opinion in Biotechnology, 57*, 197-204.

Koutsoyiannis, D., Kozonis, D., & Manetas, A. (1998). A mathematical framework for studying rainfall intensity-duration-frequency relationships. *Journal of Hydrology, 206*(1), 118-135. doi:https://doi.org/10.1016/S0022-1694(98)00097-3

Krishnappan, B. G., Chambers, P. A., Benoy, G., & Culp, J. (2009). Sediment source identification: a review and a case study in some Canadian streams. *Canadian Journal of Civil Engineering, 36*(10), 1622-1633. doi: https://doi.org/10.1139/L09-110

Kunze, M. D., & Stednick, J. D. (2006). Streamflow and suspended sediment yield following the 2000 Bobcat fire, Colorado. *Hydrological Processes: An International Journal*, *20*(8), 1661-1681. doi: https://doi.org/10.1002/hyp.5954

Kuo, K. T., Sekiyama, A., & Mihara, M. (2016). Determining C factor of universal soil loss equation (USLE) based on remote sensing. *International Journal of Environmental and Rural Development*, *7*(2), 154-161. doi:https://doi.org/10.32115/ijerd.7.2_154

Lanorte, A., Cillis, G., Calamita, G., Nolè, G., Pilogallo, A., Tucci, B., & De Santis, F. (2019). Integrated approach of RUSLE, GIS and ESA sentinel-2 satellite data for post-fire soil erosion assessment in Basilicata region (southern Italy). *Geomatics, Natural Hazards and Risk*, *10*(1), 1563-1595. doi:https://doi.org/10.1080/19475705.2019.1578271

Larsen, I. J., & MacDonald, L. H. (2007). Predicting postfire sediment yields at the hillslope scale: Testing RUSLE and disturbed WEPP. *Water Resources Research*, *43(*11) doi:https://doi.org/10.1029/2006WR005560

Larsen, I. J., MacDonald, L. H., Brown, E., Rough, D., Welsh, M. J., Pietraszek, J. H., . . . Schaffrath, K. (2009). Causes of post-fire runoff and erosion: Water repellency, cover, or soil sealing? *Soil Science Society of America Journal*, *73*(4), 1393-1407. doi:https://doi.org/10.2136/sssaj2007.0432

Larson-Nash, S. S., Robichaud, P. R., Pierson, F. B., Moffet, C. A., Williams, C. J., Spaeth, K. E., . . . Lewis, S. A. (2018). Recovery of small-scale infiltration and erosion after wildfires. *Journal of Hydrology and Hydromechanics*, *66*(3), 261-270. doi:https://doi.org/10.1515/johh-2017-0056

Lim, K. J., Sagong, M., Engel, B. A., Tang, Z., Choi, J., & Kim, K. (2005). GIS-based sediment assessment tool. *Catena*, *64*(1), 61-80. doi:https://doi.org/10.1016/j.catena.2005.06.013

Liu, J., Engel, B. A., Wang, Y., Wu, Y., Zhang, Z., & Zhang, M. (2019). Runoff response to soil moisture and micro-topographic structure on the plot scale. *Scientific Reports*, *9*(1), 2532. doi:https://doi.org/10.1038/s41598-019-39409-6

Martens, A.M., Silins, U., Proctor, H.C., Williams, C.H.S., Wagner, M.J., Emelko, M.B., Stone, M. (2019). Long term impact of severe wildfire on macroinvertebrate assemblage structure in Alberta's Rocky Mountains. *International Journal of Wildland Fire*. *28*(10), 738-749. doi:https://doi.org/10.1071/WF18177

Mataix-Solera, J., Cerdà, A., Arcenegui, V., Jordán, A., & Zavala, L. M. (2011). Fire effects on soil aggregation: A review. *Earth-Science Reviews*, *109*(1-2), 44-60. doi:https://doi.org/10.1016/j.earscirev.2011.08.002

Matula, J. (2009). Possible phosphorus losses from the top layer of agricultural soils by rainfall simulations in relation to multi-nutrient soil tests. *Plant, Soil and Environment*, *55*(12), 511-518. doi:https://doi.org/10.17221/80/2009-PSE

Meyer, L. D., & Harmon, W. C. (1979). Multiple-intensity rainfall simulator for erosion research on row side slopes. *Transactions of the ASAE, 22*(1), 100-0103. doi:https://doi.org/10.13031/2013.34973

Meusburger, K., Konz, N., Schaub, M., & Alewell, C. (2010). Soil erosion modelled with USLE and PESERA using QuickBird derived vegetation parameters in an alpine catchment. *International Journal of Applied Earth Observation and Geoinformation, 12*(3), 208-215. doi:https://doi.org/10.1016/j.jag.2010.02.004

Mhaske, S. N., Pathak, K., Dash, S. S., & Nayak, D. B. (2021). Assessment and management of soil erosion in the hilltop mining dominated catchment using GIS integrated RUSLE model. *Journal of Environmental Management, 294*, 112987. doi:https://doi.org/10.1016/j.jenvman.2021.112987

Mitasova, H., Barton, M., Ullah, I., Hofierka, J., & Harmon, R. S. (2013). GIS-based soil erosion modeling. In *Remote Sensing and GIScience in Geomorphology* (pp. 228-258). Elsevier Inc. doi:https://doi.org/10.1016/B978-0-12-374739-6.00052-X

Mitasova, H., Brown, W. M., Hohmann, M., & Warren, S. (2001). Using soil erosion modeling for improved conservation planning: A GIS-based tutorial. *University of Illinois at Urban-Champaign, Geographic Modeling Systems Laboratory, Champaign, IL. Available online at http://www.ncsu.edu/hmitaso/gmslab/reports/CerlErosionTutorial/denix/denixstart.html*.

Moody, J. A., & Ebel, B. A. (2014). Infiltration and runoff generation processes in fire-affected soils. *Hydrological Processes, 28*(9), 3432-3453. doi: https://doi.org/10.1002/hyp.9857

Moody, J. A., & Martin, D. A. (2001). Initial hydrologic and geomorphic response following a wildfire in the Colorado Front Range. *Earth Surface Processes and Landforms: The Journal of the British Geomorphological Research Group, 26*(10), 1049-1070. doi: https://doi.org/10.1002/esp.253

Moody, J. A., & Martin, D. A. (2009). Synthesis of sediment yields after wildland fire in different rainfall regimes in the western United States. *International Journal of Wildland Fire*, *18*(1), 96-115. doi:https://doi.org/10.1071/WF07162

Moody, J. A., Shakesby, R. A., Robichaud, P. R., Cannon, S. H., & Martin, D. A. (2013). Current research issues related to post-wildfire runoff and erosion processes. *Earth-Science Reviews, 122*, 10-37. doi:https://doi.org/10.1016/j.earscirev.2013.03.004

Nunes, J.P., Doerr, S.H., Sheridan, G., Neris, J., Santin, C., Emelko, M.B., Silins, U., Robichaud, P.R., Elliot, W.J., Keizer, J. (2018). Assessing water contamination risk from vegetation fires: Challenges, opportunities and a framework for progress. *Hydrological Processes*, 32(5), 687-694. doi:https://doi.org/10.1002/hyp.11434

Parks Canada. (2018a). Kenow wildfire. Retrieved from https://www.pc.gc.ca/en/pn-np/ab/waterton/securite-safety/feu-fire-kenow

Parks Canada. (2018b). Waterton Lakes National Park Climate. Retrieved from https://www.pc.gc.ca/en/pn-np/ab/waterton/nature/environment/climat-climate

Parks Canada. (2018c). Waterton Lakes National Park Climate. Retrieved from https://www.pc.gc.ca/en/pn-np/ab/waterton/nature/environment/verdure-green

Price, J.I., Renzetti, S., Dupont, D., Adamowicz, W., Emelko, M.B. (2017). Production costs, inefficiency, and source water quality: A stochastic cost frontier analysis of Canadian water utilities. *Land Economics, 93*(1), 1-11. doi:https://doi.org/10.3368/le.93.1.1

Pierson, F. B., Robichaud, P. R., & Spaeth, K. E. (2001). Spatial and temporal effects of wildfire on the hydrology of a steep rangeland watershed. *Hydrological processes, 15*(15), 2905-2916. doi:https://doi.org/10.1002/hyp.381

Planet Team (2020). Planet Application Program Interface: In Space for Life on Earth. San Francisco, CA. https://api.planet.com.

Pulley, S., & Collins, A. L. (2019). Field-based determination of controls on runoff and fine sediment generation from lowland grazing livestock fields. *Journal of environmental management*, *249*, 109365. doi:https://doi.org/10.1016/j.jenvman.2019.109365

Puntenney-Desmond, K. C., Bladon, K. D., & Silins, U. (2020). Runoff and sediment production from harvested hillslopes and the riparian area during high intensity rainfall events. *Journal of Hydrology*, *582*, 124452. doi:https://doi.org/10.1016/j.jhydrol.2019.124452

R Core Team (2019). R: A language and environment for statistical computing. R Foundation for Statistical Computing, Vienna, Austria. URL https://www.R-project.org/

Renard, K. G., Laflen, J. M., Foster, G. R., & McCool, D. K. (1994). The revised universal soil loss equation. Soil Erosion Research Methods 2nd edn, ed R Lal (Delray Beach, FL.

Renard, K. G., Foster, G. R., Weesies, G. A., McCool, D. K., & Yoder, D. C. (1996). Predicting soil erosion by water: A guide to conservation planning with the Revised Universal Soil Loss Equation (RUSLE). *Agriculture handbook, 703*, 25-28.

Renard, K. G., Foster, G. R., Weesies, G. A., & Porter, J. P. (1991). RUSLE: Revised universal soil loss equation. *Journal of soil and Water Conservation*, *46*(1), 30-33.

Requena, A. I., Burn, D. H., & Coulibaly, P. (2019). Pooled frequency analysis for intensity–duration–frequency curve estimation. *Hydrological Processes, 33*(15), 2080-2094. doi:https://doi.org/10.1002/hyp.13456

Robichaud, P. R., Jordan, P., Lewis, S. A., Ashmun, L. E., Covert, S. A., & Brown, R. E. (2013). Evaluating the effectiveness of wood shred and agricultural straw mulches as a treatment to reduce post-wildfire hillslope erosion in southern British Columbia, Canada. *Geomorphology, 197*, 21-33. doi:https://doi.org/10.1016/j.geomorph.2013.04.024

Robichaud, P. R. (2005). Measurement of post-fire hillslope erosion to evaluate and model rehabilitation treatment effectiveness and recovery. *International Journal of Wildland Fire, 14*(4), 475-485. doi:https://doi.org/10.1071/WF05031

Robichaud, P. R., Wagenbrenner, J. W., Pierson, F. B., Spaeth, K. E., Ashmun, L. E., & Moffet, C. A. (2016a). Infiltration and interrill erosion rates after a wildfire in western Montana, USA. *Catena, 142*, 77-88. doi:https://doi.org/10.1016/j.catena.2016.01.027

Robichaud, P. R., Elliot, W. J., Lewis, S. A., & Miller, M. E. (2016b). Validation of a probabilistic post-fire erosion model. *International Journal of Wildland Fire*, *25*(3), 337-350. doi:https://doi.org/10.1071/WF14171

Robinne, F.N., Miller, C., Parisien, M.A., Emelko, M.B., Bladon, K.D., Silins, U., Flannigan, M. (2016). Global index for mapping water resources exposure to wildfire activity. *Forests, 7*(1) 22. doi:https://doi.org/10.3390/f7010022

Robinne, F.N., Bladon, K.D., Silins, U., Emelko, M.B., Flannigan, M.D., Parisien, M-A., Wang, X., Kienzle, S.W., Dupont, D.P. (2019). A regional-scale index for assessing the exposure of drinking water sources to wildfires. *Forests*. *10*(5), 384. doi:https://doi.org/10.3390/f10050384

Ryan, S. E., Dwire, K. A., & Dixon, M. K. (2011). Impacts of wildfire on runoff and sediment loads at Little Granite Creek, western Wyoming. *Geomorphology*, *129*(1-2), 113-130. doi:https://doi.org/10.1016/j.geomorph.2011.01.017

Santikari, V. P., & Murdoch, L. C. (2019). Effects of construction-related land use change on streamflow and sediment yield. *Journal of environmental management*, *252*, 109605. doi:https://doi.org/10.1016/j.jenvman.2019.109605

Shakesby, R. A., & Doerr, S. H. (2006). Wildfire as a hydrological and geomorphological agent. *Earth-Science Reviews*, *74*(3-4), 269-307. doi:https://doi.org/10.1016/j.earscirev.2005.10.006

Silins, U., Bladon, K.D., Kelly, E., Esch, E., Spence, J., Stone, M., Emelko, M.B., Boon, S., Wagner, M.J., Williams, C.H.S., Tichkowsky, I. (2014). Five-year legacy of wildfire and salvage logging impacts on nutrient runoff and aquatic plant, invertebrate, and fish productivity. *Ecohydrology*, *7*(6), 1508-1523. doi:https://doi.org/10.1002/eco.1474

Silins, U., Stone, M., Emelko, M. B., & Bladon, K. D. (2009). Sediment production following severe wildfire and post-fire salvage logging in the Rocky Mountain headwaters of the Oldman River Basin, Alberta. *Catena*, *79*(3), 189-197. doi:https://doi.org/10.1016/j.catena.2009.04.001

Sheridan, G. J., Lane, P. N., & Noske, P. J. (2007). Quantification of hillslope runoff and erosion processes before and after wildfire in a wet Eucalyptus forest. *Journal of Hydrology*, *343*(1-2), 12-28. doi:https://doi.org/10.1016/j.jhydrol.2007.06.005

Spencer, S.A., Silins, U., & Anderson, A.E. 2019. Precipitation-runoff and storage dynamics in watersheds underlain by till and permeable bedrock in Alberta's Rocky Mountains. *Water Resources Research*, *55*(12): 10690-10706. doi:https://doi.org/10.1029/2019WR025313

Spigel, K. M., & Robichaud, P. R. (2007). First-year post-fire erosion rates in Bitterroot National Forest, Montana. *Hydrological Processes: An International Journal*, *21*(8), 998-1005. doi:https://doi.org/10.1002/hyp.6295

Stone, M., Emelko, M. B., Droppo, I. G., & Silins, U. (2011). Biostabilization and erodibility of cohesive sediment deposits in wildfire-affected streams. *Water Research*, *45*(2), 521-534. doi: https://doi.org/10.1016/j.watres.2010.09.016

Stone, M., Collins, A., Silins, U., Emelko, M.B., Zhang, Y. (2014). The use of composite fingerprints to quantify sediment sources in a wildfire impacted landscape, Alberta, Canada. *Science of the Total Environment*, *473*, 642-650. doi:https://doi.org/10.1016/j.scitotenv.2013.12.052

Stone, M., Krishnappan, B.G., Emelko, M.B., Silins, U., Williams, C.H.S., Collins, A.L., Spencer, S. (2021). A new framework for modelling fine sediment transport in rivers includes flocculation to inform reservoir management in wildfire impacted watersheds. *Water*, *13*(17), 2319. doi:https://doi.org/10.3390/w13172319

Stone, R. P., & Hilborn, D. (2012). Universal Soil Loss Equation (USLE). Factsheet. Ministry of Agriculture. *Food and Rural Affairs, Ontario*.

Terranova, O., Antronico, L., Coscarelli, R., & Iaquinta, P. (2009). Soil erosion risk scenarios in the Mediterranean environment using RUSLE and GIS: an application model for Calabria (southern Italy). *Geomorphology*, *112*(3-4), 228-245. doi:https://doi.org/10.1016/j.geomorph.2009.06.009

USGS. (2007). Glacier national park and Waterton Lakes National Park vegetation mapping project - spatial vegetation data

USGS. (2019). Landsat-8 image courtesy of the U.S. Geological Survey

Varela, M. E., Benito, E., & Keizer, J. J. (2010). Wildfire effects on soil erodibility of woodlands in NW Spain. *Land Degradation & Development*, *21*(2), 75-82. doi:https://doi.org/10.1002/ldr.896

Wagner, M.J., Silins, U., Bladon, K.D., Williams, C.H.S., Boon, S., MacDonald, R.J., Stone, M., Emelko, M.B., Martens, A.M., Anderson, A. (2014). Catchment-scale stream temperature response to land disturbance by wildfire governed by surface-subsurface energy exchange and atmospheric controls. *Journal of Hydrology*, *517*, 328-338. doi:https://doi.org/10.1016/j.jhydrol.2014.05.006

Waterton Lakes National Park Resource Guide. (WLNPRG; 2020). Waneeta Fisher, Parks Canada. Retrieved from https://www.watertonpark.com/reference/unique_vegetation.htm

Waterton Park Information Services. (WPIS; 2019). Geological information for Waterton lakes park. Retrieved from https://www.watertonpark.com/reference/geology.htm

Watt, C., Emelko, M.B., Silins, U., Collins, A.L., Stone, M. (2021). Anthropogenic and climate-exacerbated landscape disturbances converge to alter phosphorus bioavailability in an oligotrophic river under pressure. *Water, 13(22), 3151.* doi:https://doi.org/10.3390/w13223151

Westerling, A. L., Hidalgo, H. G., Cayan, D. R., & Swetnam, T. W. (2006). Warming and earlier spring increase western US forest wildfire activity. *science*, *313*(5789), 940-943. doi:https://doi.org/10.1126/science.1128834

Williams, C.H.S., Silins, U., Spencer, S.A., Wagner, M.J., Emelko, M.B., Stone, M. (2019). Net precipitation in burned and unburned subalpine forest stands after wildfire in the northern Rocky Mountains. *International Journal of Wildland Fire*. *28*(10), 750-760. doi:https://doi.org/10.1071/WF18181

Wischmeier, W. H., & Smith, D. D. (1978). *Predicting rainfall erosion losses: a guide to conservation planning* (No. 537). Department of Agriculture, Science and Education Administration.

Woods, S. W., & Balfour, V. N. (2010). The effects of soil texture and ash thickness on the post-fire hydrological response from ash-covered soils. *Journal of Hydrology*, *393*(3-4), 274-286. doi:https://doi.org/10.1016/j.jhydrol.2010.08.025

Wu, L., Long, T. Y., Liu, X., & Ma, X. Y. (2013). Modeling impacts of sediment delivery ratio and land management on adsorbed non-point source nitrogen and phosphorus load in a mountainous basin of the Three Gorges reservoir area, China. *Environmental Earth Sciences*, *70*(3), 1405-1422. doi:https://doi.org/10.1007/s12665-013-2227-0

Zhou, Q., Zhou, X., Luo, Y., & Cai, M. (2018). The effects of litter layer and topsoil on surface runoff during simulated rainfall in Guizhou Province, China: A plot scale case study. *Water*, *10*(7), 915. doi:https://doi.org/10.3390/w10070915

# Appendix A

## A.1 Data Dictionary

*Table A.1: File level metadata for the GIS analysis used to model sediment erosion with RUSLE.*

| Data Type | File Name | Year | Source | Citation |
|---|---|---|---|---|
| Primary Data | Soil Texture Class | 2020 | Fleming | Fleming (unpublished) |
| | Rainfall Erosivity (Plot-scale) | 2020 | Fleming | Fleming (unpublished) |
| | Soil Erodibility (Plot-scale) | 2020 | Fleming | Fleming (unpublished) |
| | LS-Factor (Plot-scale) | 2020 | Fleming | Fleming (unpublished) |
| Secondary Data | River | 2017 | CanVec | CanVec (2017) |
| | Road | 2017 | CanVec | CanVec (2017) |
| | Catchments | 2017 | CanVec | CanVec (2017) |
| | Lake | 2017 | CanVec | CanVec (2017) |
| | Landsat-8 imagery | 2017; 2018 | USGS | USGS (2019). Landsat-8 image courtesy of the U.S. Geological Survey |
| | Planet Labs imagery | 2018 | Planet Labs | Planet Team (unpublished). Planet Application Program Interface: In Space for Life on Earth. San Francisco, CA. https://api.planet.com. |
| | Soil Survey | 2018 | Parks Canada | Parks Canada (unpublished) |
| | Soil Samples | 2018 | Parks Canada | Parks Canada (unpublished) |
| | Alberta | 2016 | CanVec | CanVec (2017) |
| | Burn Severity | 2020 | Fleming | Fleming (unpublished) |
| | Vegetation Cover | 2020 | Fleming | Fleming (unpublished) |
| | Rainfall Erosivity (Watershed-scale) | 2020 | Fleming | Fleming (unpublished) |
| | Soil Erodibility (Watershed-scale) | 2020 | Fleming | Fleming (unpublished) |
| | LS-Factor (Watershed-scale) | 2020 | Fleming | Fleming (unpublished) |
| | C-Factor (Watershed-scale) | 2020 | Fleming | Fleming (unpublished) |